

**PREPARATION AND CHARACTERISATION OF PLANTAIN WASTE BASED
CELLULOSIC NANOCOMPOSITES FOR THE REMOVAL OF SELECTED
HEAVY METALS FROM BATTERY EFFLUENT**

BY

**SHAIBU, Blessing Mamudu
MTech/SPS/2017/6863**

**DEPARTMENT OF CHEMISTRY
FEDERAL UNIVERSITY OF TECHNOLOGY, MINNA**

SEPTEMBER, 2021

ABSTRACT

In this study, Ag NPs and Ag-CNCs impregnated on CNTs nano adsorbents were developed using a combination of green chemistry protocol and chemical vapor deposition techniques and subsequently characterized using, HRTEM, HRSEM, XRD, EDS and SAED. The adsorption capability of silver-carbon nanotubes (Ag-CNTs) and silver-cellulose nanocrystals are modified multiwalled carbon nanotube (Ag-CNTs-CNCs), the nanocomposites are for rapid and efficient removal of selected heavy metals (Fe, Cu, Ni, Zn and Pb) as well as analysis of physico-chemical parameters such as, pH, total dissolved solids (TDS), chemical oxygen demand (COD), biochemical oxygen demand (BOD), nitrates, sulphates, and chlorides from battery effluent using a batch process. The aim of the study is the preparation and characterization of plantain waste based cellulosic nanocomposites for the removal of selected heavy metals from battery effluent. The result showed successful deposition of Ag and the grafting of CNCs into the matrix of CNTs as confirmed by the microstructures, morphology, crystalline nature, and elemental characteristics of the Ag-CNTs-CNCs. Optimum batch adsorption parameters include; contact time (90 min) and adsorbent dosage (0.03 g) for Ag-CNTs and contact time (90 min), adsorbent dosage of (0.02 g) for Ag-CNTs-CNCs. The adsorption capacities were obtained as follows; Fe^{2+} (105.263 mg/g), Cu^{2+} (238.095 mg/g) Ni^{2+} (166.667 mg/g), Zn^{2+} (121.951 mg/g) and Pb^{2+} (119.048 mg/g), for Ag-CNTs. Langmuir isotherm and pseudo-second order kinetic model best described the experimental data in the batch adsorption with Ag-CNTs adsorbent. The adsorption capacities using the Ag-CNTs-CNCs adsorbent were obtained as follows; Fe^{2+} (200.000 mg/g), Cu^{2+} (263.158 mg/g) Ni^{2+} (238.095 mg/g), Zn^{2+} (169.492) and Pb^{2+} (181.818mg/g), with a higher adsorption capacity following more physical adsorption, electrostatic interactions and surface complexation. On the contrary, the Freundlich isotherm and pseudo-second order kinetic model best described the experimental data in batch adsorption for Ag-CNTs-CNCs, which validated the chemisorption and multilayered nature of the adsorption process. The high physico-chemical parameters in the effluent were successfully analyzed in the batch systems to fall within WHO permissible concentrations. This study establishes that Ag-CNTs-CNCs is efficient for the treatment of industrial effluent when compared to Ag-CNTs.

TABLE OF CONTENTS

Content	Page
Cover page	i
Title page	ii
Declaration	iii
Certification	iv
Dedication	v
Acknowledgement	vi
Abstract	vii
Table of Contents	viii
List of Tables	xv
List of Figures	xvi
List of Plates	xviii
Lists of Appendices	xix
Lists of Abbreviations	xx
 CHAPTER ONE	 1
1.0 INTRODUCTION	1
1.1 Background to the Study	1
1.2 Statement of the Research Problem	4
1.3 Justification of the Study	5
1.4 Aim and objectives of the Study	7
 CHAPTER TWO	 9
2.0 LITERATURE REVIEW	9
2.1 Effluents and their Management	9
2.2 Heavy Metals, Sources and Impact on Humans and Environment	11

2.2.1	Heavy metal and their sources	11
2.2.2	Impact of heavy metals on human and environment	11
2.2.3	Physicochemical composition of effluents	16
2.3	Conventional Methods for Heavy Metal Removal	18
2.3.1	Chemical precipitation	18
2.3.2	Ultra filtration	19
2.3.3	Ion-exchange	19
2.3.4	Reverse osmosis	19
2.3.5	Electro winning	20
2.3.6	Carbon adsorption	20
2.3.7	Phytoremediation	20
2.3.8	Adsorption	21
2.3.8.1	Physisorption	21
2.3.8.2	Chemisorption	22
2.4	Nanotechnology and the history of nanotechnology	22
2.4.1	Nanotechnology in effluent management	23
2.4.2	Carbon-based nano-adsorbents	23
2.5	Carbon Nanotubes (CNTs)	24
2.5.1	Synthesis of carbon nanotubes	26
2.6	Metal Nanoparticles for Effluent Remediation	29
2.6.1	Silver nanoparticles	30
2.6.2	Synthesis of silver nanoparticles	31
2.6.3	Green synthesis of silver nanoparticles	34
2.6.4	Green synthesis of silver nanoparticles using plant extract	35
2.7	Alternative Source of Biodegradable Polymers for Environmental Remediation	36

2.7.1	Cellulose and cellulose nanocrystals (CNCs)	36
2.7.2	Plantain	38
2.8	Nanocomposites	42
2.8.1	Polymer membranes	43
2.9	Characterization of the as-synthesized nanomaterials	44
2.9.1	X –ray diffraction	45
2.9.2.	High resolution transmission electron microscopy (HRTEM) and high resolution scanning electron microscopy (HRSEM)	45
2.10	Adsorption Models in Batch Tests	46
2.11	Factors Affecting the Adsorption Capacity of Effluent	47
2.11.1	Effect of contact time	47
2.11.2	pH	48
2.11.3	Temperature	48
2.11.4	Effect of initial concentration	49
2.11.5	Adsorbent dosage	49
2.12	Kinetics Model of Adsorption	49
2.12.1	Pseudo first-order kinetics	49
2.12.2	Pseudo second-order kinetics	50
2.12.3	Elovich model	51
2.12.4	Isotherm studies	51
2.12.5	Langmuir isotherm	52
2.12.6	Freundlich isotherm	52
2.12.7	Temkin isotherm	53
2.13	Review of Literature on the Removal of Selected Heavy Metals from Industrial Effluent by Agricultural Biomass or CNTs/Ag Modified Nanocomposites and Research Gaps	54
2.14	Chapter Summary	62

CHAPTER THREE	64
3.0 MATERIALS AND METHODS	64
3.1 Materials, Reagents and Equipment	64
3.2 Methods	66
3.2.1 Sample collection and pre-treatment for plantain trunk	66
3.2.2 Preparation of cellulose nanocrystals (CNCs)	66
3.2.3 Green synthesis of silver nanoparticles	68
3.2.4 Carbon nanotube synthesis	68
3.2.4.1 Purification of the synthesized CNTs	69
3.2.5 Preparation of CNCs-Ag-CNTs nanocomposite	71
3.2.6 Characterisation of the as-synthesized nanomaterials	71
3.2.6.1 X-Ray diffraction (XRD)	71
3.2.6.2 High resolution scanning electron microscope / electron dispersive x-ray spectroscopy (HRSEM/EDS)	72
3.2.6.3 High resolution transmission electron microscope / selected area electron diffraction spectroscopy (HRTEM/SAED)	73
3.2.7 Sampling and sample pre-treatment for battery effluent	73
3.2.7.1 Acid digestion of the battery effluent for heavy metal determination	74
3.2.8 Determination of selected heavy metals in the battery effluent	74
3.2.9 Physicochemical characterisation of battery effluent sample	75
3.2.9.1 Determination of water pH	75
3.2.9.2 Determination of total dissolved solid and total suspended solid	75
3.2.9.3 Determination of the biochemical oxygen demand (BOD)	76
3.2.9.4 Determination of the chemical oxygen demand (COD)	76
3.2.9.5 Determination of turbidity	77
3.2.9.6 Determination of sulphate concentration	77

3.2.9.7 Chloride determination	77
3.2.9.8 Dissolved oxygen (DO)	77
3.2.9.9 Fluoride determination	77
3.2.9.10 Determination of cyanide	78
3.2.9.11 Determination of ammonium	78
3.3 Batch Adsorption of Selected Heavy Metals using the Prepared Nanomaterial	79
3.3.1 Effect of contact time on adsorption	79
3.3.2 Effect of adsorbent dosage	79
3.3.3 Adsorption data analysis	80
3.4 Adsorption Kinetics	80
3.4.1 Pseudo first-order kinetic model	80
3.4.2 Pseudo second-order kinetic model	81
3.4.3 Elovich kinetic model	81
CHAPTER FOUR	83
4.0 RESULTS AND DISCUSSION	83
4.1 Characterisation of Nanomaterials	83
4.1.1. UV-Vis Analysis of Ag NPs	83
4.1.2 HRSEM analysis	83
4.1.3 EDS profile of synthesized silver nanoparticles	86
4.1.4 XRD Analysis	88
4.1.5 HRTEM analysis	91
4.1.6 SAED analysis	94
4.2 Physiochemical Characterization of Effluent before Batch Adsorption	96
4.3 Adsorption Parameters	99
4.3.1 Effect of contact time	99

4.3.2	Effect of dosage	102
4.4	Physicochemical Parameters of Battery Effluent at Batch Adsorptions	104
4.5	Adsorption Isotherms	106
4.6	Kinetic Studies	114
4.7	Adsorption Mechanism	118
	CHAPTER FIVE	121
5.0	CONCLUSIONS AND RECOMMENDATIONS	121
5.1	Conclusion	121
5.2	Recommendations	122
5.3	Contribution to Knowledge	123
	REFERENCES	124
	APPENDICES	144

LIST OF TABLES

Table	Page
2.1 Summary and Comparison of the Three Common Methods Employed in the Synthesis of CNT	29
2.2 Scientific Classification of Plantain	39
2.3 Chemical Composition of Plantain Pseudo-stem (Based on Different Literatures)	41
3.1 List of Reagents	65
3.2 List of Equipment and Apparatus	66
3.3 HRSEM Operating Settings	71
3.4 HRTEM experimental conditions	72
4.1 Elemental Composition from EDS of Ag, CNCs, CNTs, Ag-CNTS and Ag-CNTs-CNCs	71
4.2 Initial Concentration Metals Ion in Battery Effluent	96
4.3 Physicochemical Characteristics of Battery Effluent Before Adsorption	96
4.4 Physicochemical Characteristics of Battery Effluent after Adsorption Process with Ag-CNTs and Ag-CNTs-CNCs	105
4.5 Isotherm Parameters for the Selected Heavy Metal Removed from Battery Effluent using Ag-CNTs	108
4.6 Isotherm Parameters for the Selected Heavy Metal Removed From Battery Effluent using Ag-CNTs-CNCs	111
4.7 Pseudo First, Second, and Elovich Diffusion Kinetic Parameters for Adsorption of Selected Heavy Metals on Ag-CNTs	115
4.8 Pseudo First, Second, and Elovich Diffusion Kinetic Parameters for Adsorption of Selected Heavy Metals on Ag-CNTs-CNCs	116

LIST OF FIGURES

Figure	Page
2.1 Convectional ways to Treat Effluent and their Shortcomings	18
2.2 Basic Terms of Adsorption	21
2.3 Schematic Structure of SWCNT and MWCNT	24
2.4 Functionalization of CNTs	25
2.5 Different Approaches of Synthesis of Silver Nanoparticles	33
2.6 Protocols Employed for Synthesis of Nanoparticles (a) Bottom to Top Approach and (b) Top to Bottom Approach	32
2.7 Protocol for Synthesis of Silver Nanoparticles Using Plant Extract	35
2.8 (a) Plantain plant (b) Plantain Trunk	39
2.9 Synthesis of Polymer Nanocomposites	42
2.10 Typical Types of Nanocomposite Membranes	44
3.1 Reaction Scheme for the TEMPO-mediated Oxidation of Cellulose	67
4.1 UV-Vis Absorption Spectrum of Biosynthesized Ag NPs	83
4.2 EDX Spectrum of Green Synthesized Ag NPs	87
4.3 XRD Graph of Ag-NPs, Carbon Nanotubes (CNTs), Cellulose Nanocrystals (CNCs), Ag-CNTs and Ag-CNTs-CNCs Composites	90
4.4 Effect of Contact Time on Percentage Removal of Heavy Metal using Ag-CNTs	99
4.5 Effect of Contact Time on Percentage Removal of Heavy Metal using Ag-CNTs-CNCs	100

4.6 Effect of Dosage on Percentage Removal of Heavy Metal using Ag-CNTs	102
4.7 Effect of Dosage on Percentage Removal of Heavy Metal using Ag-CNTs-CNCs	103
4.8 Possible Adsorption Mechanism of Fe(II), Cu(II), Zn(II), Ni(II), and Pb (II) Ions Adsorption by Ag-CNTs-CNCs	119

LIST OF PLATES

Plate		Page
I	HRSEM Micrographs of (a) Silver Nanoparticles (Ag NPs), (b) Carbon Nanotubes (CNTs), (c) Cellulose Nanocrystals (CNCs), (d) Ag NPs-CNTs Composites, (e) Ag NPs-CNTs-CNCs composites	85
II	HRTEM Micrographs of (a) Silver Nanoparticles (Ag NPs), (b) Carbon Nanotubes (CNTs), (c) Cellulose Nanocrystals (CNCs), (d) Ag NPs-CNTs Composites, (e) Ag NPs-CNTs-CNCs Composites	92
III	SAED Micrographs of (a) Silver Nanoparticles (Ag NPs), (b) Carbon Nanotubes (CNTs), (c) Cellulose Nanocrystals (CNCs), (d) Ag NPs-CNTs composites, (e) Ag NPs-CNTs-CNCs Composites	94

LIST OF APPENDICES

Appendix	Page
A Preparation of Reagents	144
B Calibration Curves	145
C Adsorption Isotherm Plots for Heavy Metal Removal by Adsorbents	150
D Kinetics Plots for Heavy Metal Adsorption by Prepared Adsorbents	153

LIST OF ABBREVIATIONS

$Al_2Si_2O_5(OH)_4$	Kaolin
AAS	Atomic Absorption Spectrophotometer
Ag-CNTs	Silver-carbon nanotubes composite
Ag-CNTs-CNCs	Carbon nanotubes modified with Silver and Cellulose nanocrystals
At %	Atomic percentage
BET	Brunauer Emmett Teller
BOD	Biological oxygen demand
CCVD	Catalytic Chemical Vapour Deposition
CNCs	Cellulose Nanocrystals
CNTs	Carbon nanotubes
COD	Chemical oxygen demand
CVD	Chemical vapour deposition
EDS	Energy Dispersive X-ray Spectroscopy
EDX	Energy dispersive X-ray spectroscopy
FTIR	Fourier Transform Infrared Spectroscopy
FWHM	Full width at half maximum
h	Hour(s)
HRSEM	Scanning Electron Microscopy
HRTEM	Transmission Electron Microscopy
Min	Minute
mL/min	Millilitre per minute
mM	Milli molar
MWCNT	Multiwalled carbon nanotubes
nm	Nanometre
NM	Nanomaterials
NPs	Nanoparticles
Pb	Lead
SAED	Selected Area Electron Diffraction
SWCNT	Single-walled carbon nanotube

TGA	Thermogravimetric Analyses
wt %	Weight percentage
XRD	X-Ray Diffraction
XRF	X-Ray Fluorescence
ΔH	Enthalpy
ΔS	Enthropy

CHAPTER ONE

1.0

INTRODUCTION

1.1 Background to the Study

Water is a universal liquid in the world and vital for domestic purposes such as drinking, cooking, washing, bathing among others, with 75% of the human body made up of water because of its specific gravity (Seiyaboh and Izah, 2017). Nevertheless, environmental pollution is currently one of the most important issues faced by humanity and has increased exponentially to alarming levels in terms of its effects on living creatures (Renge *et al.*, 2012). Increased industrial and agricultural activities have resulted in the generation of various types of toxic pollutants, which are the main cause of environmental water pollution on a global scale. However, years of increased industrial, agricultural and domestic activities have resulted in the generation of large amount of effluent containing a number of toxic pollutants which are polluting the available fresh water continuously (Bhatnagar and Sillanp, 2010).

With a swift increase in the population of the world, demand for drinking water has been on the increase and it is expected that there would be a corresponding upsurge in domestic, agriculture and industrial water sources, especially in developing countries where the need of water is greater as compared to its economic status and population (Zahid *et al.*, 2018). Rapid industrialization in developed and developing countries has led to a substantial increase in the generation of industrial effluents. These effluents are a great concern to health scientists all over the world as they constantly pollute water bodies when discharged without adequate treatment (Sweetly *et al.*, 2015).

Effluents from numerous industries such as paints and pigments, glass production, mining operations, metal plating, and battery manufacturing processes are known to

contain contaminants such as heavy metal, chlorides, sulphides, and pathogens to mention but a few (Manjuladevi and Sri, 2017). Most of these pollutants present in industrial effluents, are not biodegradable and their existence in receiving lakes and streams cause bioaccumulation in living organisms, which leads to several health problems in animals, plants and human beings such as cancer, kidney failure, metabolic acidosis, oral ulcer, renal failure and damage in the stomach of the rodents (Mehmet *et al.*, 2006).

Batteries may be hazardous wastes because they contain heavy metals and corrosive electrolyte solutions that are the sources of their energy (Sweetly *et al.*, 2015). Battery industries discharge mostly inorganic pollutants containing heavy metals such as, lead, zinc, lithium, cadmium as well as sulfuric acid (Iloms *et al.*, 2020). It is, therefore, essential to remove or reduce the presence of these inorganic contaminants in order to diminish the possibility of uptake by animals, plants, humans and eventual accumulation in the food chain to prevent them from contaminating surface and groundwater by dissolution or dispersion (Ibigbami *et al.*, 2016).

To address the undeniable need of alleviating water pollution from industrial activities, various water treatment technologies have been proposed and applied at experimental and field levels. These technologies commonly fall into primary (screening, filtration, centrifugation, separation, sedimentation, coagulation and flocculation); secondary (aerobic and anaerobic treatments); and tertiary (distillation, crystallization, evaporation, solvent extraction, oxidation, precipitation, ion exchange, reverse osmosis (RO), nanofiltration (NF), ultrafiltration (UF), microfiltration (MF), electrolysis and electrodialysis) level water treatment technologies (Gupta *et al.*, 2012). However, the most used of these technologies are not capable of fixing water pollutants present in battery effluents in an effective way. Some of the mentioned methods are energy and

operationally intensive and thus are not affordable on a commercial scale. Adsorption techniques are easy and simple and can be carried out with polymeric materials or membranes.

Polymer nano-composite membranes are basically modified type of polymeric membranes with nano-materials dispersed in their matrices (Qalyoubi *et al.*, 2021). Polymer nano-composite membranes are applied in organic solvent nanofiltration, pervaporation, effluent treatment, direct methanol fuel cells, sensor applications, gas separation and proton exchange membrane fuel cells (Rasheed *et al.*, 2020). Polymeric membranes have been widely used for water treatment. These include; waste streams from agro-food (Castro-Muñoz *et al.*, 2016), textile (Van der Bruggen *et al.*, 2004), and petroleum industries (Alzahrani, and Wahab *et al.*, 2014) or removal of pollutants from drinking water (Kim and van der Bruggen, 2010) enabling the concentrate to be treated or discharged and, thereby, reducing the contaminants directly or indirectly discharged into wastewater (Castro-Muñoz *et al.*, 2016). However, the basic setback associated with polymeric membrane in the industrial scale includes high cost of maintenance and membrane fouling (Ursino *et al.*, 2018).

Over the past decade, numerous trials have been devoted to make use of agricultural wastes from fruits such as, plantain and pineapple peels which contains appreciable amount of natural cellulose for the manufacture of nanocomposites with particular applications having appropriate features such as permeability, selectivity, and specific chemical and physical properties. Cellulose is the most abundant polysaccharide in the world and it is widely considered to be a long-term renewable alternative to synthetic plastics. Cellulose is a long chain linear homo-polymer comprising anhydro- β -D-glucopyranose units linked by (1 \rightarrow 4) glycosidic bonds (Spinella *et al.*, 2016; Yadav *et al.*, 2017). Cellulose has received increasing research interest owing to its

environmental friendly advantages and attractive features, such as nontoxicity, biological biodegradation, biocompatibility, excellent thermal and mechanical properties, renewability and easy modification (Dai & Huang 2016, 2017a, b; Khawas & Deka 2016; Zhang *et al.*, 2017). Recently, highly crystalline nanoscale materials, namely cellulose nanocrystals (CNCs) and cellulose nanofibrils (CNFs) have been produced from cellulose and combined with other nanomaterials via techniques such as, track-etching, stretching, sintering, phase inversion, electrospinning and interfacial polymerization with superior properties (Lalia *et al.*, 2013). Likewise, nanoparticles (NPs)-based membranes have demonstrated low-fouling process through adding the inorganic particles (Kim and van der Bruggen, 2010). Dispersing the NPs into the natural polymer generally forms nanocomposite membranes, which are also a suitable tool to improve the performances, such as permeability and selectivity (Madaeni *et al.*, 2015). The unique features exhibited by natural polymeric membranes such as, nanocellulosic crystals when reinforced with silver (Ag) nanoparticles and carbon nanotubes (CNTs) to form nanocomposites is what this research intends to utilize for effluent treatment in a battery manufacturing factory at industrial scale.

1.2 Statement of the Research Problem

Noxious and hazardous electrolytes and materials are widely used in the battery industry (Fedorov, *et al.*, 2017). The problems of low pH and high concentration of lead are often associated with battery effluent (Vu *et al.*, 2019). Consumption and exposure of aquatic species and humans to battery effluent have caused challenges which has led to several health problems in animals, plants and human beings such as cancer, kidney failure, metabolic acidosis, oral ulcer, renal failure and damage in the stomach of the

rodents (Mehmet *et al.*, 2006). Besides, the effluents have offensive odour and contains a lot of contaminants.

In addition, accidental discharge of such battery effluent into water bodies will deteriorate and degrade the quality of limited clean water. Many traditional methods such as chemical precipitation, electrochemical reduction, ion exchange, activated carbon and biosorption to mention a few, has been used for the removal of one of the major constituent of battery effluent (Pb^{2+}). This method can only be used effectively for heavy metal extraction when the concentration of the heavy metal is less than 100 mg/L (Inbaraj *et al.*, 2009). Furthermore, the use of polymeric materials alone for the treatment of industrial effluent can be prone to fouling. Likewise, pristine CNTs alone often forms aggregates when put to use over time which significantly decreases water flux and pollutant rejection capacities of the membranes. CNTs are generally contaminated with metal catalysts, impurities and physical heterogeneities (Madaeni, 2007). Also, reinforcement of CNTs into metal matrix or natural polymer remains a challenge due to their entangled structure. The CNTs are held together by weak, non-covalent interactions. These interactions are π - π attractive bonding, electrostatic and van der Waal forces which is the main reason CNTs have tendencies to agglomerate. Plantain is an important plant whose fruits are consumed on daily basis. However, the peel and trunk fiber of this fruits are underutilized and are usually discarded after consumption and left to decompose in this part of the world. This plantain tree waste can cause serious environmental threat if not properly managed, and can produce greenhouse gas such as (methane) if dumped in wet condition.

1.3 Justification for the Study

In order to avoid some disadvantages of conventional adsorbents based on synthetic polymers (high prices, difficulties in production, pollution produced during their synthesis), unconventional materials are increasingly being used for effluents analysis and treatment (Suteu *et al.*, 2007). The abundant availability of natural polymeric adsorbents such as clay, kaolin and several agricultural wastes which includes plantain trunk and stalks makes them to be considered as alternative sources of effective and eco-friendly adsorbents for removal of pollutants from effluents in battery manufacturing factories. Modification of this polymeric materials or membrane both enhance the surface area and adsorption capacity.

Carbon nanotubes (CNTs) have recently attracted the attention of researchers due to their extraordinary electrical, mechanical, and thermal properties and antibacterial activity. Indeed, they alter the physico-chemical properties of polymer membranes, which encourage their potentiality for several applications. Typically, the inner pores of CNTs tend to act as selective nanopores. Therefore, the CNT-filled membranes show an enhanced permeability without a decrease in selectivity, coupled with enhancements in mechanical and thermal properties (Fontananova *et al.*, 2017). Silver (Ag)-based NPs when present in polymer membranes, generally offer antimicrobial properties that give them potential for several applications including water treatment and disinfection of medical devices (Ursino *et al.*, 2018). Therefore, since silver nanoparticles is among the most often used nanoparticles for antimicrobial applications with less health and environmental consequences. A synergistic nanocomposition of Ag NPs, CNTs and CNCs would improve the performance of the base cellulosic natural polymeric with several attractive features including surface hydrophilicity, thermal and mechanical

stability, antimicrobial and anti-fouling properties which are relevant in water treatment or industrial effluents remediation.

1.4 Aim and Objectives of the Study

The aim of this study is to prepare cellulose nanocrystals from plantain waste (pseudo-stem/trunk) and modify them with carbon nanotubes and biosynthesized silver nanoparticles for the sequestration of selected heavy metals from battery effluents.

The aim was achieved through the following objectives;

- i. Biosynthesis of Ag nanoparticles (AgNPs) using AgNO_3 as a precursor and tea leaves extract.
- ii. Synthesis of CNTs via catalytic chemical vapor deposition method.
- iii. Preparation of Ag-CNTs nanocomposite
- iv. Preparation of cellulose nanocrystals (CNCs) using dried plantain trunk (DPT) and to modify it with the prepared Ag-CNTs nanocomposite via ultrasonic cavitation to obtain Ag-CNTs-CNCs.
- v. Characterisation of the Ag NPs, CNTs and Ag-CNTs, and Ag-CNTs-CNCs nanomaterials produced to determine the morphologies, microstructures and crystallinities using High Resolution Scanning Electron microscopy (HRSEM-EDS), High Resolution Transmission Electron Microscopy (HRTEM-SAED) and X-ray Diffraction (XRD) respectively.
- vi. Evaluation of the adsorption potentials of the developed Ag-CNTs & Ag-CNTs-CNCs for the removal of the selected heavy metals from battery effluent by

varying the contact time and dosage of the nanosorbents via batch adsorption process.

- vii. Evaluation of the adsorption kinetics of the developed Ag-CNTs and Ag-CNTs-CNCs using pseudo-first order, pseudo second order and Elovich models, as well as to investigate the adsorption isotherms using Freundlich, Langmuir and Temkin isotherms.

CHAPTER TWO

2.0 LITERATURE REVIEW

2.1 Effluents and their Management

An effluent refers to any water whose quality has been adversely affected by anthropogenic influence. In a general term, effluent refers to the municipal effluent that contains a broad spectrum of contaminants (Alves *et al.*, 2000). It includes waste materials containing heavy metals, cyanides, toxic organic compounds, nutrients and sewages that are discharged by domestic residences, industry and agriculture processes into a water bodies. Effluents have been recognized as a major environmental problem, since all life activities ranging from natural to anthropogenic, biological, physical and chemical all rely on the use of water. Early generation suffered little effluent problem due to the natural cleansing mechanisms available then which often get rid of most of these pollutants in water within a short period. However, the advent of urbanization and industrialization has resulted into increase in pollution of wastewater/effluent system. Man's quest for comfort as contributed largely to high level of contaminants that general environment especially water bodies have little or no capacity to remove.

One of the most critical problems of developing countries is improper management of the vast amount of wastes generated by various anthropogenic activities. More challenging is the unsafe disposal of these wastes into the ambient environment (Kanu and Achi, 2011). Water bodies especially freshwater reservoirs are the most affected. This has often rendered these natural resources unsuitable for both primary and/or secondary usage (Fakayode, 2005). These effluents from industries can alter the physical, chemical and biological nature of the receiving water body (Nwagwu *et al.*, 2016).

In addition to the foregoing, increased industrial activities have led to pollution stress on surface waters both from industrial, agricultural and domestic sources (Kanu and Achi, 2011). Wastes entering these water bodies are both in solid and liquid forms. These are mostly derived from industrial, agricultural and domestic activities. As a result, water bodies that are major receptacles of treated and untreated or partially treated industrial wastes have become highly polluted (Osibanjo *et al.*, 2011). The resultant effects of this on public health and the environment are usually high in magnitude (Osibanjo *et al.*, 2011). Over the last decades, a considerable population growth has taken place. In many African countries accompanied by a steep increase in urbanization. This was industrialization and agricultural process use. This has entailed a tremendous increase in discharge of a wide diversity of pollutants to receiving water bodies and has caused undesirable effects on the different components of the aquatic environment and on fisheries (Kanu and Achi, 2011).

There is a growing appreciation that nationally, regionally, and globally, the management and utilization of natural resources need to be improved and that the amount of waste and pollution generated by human activity need to be reduced on a large scale (Kanu and Achi, 2011). Furthermore, industries are the primary sources of pollution in all environments. Based on the type of industry, various levels of pollutants can be discharged into the environment directly or indirectly through the public sewer lines. Effluents from industries include employees' sanitary waste, process wastes from manufacturing, wash waters and relatively uncontaminated water from heating and cooling operations. High levels of pollutants in river water systems cause an increase in biological oxygen demand (BOD), chemical oxygen demand (COD), total dissolved solids (TDS), total suspended solids (TSS), toxic metals such as Cd, Cr, Ni and Pb and fecal coliform and hence make such water unsuitable for drinking, irrigation and aquatic

life (Kanu and Achi, 2011). Additionally, industrial effluents come with high biochemical oxygen demand (BOD) from biodegradable wastes such as those from human sewage, pulp and paper industries, slaughterhouses, battery production, tanneries and chemical industry. Others include those from plating shops and textiles, which may be toxic and require on-site physico- chemical pre-treatment before discharge into municipal sewage system (Emongor *et al.*, 2005; Otokunefor and Obiukwu, 2005). Organic pollution of inland water systems in Africa is often the result of extreme poverty and economic and social underdevelopment in contrast to the situation in developed countries of the world. According to Kanu and Achi (2011), it is in these countries that the quality of water, and often the quantity, is lowest, sanitation and nutrition the worst and disease most prevalent. Unfortunately, there are very few studies on the social, economic and health implications of waste discharge into inland waters in Africa.

2.2 Heavy Metals, Sources and Impact on Humans and Environment

2.2.1 Heavy metal and their sources

The heavy metals are usually defined based on their atomic weights; however, term heavy metals are also referred to elements toxic to living creatures (Appenroth, 2010). Certain heavy metals are lethal to the human health and other living creatures in their different forms and doses. Frequently, heavy metals are thought of as toxic; however, lighter metals may likewise be lethal, for example, beryllium and lithium. Natural and anthropogenic activities are sources of heavy metal contamination. Specifically, point and non-point sources such as industrialization expansion, urbanization drive, manufacturing, metallurgical, paint pigment production, mining activities, agricultural practices and battery effluent have been identified as possible routes through which

heavy metals are introduced into the environment (Ejazul *et al.*, 2007). Generally, heavy metals are non-biodegradable and enter the environment due to inappropriate treatment and their presence pose a serious threat to both environment and the living things.

2.2.2 Impact of heavy metals on human and environment

Not all heavy metals are poisonous to health, as some are fundamental, for example, iron and Cr (III). Most commonly known toxic metals are Pb, Cd, Cr, Mn, Hg, As, and radioactive metals. Radioactive metals have both radiological and chemical toxicity. Heavy metal toxicity has turned out to be a major threat, and there are many health risks associated with them. The lethal impact of these metals is the fact that they do not have any biological role; however, they may mimic as an element of the body and interfere with the metabolic and other biological processes (Baby *et al.*, 2019). Some metals like aluminum can easily be eliminated by the excretion system, while certain metals accumulated in the food chain and body. Metal-induced toxicity depends on dose, exposure route, and contact time (acute or chronic).

The heavy metals detected in water, air, soils, rocks and living organisms originate from different point and non-point sources. Some of the heavy metals are key to living creatures in very low concentrations especially iron and zinc (Lieu *et al.*, 2001), however some are exceptionally poisonous even at relatively low concentration for instance, nickel, cadmium and chromium (Telisman *et al.*, 2007).

Effluents generated from battery manufacturing industries contain metal ions whose concentrations are higher than the permissible limits and are regarded as toxic or carcinogenic. As a result of their high toxicity, industrial effluent containing metals must be treated before being discharged into the environment (Nwabanne & Okoye

2013). Examples of toxic heavy metals are zinc, copper, mercury, cadmium, lead, and chromium.

(i) Mercury (Hg)

Mercury is a d-block element with an atomic number 80 and is in liquid form under standard conditions. Mercury is found in deposits of mercuric sulfide called cinnabar. Mercury pollution is caused by pharmaceutical industries, pulp and paper preservation, caustic soda production industry, agriculture industry amongst others (Morais & Pereira, 2012). Mercury is the most toxic heavy metal in the environment, and mercury poisoning is called pink disease also known acrodynia. Mercury can combine with organic and inorganic compounds. Elevated exposure levels of mercury in any form can damage the kidneys, brain, developing fetus amongst others (Alina *et al.*, 2012). The environmental protection agency has declared methyl mercury and mercuric chloride as carcinogenic. Mercury exposure can also cause lung damage, skin rashes, memory problems, and hair loss. The World Health Organization (WHO) has set the standard for drinking water with lower levels of mercury to 0.01 mg/l (WHO, 2004).

(ii) Copper (Cu)

Copper as an element does essential work in animal metabolism but the excessive ingestion brings out serious toxicological concerns such as vomiting, cramps, convulsions, or even death (Nwabanne & Okoye 2013).

(iii) Lead (Pb)

Lead is an element with an atomic number of 82 and is considered as a heavy metal with silvery bluish appearance which turns dull gray by the action of air (Jaishankar *et al.*, 2014). There are various sources of lead pollution, mainly wastes of battery

industries, fertilizers and pesticides, metal plating and finishing operations, exhaust, additives in gasoline, pigment in automobiles, and smelting of ores. This metal is becoming an environmental and health concern around the globe due to its widespread use (Sharma & Dubey, 2005). Lead (Pb) is a carcinogenic element declared by the Environmental Protection Agency (EPA). Lead poisoning is a term used for its toxicity, and it may be acute or chronic. Lead poisoning can cause mental retardation, birth defects like autism, allergies, dyslexia, paralysis, brain damage, and kidney damage and may also result in death (Martin & Griswold, 2009).

(iv) Arsenic (As)

Arsenic is a metalloid element having an atomic number of 33 and occurs in mineral form commonly in combination with sulfur, some other metals, salts of iron, calcium, sodium, and copper, and also in pure elemental form (Waalkes *et al.*, 2001). The water is contaminated by arsenic-based pesticides, deposits of natural minerals, and inappropriate disposal of arsenic-based reagents or chemicals. Arsenic in the form of arsenate and arsenite is lethal to the environment and living creatures. Arsenic disturbs protoplasm of the cells by interacting with the sulphhydryl group of the cells causing respiration malfunctioning and affecting mitosis and cell enzymes (Jaishankar *et al.*, 2014).

(v) Cadmium (Cd)

Cadmium has an atomic number of 48 and is bluish-white soft metal having chemical properties similar to mercury and zinc of group 12 (Jaishankar *et al.*, 2014). It is produced from smelting of its ores, electroplating, batteries, plasticizers, alloys, pigments, nuclear industry, and cigarette smoke. Generally, cadmium is present at low levels in the environment; however, industrial wastes have greatly increased those levels.

Cadmium-induced toxicity can cause damage to the kidneys, respiratory systems, and skeleton and is carcinogenic to humans (Waalkes *et al.*, 2001; Jaishankar *et al.*, 2014). Cadmium is ranked the seventh most toxic metal by the Agency for Toxic Substances and Disease Registry (ATSDR).

(vi) Chromium (Cr)

Chromium is an element having an atomic number 24, with steely gray appearance (Martin and Griswold, 2009). Chromium occurs in different states, e.g., divalent, tetravalent, pentavalent, and hexavalent states; however, trivalent and hexavalent forms are the most stable. Chromium (III) is an essential nutritional supplement for humans and animals. However, chromium (VI) form is highly toxic and carcinogenic in nature (Zhitkovich *et al* 2005; Wilbur *et al.*, 2012). Chromium is produced in environment matrices (air, water, and soil) from different sources, such as, effluent and air mainly released from metallurgical and chemical industries. The hexavalent chromium Cr (VI) is an industrial pollutant established as a human carcinogen (Jacobs & Testa, 2005). Concentration of Cr (VI) in ground water and surface water is increasing and the World Health Organization has set the limit of 50 µg per liter (Velma *et al.*, 2009).

(vii) Zinc (Zn)

Zinc is an element having an atomic number 30 and placed in group 2 of the periodic table. Although zinc is an essential trace metal for humans, excessive absorption of zinc can suppress the iron absorption. Zinc ions are highly toxic to plants, vertebrate fishes, invertebrates amongst others (Brita *et al.*, 2006; Fosmire, 2006). Zinc is a trace element essential for human health. It is important for the physiological functions of living tissue and regulates many biological processes. However, too much zinc can cause eminent

health problems such as stomach cramps, skin irritations, vomiting, nausea and anemia (Oyaro *et al.*, 2007).

2.2.3 Physicochemical composition of effluents

The pollution level of water is frequently described using aggregate parameters, sometimes called sum parameters, such as the chemical oxygen demand (COD), biochemical oxygen demand (BOD), total organic carbon (TOC) or the spectral absorption coefficients (SAC) (Werner, 2018). The organic carbon in water and effluent is composed of a variety of organic compounds in various oxidation states. Biological or chemical processes can oxidize some of these carbon compounds further, and the BOD and COD may be used to characterize these fractions. COD is the total measurement of all chemicals (organics and in-organics) in the water/effluent. BOD is a measure of, the amount of oxygen that is required for bacteria to degrade the organic components present in water/effluent (Power, 2016). It is a standard test for assaying the oxygen-demanding concentration of microbes to degrade organic matter over a given time period, usually 5 days but can be extended to 30 days. COD is a standard test for water to consume oxygen in the form of potassium dichromate during the degradation of organic matter and inorganic chemicals such as ammonia and nitrite for few hours. The potassium dichromate is not specific to oxygen-consuming chemicals either organic or inorganic and therefore, both chemicals are included in COD. As a result, the BOD/COD ratio should be equal or less than 1.0 (Samudro & Mangkoedihardjo, 2010).

Unlike BOD or COD, TOC is independent of the oxidation state of the organic matter and does not measure other organically bound elements, such as nitrogen and hydrogen, and inorganics that can contribute to the oxygen demand measured by BOD and COD. The TOC therefore, is a measure of the amount of electrons available in the organic

carbon for reduction of oxygen to water. Similarly, since TOC measures the amount of carbon bound to an organic compound, hence the relation between COD and TOC are supposed to be directly proportional to each other. Biochemical Oxygen Demand, currently a five-day laboratory test labeled BOD₅, is one of the most broadly used parameters for water & effluent quality in the world and the standard for municipal water & sewage treatment. COD, typically a two-hour test, is more widely used in industrial applications. Often, both of these laboratory methods are measured, recorded and compared over time. TOC analysis is a well-known analytical method used in diverse water and municipal and industrial effluent quality applications. There are multiple TOC measurement methods and technologies available in the laboratory and online configurations, and typical analytical times are 3-10 minutes depending on the mode of analysis. TOC analysis is faster and more accurate than either oxygen demand method and is a direct measurement of the organic load. The speed of analysis and online operation of TOC instruments provide advantages over oxygen demand measurements, providing near real-time analysis for event detection and integrated process control. Additionally, TOC is a direct measure of the quantity of organics in the water, whereas COD and BOD are indirect measurements (Chihoon *et al.*, 2016; Katarzyna *et al.*, 2006; Waziri, 2010). It is now not very uncommon in the world that many organization especially municipal sewage and industrial effluent plants are conducting short-term and long-term studies to determine the correlation between organic pollutants and oxygen demand (Khaled, 2014). If a repeatable empirical relationship is established between TOC and BOD or COD, then TOC can be used to estimate the accompanying BOD or COD. To insure the practical capability, this relationship must be established independently for each set of matrix conditions, such as various points in a treatment process.

2.3 Conventional Methods for Heavy Metal Removal

For the last few decades, various methods have been used for the removal of heavy metals from polluted water and effluents.

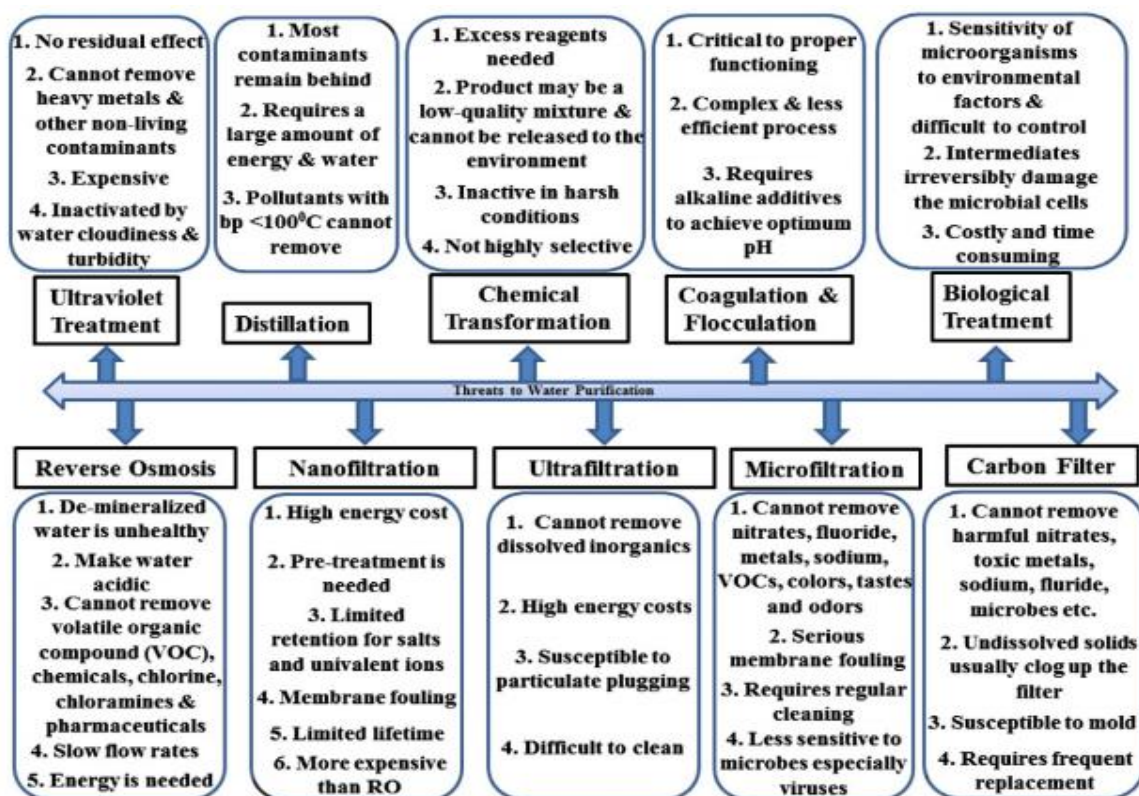


Figure 2.1: Convectional Ways to Treat Effluent and their Shortcomings (Das *et al.*, 2014)

The commonly used methods for the removal of heavy metals and general pollutants from contaminated effluent and their shortcomings are shown in Figure 2.1, These methods includes chemical precipitation, ultra-filtration, ion exchange, reverse osmosis, electro winning, carbon adsorption and were discussed in section 2.3.1 to 2.3.8

2.3.1 Chemical precipitation

The precipitation of metals takes place by the addition of coagulants such as alum, lime, iron salts and other organic polymers. The accumulation of large amounts of sludge containing toxic compounds during the process is the main disadvantage. Precipitation

is used as the treatment method to extract metals ions from solutions by almost 75 percent of plating companies. The most common of these precipitation methods used by industries are carbonate precipitation, sulphide precipitation and sodium hydroxide precipitation (ATSDR, 2017).

2.3.2 Ultra filtration

Ultra filtration is a pressure driven membrane operation which uses porous membranes for removal of heavy metals. The main disadvantage of this process is the production of sludge. Franko *et al.* (2015) reported that at the best operating condition (pH 9.0) using diethyl aminoethyl cellulose, the removal of Cd (II) and Zn (II) more than 95 and 99 %, respectively have been achieved.

2.3.3 Ion-exchange

Ion exchange technologies have been successfully used by metal finishing industries for many decades. During this process, metal ions from dilute solutions are exchanged with ions held by electrostatic forces on the exchange resin. There are a lot of disadvantages, these include, high cost and partial removal of certain ions. For large quantities of competing mono and divalent ion, sodium ion and calcium ion exchange is almost totally ineffective (ATSDR, 2017).

2.3.4 Reverse osmosis

Reverse osmosis is mostly used in desalination of the water (H₂O). However, in the past decades, a particular effort has been made for the application of reverse osmosis in recovery of concentrated solution of metal salts and to clean up water. During this process, heavy metal ions are separated by a semi-permeable membrane at a pressure

greater than osmotic pressure caused by the dissolved solids in the effluent. The only disadvantage of this technique is that it is expensive (ATSDR, 2017).

2.3.5 Electro winning

An electro-winning design consists of components such as rectifier and a reaction chamber containing the electrolyte and electrodes (Li *et al.*, 2018). Metal ions from solutions are reduced on the cathode at a rate that depends on the amount of metal ion in the electrolyte, the current, cathode area and the species of metal being recovered. Although there is no sludge generation the technology has disadvantages such as cost implication, unavailability of steady power supply to mention a few.

2.3.6 Carbon adsorption

The carbon adsorption method removes heavy metals from single phase liquid streams using granular activated carbon as an adsorbent (Li *et al.*, 2018). Activated carbon consists of amorphous form of carbon that has been treated to increase the surface area or volume ratio of the carbon. Granular activated carbon has some disadvantages such as high cost, water soluble component which are not properly absorbed and streams with high suspended solids may result into fouling of the carbon and may require a pretreatment.

2.3.7 Phytoremediation

Phytoremediation is the use of some plants to clean up soil, sediment and water contaminated with metals. Aquatic plants in fresh water, marine and estuarine systems are used as receptacle for several heavy metals. This is because gymnosperms, aquatic macrophytes, bryophytes and tree crops have resistance to metals and have potential to clean up toxic metals in all compartment of atmosphere (Cannon *et al.*, 2016). The

disadvantages of phytoremediation methods are that it takes a long time to remove heavy metals and the regeneration of the plant for further biosorption is difficult.

2.3.8 Adsorption

Adsorption is defined as a separation technique by which the solute is removed from a solution by attachment to the surface of the solid, granular material called “adsorbent”. The solute to be removed is called the “adsorbate”. The attachment of solutes to the solid surfaces takes place by bond formation between adsorbate and adsorbent. Depending on the type of adsorbent – adsorbate bonds formed, there are two forms of adsorption. Basic terms to describe adsorption are shown in Figure 2.2.

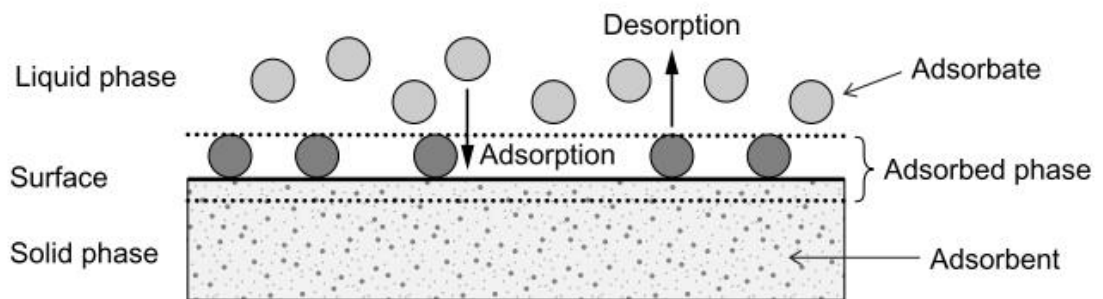


Figure 2.2: Basic Terms of Adsorption (Worch, 2021)

2.3.8.1 Physisorption

Physisorption is the type of adsorption in which the adsorbate (the solute to be adsorbed) is joined to the adsorbent micropores by weak Van der Waal forces (Somorjai, 2014). This makes the physisorption process mostly reversible that is the adsorption bonds are easily formed and broken, due to the low energy of adsorption that characterizes such systems.

2.3.8.2 Chemisorption

Chemisorption is a result of chemical interaction between adsorbate molecules and adsorbent surface. During the chemisorption process, “ionic and covalent bonds are normally formed and a high energy of adsorption is liberated” (Somorjai, 2014). This process is irreversible as the bonds formed are semi-permanent; therefore in order for desorption to occur, the adsorbate undergoes a chemical change. Thermodynamically speaking, when an atom or molecule strikes a surface and forms a bond with it, heat is evolved, as heat of adsorption ΔH_{ads} (Somorjai, 2014). This heat evolved is usually measured as desorption – breaking the bonds.

2.4 History of Nanotechnology

Almost 15 years after Feynman’s lecture, a Japanese scientist, Norio Taniguchi, was the first to use “nanotechnology” to describe semiconductor processes that has been occurring in the order of a nanometer. He mentioned that nanotechnology consisted of the processing, separation, consolidation, and deformation of materials by one atom or one molecule (Du-Bois *et al.*, 1991). The golden era of nanotechnology began in the 1980s when Kroto, Smalley, and Curl discovered fullerenes and Eric Drexler of Massachusetts Institute of Technology (MIT) used ideas from Feynman’s “There is Plenty of Room at the Bottom” and Taniguchi’s term nanotechnology in his 1986 book titled, “Engines of Creation: The Coming Era of Nanotechnology.” Drexler proposed the idea of a nanoscale “assembler”. Drexler’s vision of nanotechnology is also called “molecular nanotechnology.” The science of nanotechnology was advanced further when Iijima, another Japanese scientist, developed carbon nanotubes (Anusha, 2020).

Nanotechnology is basically a manipulation of matter at the molecular and atomic levels to craft a new structure, device and system with superior electronic, optical, magnetic,

conductive and mechanical properties (Khan *et al.*, 2019). Nanotechnology is being explored as a promising technology and has demonstrated remarkable accomplishments in various fields including effluent treatment. Nanostructures offer unparalleled opportunities to make more effective catalysts and redox active media for effluent purification, owing to their small size, large surface area, and ease of functionalization. Nanomaterials have been found to be effective in the elimination of several pollutants from effluent such as heavy metals, organic and inorganic solvents, color as well as biological toxins, and pathogens that cause diseases like cholera and typhoid (Kumar *et al.*, 2014).

2.4.1 Nanotechnology in effluent management

There are various types of nanomaterials reported, which could be used in the effluent treatment such as polymeric nanoparticles (NPs), metal NPs, carbon-based nanomaterials, zeolite, self-assembled monolayer on mesoporous supports (SAMMS), biopolymers and many more (Baruah *et al.*, 2019). Nanotechnology-based pathway which are being employed for effluent remediation are adsorption and biosorption, nanofiltration, photocatalysis, disinfection and pathological control, sensing and monitoring and so on (Jain *et al.*, 2021).

2.4.2 Carbon-based nanoadsorbents

In various fields of science and technology, carbon based materials has been studied for decades. Nanostructures of carbon are known to have different low-dimension allotropes of carbon such as activated carbons, carbon nanotubes (CNTs), and the C₆₀ family of Bulky balls, graphite, and graphene (Nasir *et al.*, 2018). Carbon nanostructures are widely used as nanoadsorbents for effluent treatment owing to their abundant availability, cost-effectiveness, high chemical and thermal stabilities, high

active surface areas, excellent adsorption capacities, and environmental friendly nature (Sayed *et al.*, 2020). For years, activated carbon have been in use as the most common adsorbent due to their high porosity and large surface area. Although, high cost confines their use, therefore different allotropes of carbon and functionalized carbon are being examined as nanoadsorbents (Ray *et al.*, 2020).

2.5 Carbon nanotubes (CNTs)

Carbon nanotubes are hollow graphitic nanomaterials comprising one (single walled carbon nanotubes, SWNTs) or multiple (multi-walled carbon nanotubes, MWNTs) layers of graphene sheets as illustrated in Figure 2.3. The lengths of the nanotubes can range from several hundred nanometers to several micrometers, and the diameters from 0.2 to 2 nm for a SWNT and from 2 to 100 nm for a coaxial MWNT (Chang *et al.*, 2008). CNTs have recently attracted the attention of researchers due to their extraordinary electrical, mechanical, and thermal properties and partial antibacterial activity.



(a) Single-walled Carbon Nanotube (SWCNT) (b) Multiple-walled Carbon Nanotube (MWCNT)

Figure 2.3: Schematic Structure of SWCNT and MWCNT (Eatemadi *et al.*, 2014)

Indeed, functionalization of CNT alters their physico-chemical properties, which encourage their potentiality for several applications as illustrated in Figure 2.4. Typically, the inner pores of CNTs tend to act as selective nano-pores; thereby, the

CNT-filled polymers show an enhanced permeability without a decrease in selectivity, coupled to enhancements in mechanical and thermal properties (Fontananova *et al.*, 2017).

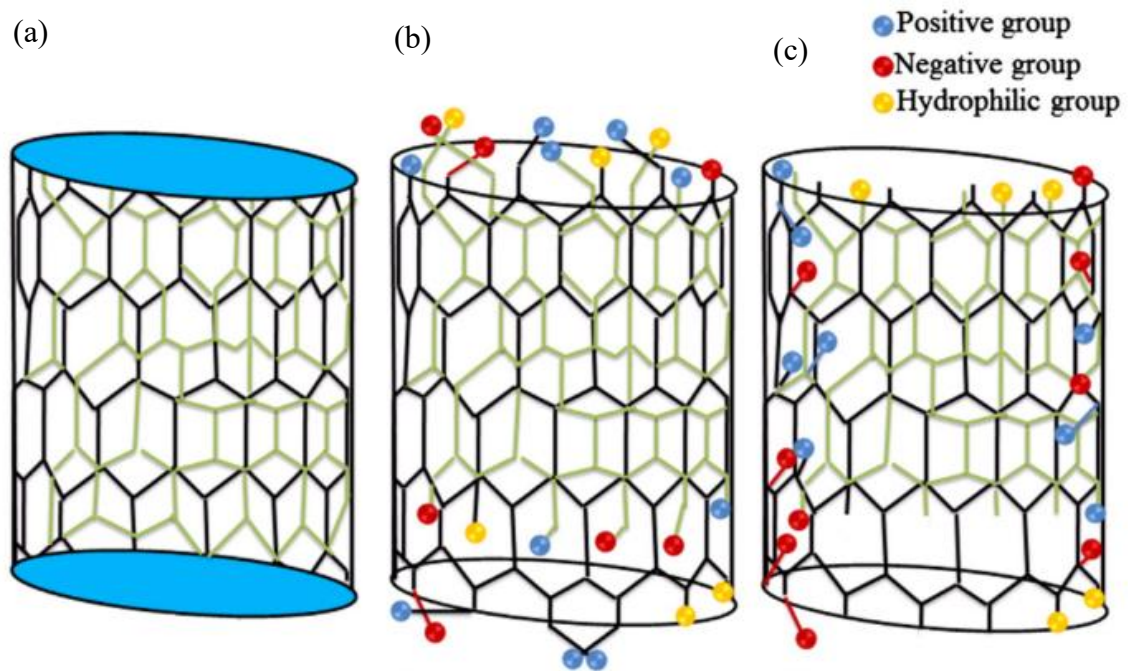


Figure 2.4: Functionalization of CNTs (a) Pristine CNT (b) Tip Modified CNT (c) Core Modified CNT (Das et al., 2014)

For example, Celik *et al.* (2011) enhanced the hydrophilicity of PES membranes blending with CNTs; the generated nanocomposite membranes (at 2 wt %) displayed higher pure water flux and slower fouling rate than the pure PES membranes. Similarly, Daraei *et al.* (2013) enhanced the hydrophilicity of PES membranes by means of incorporating chemically modified multi-walled CNTs, showing higher pure water flux compared to pristine one; basically, the hyper-branched polycitric acid on CNTs offered many functional groups and significantly improved membrane fouling resistance against the proteins. The acid-modified CNTs developed surface functional groups that increased their hydrophilicity, tending to increase the rejection of hydrophobic pollutants. This was reported by Kim *et al.* (2013) during the incorporation of such filler

in polyamide (PA) thin-film composite membranes. On the other hand, a thin-film layer enhanced the pure water permeability of the n-TFN membrane by 23%, compared to the one unfilled layer. In addition, the membranes indicated greater anti-adhesive and antibacterial properties (using *Pseudomonas aeruginosa*). In the same way, coated nitrocellulose membranes with a nanocomposite containing 3 wt % of single-walled CNTs exhibited significant antimicrobial activity (80–90%) toward Gram-positive and Gram-negative bacteria as well as virus removal (Ahmed *et al.*, 2013). Moreover, these nanocomposite polymeric membranes are potential candidates for water purification because they did not present any toxicity against fibroblast cells, so they could be used as membrane filter for drinking water treatment.

The preparation of amino-functionalized-multi-walled CNTs-PSF composite membranes was carried by Shah and Murthy (2013); such membranes were tested for heavy metal removal displaying maximum removals of about 94.2% and 78.2% for Cr(VI) and Cd(II), respectively, which was just 10.2% and 9.9%, respectively, with pristine PSF membranes. In the case of these composite membranes, the percentage rejection of heavy metal was found to increase with increase in loading of MWNTs. On the other hand, thin-film nanocomposite membranes embedded with poly (methyl methacrylate) (PMMA) hydrophobic modified multi-walled CNTs by interfacial polymerization were prepared by Shen *et al.* (2013). These membranes presented high Na₂SO₄ rejection (99%), and the water permeate flux was enhanced about 62% compared to the pristine thin-film composite membrane.

2.5.1 Synthesis of carbon nanotubes

There are several techniques that have been developed for fabricating CNT structures which mainly involve gas phase processes. Commonly, three procedures are being used

for producing CNTs: (1) the chemical vapor deposition (CVD) technique (Abbasi *et al.*, 2014), (2) the laser-ablation technique (Ajayan and Ebbesen, 1997), and (3) the carbon arc-discharge technique (Hirlekar *et al.*, 2009) as shown in Table 2.1

High temperature preparation techniques for instance laser ablation or arc discharge were first used to synthesize CNTs, but currently, these techniques have been substituted by low temperature chemical vapor deposition (CVD) methods (Ganesh, 2013).

(i) Electric arc discharge

Arc-discharge technique uses higher temperatures (above 1,700°C) for CNT synthesis which typically causes the expansion of CNTs with fewer structural defects in comparison with other methods. The most utilized methods use arc discharge between high-purity graphite (6 to 10-mm optical density (OD)) electrodes usually water-cooled electrodes with diameters between 6 and 12 mm and separated by 1 to 2 mm in a chamber filled with helium (500 torr) at sub-atmospheric pressure (helium can be replaced by hydrogen or methane atmosphere) (Grobert *et al.*, 2007). The chamber contains a graphite cathode and anode as well as evaporated carbon molecules and some amount of metal catalyst particles (such as cobalt, nickel, and/or iron). Direct current is passed through the chamber (arcing process), and the chamber is pressurized and heated to approximately 4,000 K. In the course of this procedure and arcing, about half of the evaporated carbon solidifies on the cathode (negative electrode) tip, and a deposit forms at a rate of 1 mm/min which is called ‘cylindrical hard deposit or cigar-like structure’, whereas the anode (positive electrode) is consumed (Eatemadi *et al.*, 20014).

(ii) Laser ablation method

With influence of high-power laser vaporization (YAG type), a quartz tube containing a block of pure graphite is heated inside a furnace at 1,200 °C, in an Ar atmosphere (Abbasi *et al.*, 2014). The aim of using laser is to vaporize the graphite within the quartz tube. As described about the synthesis of SWNT using arc-discharge method the technique involve addition of metal particles as catalysts to the graphite. Studies have shown that the diameter of the nanotubes depends upon the laser power. When the laser pulse power is increased, the diameter of the tubes became thinner (Thess *et al.*, 1996).

(iii) Chemical vapor deposition

One of standard methods for production of carbon nanotubes is chemical vapor deposition method (CVD). There are many different types of CVD such as catalytic chemical vapor deposition (CCVD) these can be either thermal (Van der Wal *et al.*, 2003) or plasma enhanced (PE), oxygen assisted CVD (Lijima, 1991), water assisted CVD (Journet *et al.*, 1997; He *et al.*, 2010), microwave plasma (MPECVD) (Ebbesen *et al.*, 1992), radiofrequency CVD (RF-CVD) (Bernholc *et al.*, 1997)), or hot-filament (HFCVD) (Dervishi *et al.*, 2009). However, catalytic chemical vapor deposition (CCVD) is currently the standard technique for the synthesis of carbon nanotubes. This technique allows CNTs to expand on different of materials and involves the chemical breakdown of a hydrocarbon on a substrate. The main process of growing carbon nanotubes in this method is same as arc discharge method and also its exciting carbon atoms that are in contact with metallic catalyst particles. A hydrocarbon such as acetylene is heated and decomposed onto the substrate. Since the carbon is able to make contact with the metal particles implanted in the holes, it initiates to create nanotubes which are a ‘template’ from the shape of the tunnel. With the aforementioned properties, the carbon nanotubes can grow very well aligned and very long, in the angle of the tunnel. In CVD processing,

commonly used metal catalyst particles are nickel, cobalt, iron, or a combination (Landi *et al.*, 2005).

Table 2.1: Summary and Comparison of the Three Common Methods Employed in the Synthesis of CNT

Method	Arc discharge	Laser ablation	CVD
Yield rate	>75%	>75%	>75%
SWT and MWNT	Both	Both	Both
Advantages	Simple, inexpensive high quality nanotubes	Relatively high quality, room temperature synthesis	Simple, low temperature, high purity, large-scale aligned growth
Disadvantages	High temperature, purification required, tangled nanotubes	Method limited to laboratory scale, crude product; purification required	Synthesized CNT are MWNTs, morphological defects

(Eatemadi *et al.*, 2014)

2.6 Metal Nanoparticles for effluent remediation

Metallic nanoparticles have two key properties that make them particularly attractive as sorbents. On a mass basis, they have much larger surface areas than bulk particles. Metal nanoparticles can also be functionalized with various chemical groups to increase their affinity towards target compounds. It has been found that the unique properties of nanoparticles are absorption on high capacity and selective sorbents for metal ions and anions. Characterization of the interactions of the nanoparticles with the bacteria by atomic force microscopy (AFM), Transmission Electron Microscopy (TEM) and laser confocal microscopy showed considerable changes in the integrity of the cell membranes, resulting in the death of the bacteria in most cases (Dhermendra *et al.*,

2008). Photocatalytic nanomaterials allow ultraviolet light also used to destroy pesticides, industrial solvents and germs.

2.6.1 Silver nanoparticles

Silver (Ag)-based compounds include Ag NPs, stabilized Ag salts, polymer and metal oxide composites, silver dendrimer, Ag-impregnated zeolite and activated carbon materials. Generally, these materials based on Ag tend to offer antimicrobial properties that give them potential for several applications including water treatment and disinfection of medical devices. Indeed, there are some reports of silver nanoparticles incorporated into polyethylene (PE) for medical applications, and, recently, Zapata *et al.* (2016) reported the preparation of silver nanofibers in PE. In fact, silver nanoparticles are among the most often used nanoparticles for antimicrobial applications and the health and environmental consequences when silver is released from polymeric membrane must be investigated. There are some reports about the incorporation of Ag NPs into polyethylene (PE) for medical applications, for instance, Ag NPs are among the most often used NPs for antimicrobial applications.

In general, nano-Ag, ranging from 1 to 100 nm, can be synthesized for various approaches using different precursors, reducing and capping agents (Chaloupka *et al.*, 2018). The antibacterial activity of Ag NPs has been recently discussed by López-Heras *et al.* (2015). Their activity generally depends on several physicochemical properties of the particles, including their size, shape, and chemistry. Typically, Ag-NPs reduce the activity of bacteria due to a synergistic effect between direct particle-specific biological effects and the release of Ag⁺ ions. Furthermore, Ag NPs can stick to the bacterial cell which influences negatively the permeability and respiration of the bacteria, but particles affect the cell membrane resulting in cell lysis. In this way, the Ag particles

can go through the bacterial cytoplasm, causing damage to the DNA (Wei *et al.*, 2015; Koseoglu-Imer and Koyuncu, 2017). The preparation of nanocomposites membranes using Ag has been reported by several authors (Sile-Yuksel *et al.*, 2014; López-Heras *et al.*, 2015; Chaloupka *et al.*, 2018), being cellulose acetate (CA), chitosan, polyacrylonitrile (PAN) and polysulfone (PSF) the most popular polymeric materials used for the preparation of Ag nanocomposite membranes. Sile-Yuksel *et al.* (2014) studied the effect Ag-NPs location in polymer types. Three different polymers, PES, PSF and CA, were used to fabricate nanocomposite membranes at three Ag-NPs different ratios (0.03, 0.06 and 0.09 w/w). The authors reported that Ag-NPs are homogeneously located along the membrane matrix both skin layer and sublayer but they protruded from the top surfaces of PSF and PES membranes. On the other hand, the increase of Ag-NP/polymer ratio tended to increase water permeability in PSF ($200 > 215 > 225 > 235 \text{ L/m}^2 \text{ h bar}$) while it decreased using PES and CA polymers, such as, $360 < 325 < 250 < 220$ and $80 < 67 < 46 < 40 \text{ L/m}^2 \text{ h bar}$ for PES and CA, respectively.

2.6.2 Synthesis of silver nanoparticles

Various authors have reported several methods from common precursors. Generally, nanoparticles are prepared by a variety of chemical and physical methods which are quite expensive and potentially hazardous to the environment which involve use of toxic and hazardous chemicals that are responsible for various biological risks (Vijay *et al.*, 2014). The development of biologically-inspired experimental processes for the syntheses of nanoparticles is evolving into an important branch of nanotechnology. Generally, there are two approaches which are involved in the syntheses of silver nanoparticles, either from “top to bottom” approach or a “bottom to up” approach as illustrated in Figure 2.5.

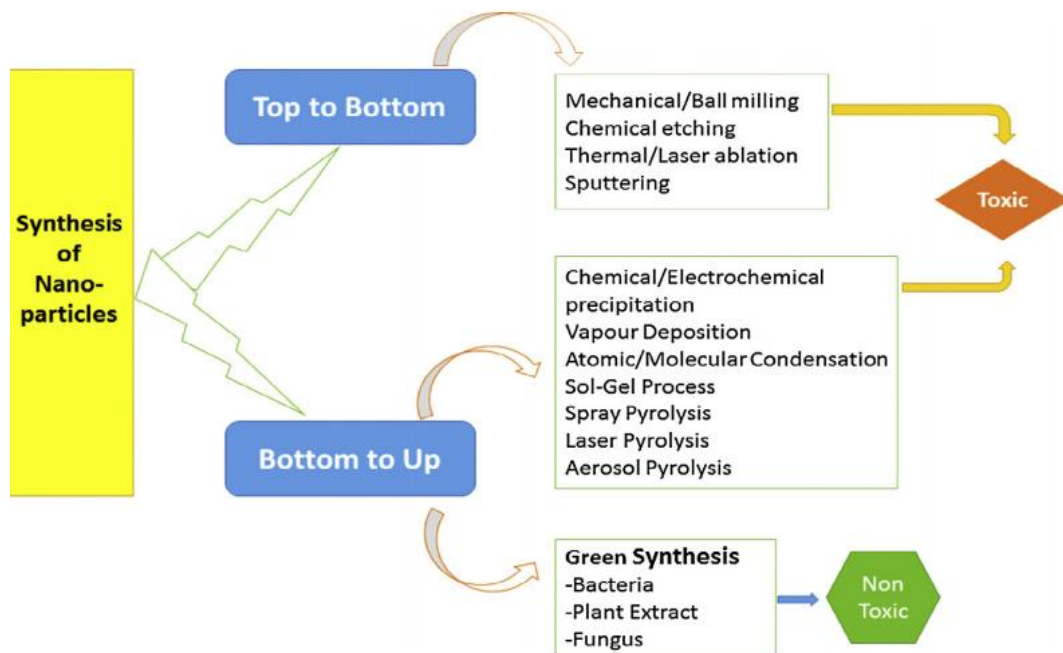


Figure 2.5: Different Approaches for the Synthesis of Silver Nanoparticles

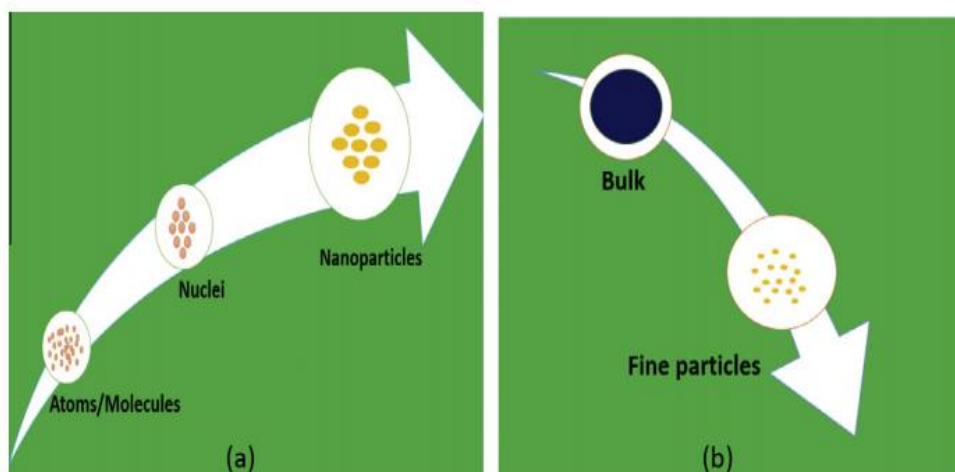


Figure 2.6: Protocols Employed for the Synthesis of Nanoparticles (a) Bottom to Top Approach and (b) Top to Bottom Approach (Ahmed *et al.*, 2016)

In bottom to top approach, nanoparticles can be synthesized using chemical and biological methods by self-assembly of atoms to new nuclei which grow into a particle of nanoscale as shown in Figure 2.5. While in top to bottom approach, suitable bulk materials are broken down into fine particles by size reduction with various lithographic techniques e.g. grinding, milling, sputtering and thermal/laser ablation as shown in

Figures 2.5 and 2.6. In bottom to top approach, chemical reduction is the most common scheme for syntheses of silver nanoparticles (Hurst *et al.*, 2006). Different organic and inorganic reducing agents, such as sodium borohydride (NaBH_4), sodium citrate, ascorbate, elemental hydrogen, Tollen's reagent, N, N-dimethyl formamide (DMF) and poly (ethylene glycol) block copolymers are used for reduction of silver ions (Ag^+) in aqueous or non-aqueous solutions (Tran *et al.*, 2013; Iravani *et al.*, 2014). Capping agents are also used for size stabilization of the nanoparticles. One of the biggest advantages of this method is that a large quantity of nanoparticles can be synthesized in a short span of time. During this type of syntheses; chemicals used are toxic and led to non-ecofriendly by-products. This may be the reason which leads to the bio-syntheses of nanoparticles via green route that does not employ toxic chemicals and hence proving to become a growing wanton want to develop environment friendly processes.

In case of top to bottom approach, nanoparticles are generally synthesized by evaporation–condensation using a tube furnace at atmospheric pressure. In this method the foundation material; within a boat; place centered at the furnace is vaporized into a carrier gas. Ag, Au, PbS and fullerene nanoparticles have previously been produced using the evaporation/condensation technique. The generation of silver nanoparticles using a tube furnace has numerous drawbacks as it occupies a large space and munches a great deal of energy while raising the environmental temperature around the source material, and it also entails a lot of time to succeed thermal stability (Samberg *et al.*, 2010; Prathna *et al.*, 2011; Vijay *et al.*, 2014). In addition, a typical tube furnace requires power up to several kilowatts and a pre-heating time of several tens of minutes to attain a stable operating temperature. One of the biggest limitations in this method is the imperfections in the surface structure of the product and the other physical

properties of nanoparticles are highly dependent on the surface structure in reference to surface chemistry.

2.6.3 Green synthesis of silver nanoparticles

The advancement of green syntheses of nanoparticles is progressing as a key branch of nanotechnology; where the use of biological entities like microorganisms, plant extract or plant biomass for the production of nanoparticles could be an alternative mass to chemical and physical methods in an ecofriendly manner (Reddy *et al.*, 2012). The advancement of green syntheses over chemical and physical methods is: environment friendly, cost effective and easily scaled up for large scale syntheses of nanoparticles, Furthermore there is no need to use high temperature, pressure, energy and toxic chemicals (Dhuper *et al.*, 2012). A lot of literature has been reported on biological syntheses of silver nanoparticles using microorganisms including bacteria, fungi and plants; Their antioxidant or reducing properties is typically responsible for the reduction of metal compounds to their respective nanoparticles. Among the various biological methods of silver nanoparticle synthesis, microbe mediated synthesis is not of industrial feasibility due to the requirements of highly aseptic conditions and their maintenance. Therefore, the use of plant extracts for this purpose is potentially advantageous over microorganisms due to the ease of improvement, the less biohazard and elaborate process of maintaining cell cultures (Kalishwaralal *et al.*, 2010). It is the best platform for syntheses of nanoparticles; being free from toxic chemicals as well as providing natural capping agents for the stabilization of silver nanoparticles.

2.6.3 Green synthesis of silver nanoparticles using plant extract

The use of plants as the production assembly of silver nanoparticles has drawn attention, because of its rapid, ecofriendly, non-pathogenic, economical protocol and providing a single step technique for the biosynthetic processes as shown in Figure 2.7.

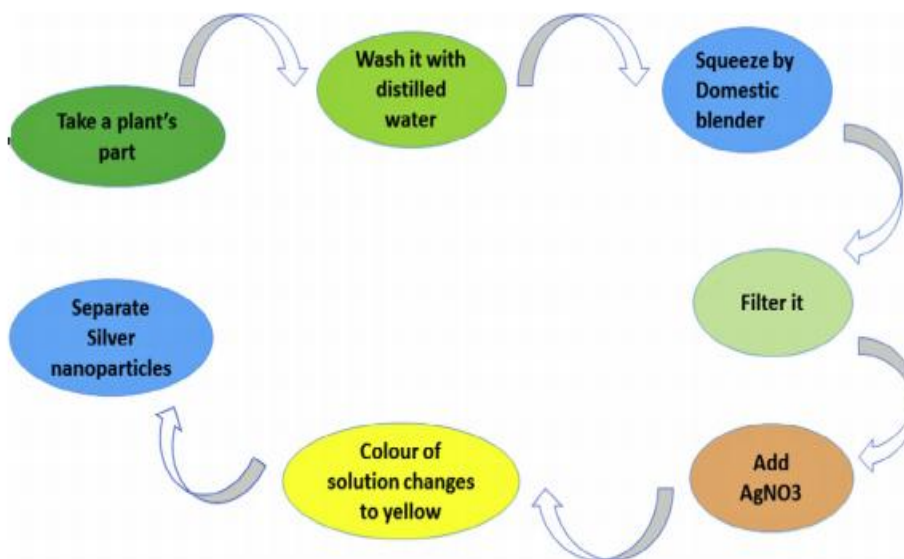


Figure 2.7: Protocol for the Synthesis of Silver Nanoparticles Using Plant Extract

The reduction and stabilization of silver ions by combination of biomolecules such as proteins, amino acids, enzymes, polysaccharides, alkaloids, tannins, phenolics, saponins, terpinoids and vitamins which are already established (Kulkarni and Muddapur, 2014). The protocol for the nanoparticle syntheses involves: the collection of the part of plant of interest from the available sites and then it was washed thoroughly twice/thrice with tap water to remove both epiphytes and necrotic plants; followed with sterile distilled water to remove associated debris. These; clean and fresh sources are shade-dried for 10–15 days and then powdered using domestic blender. For the plant broth preparation, around 10 g of the dried powder is boiled with 100 cm³ of deionized distilled water (hot percolation method). The resulting infusion is then filtered thoroughly until no insoluble

material appeared in the broth and appropriate amount of this plant extract is added to known concentration AgNO_3 solution, the reduction of pure Ag^+ ions to Ag^0 which can be monitored by measuring the UV–visible spectra of the solution at regular intervals (Sahayaraj & Rajesh, 2011).

2.7 Alternative Source of Biodegradable Polymers for Environmental Remediation

Current major threats to society are the aggregation of non-biodegradable polymers and overutilization of fossil resources (Deng *et al.*, 2016). Fossil resources are being utilized for energy and polymer production for many decades. This is one of the reasons for depleting fossil resources. The global concern has always been the rising environmental pollution, due to improper recycling techniques and non-biodegradability of petroleum-based polymers. Among the above-cited causes, non-biodegradable nature of polymers is the primary reason, for the alarming threat to the environment. Proper use of natural polymers can be the remedy for this red alert environmental problem. Thus, there is a growing interest among researchers, to develop biodegradable materials such as cellulose, chitin, chitosan to mention a few for substitution of petroleum-based polymers (Shaikh *et al.*, 2009)

2.7.1 Cellulose and cellulose nanocrystals (CNCs)

All plant materials are rich in cellulose and thus provides the incomparable renewable natural resource. Cellulose is the natural biopolymer, having a microfibril structure of both amorphous and crystalline regions. Cellulose has a wider range of applications compared to other natural polysaccharides such as starch and proteins.

Cellulose is an extensive crystalline homo-polymer of anhydroglucopyranose units (AGU) via β -1,4-glycosidic linkage and intra- and inter-molecular hydrogen bonds (Saelo *et al.*, 2016; Dai and Huang 2017a, b; Nepomuceno *et al.*, 2017). As one of the

most abundant natural polymers on the earth (a yearly production of about 1.5 × 10¹² tons). Cellulose has received increasing research interest owing to its environmental friendly advantages and attractive features, such as nontoxicity, biological biodegradation, biocompatibility, excellent thermal and mechanical properties, renewability and easy modification (Dai & Huang 2016, 2017a, b; Khawas & Deka 2016; Zhang *et al.*, 2017). Many researchers have worked on conversion of complex cellulose molecules, to simple cellulose nanofibers or cellulose nanocrystals (Kedzior *et al.*, 2017; Liu *et al.*, 2017). Agricultural wastes such as plantain and pineapple peels wastes are made of lignocellulosic materials, which is a composite of cellulose and lignin adhered by the hemicellulose (Huang *et al.*, 2017). Chemical treatment methods have been examined to be successful in the production of cellulose nanofibers & Cellulose nanocrystal from agro-wastes. These chemical treatment methods involve alkali treatment for removal of impurities and acid hydrolysis for disruption of amorphous regions in cellulose fibers.

Cellulose nanocrystals CNCs are needle-shaped nanometric or rod-like particles with at least one dimension equal to or less than 100 nm (Flauzino *et al.*, 2013). CNCs have been reported in the literature as whiskers, nanofibers, nanocelluloses, cellulose crystallites or crystals, and the interest of many researchers. This is due to their attractive characteristics, such as, biocompatibility, biodegradability, light weight, non-toxicity, stiffness, renewability, sustainability, optical transparency, low thermal expansion, gas impermeability, adaptable surface chemistry, and improved mechanical properties (Lagerwall *et al.*, 2014; Trache *et al.*, 2017). Therefore, CNCs potentially have application in nanocomposites, papers, coating additives, electrolytes, foams, aerogels, food packaging, and gas barriers (Sharmin *et al.*, 2012; Brinchi *et al.*, 2013; Hu *et al.*, 2013; Abdul-Khalil *et al.*, 2014;).

2.7.2 Plantain

Many agricultural wastes have been utilized as adsorbents among which, plantain waste has been of significant importance because it has various parts that can be utilized such as plantain fruit peels, trunks, pseudo-stems, leaves, and piths (Mohapatra *et al.*, 2010). These parts of plantain wastes have been extensively studied as an adsorbent against a wide range of pollutants. Plantain wastes have attracted researcher's attention as an effective raw material for adsorbents owing to abundantly available, post fruit harvesting no proper utilization of the plantain waste by the farmers, and a significant amount of carbon compounds present in it (Ahmad and Danish, 2018). Moreover, plantain tree waste can cause serious environmental threat if its waste not properly managed, it can produce greenhouse gas if dumped in wet conditions. Usually, farmers threw the plantain tree waste in rivers and ponds where it degraded slowly and formed methane, and other gases spread putrescible smell and affect the nearby ecosystem.

Plantain as presented in Figure 2.8 (a) is one of the fruit crops, majorly cultivated all over the world, its scientific classification is presented in Table 2.2. Every part of the plantain is useful, and they are rich in cellulose (Tibolla *et al.*, 2014). The process of plantain cultivation and industrialization produces a considerable amount of cellulose-rich residues, and the use of this biomass could help reduce environmental pollution and add value to the cellulose byproduct. In this sense, research involving this fruit and seeking sustainable development has been encouraged to use plantain peel as a potential source of cellulosic fiber, a material that is essential to produce paper and clothing and which has recently found applications in the production of nanomaterials (Elanthikkal *et al.*, 2010).

Table 2.2: Scientific Classification of Plantain

Category	Group
Kingdom	Plantae
Clade	Angiosperm
Clade	Monocot
Clade	Commelinids
Order	Zingiberales
Family	Musaceae
Genus	Musa
Specie	Paradisiaca

Plantain processing industries release tons of plantain trunk flower bracts, and saps as waste materials as presented in Figure 2.8. These waste materials can serve as a potential source of cellulose nanofibers (Tibolla *et al.*, 2014; Tibolla *et al.*, 2018). After harvesting the fruit of plantain, the matured pseudo-stems are generally disposed at a landfill or left to decompose slowly in a plantation field.

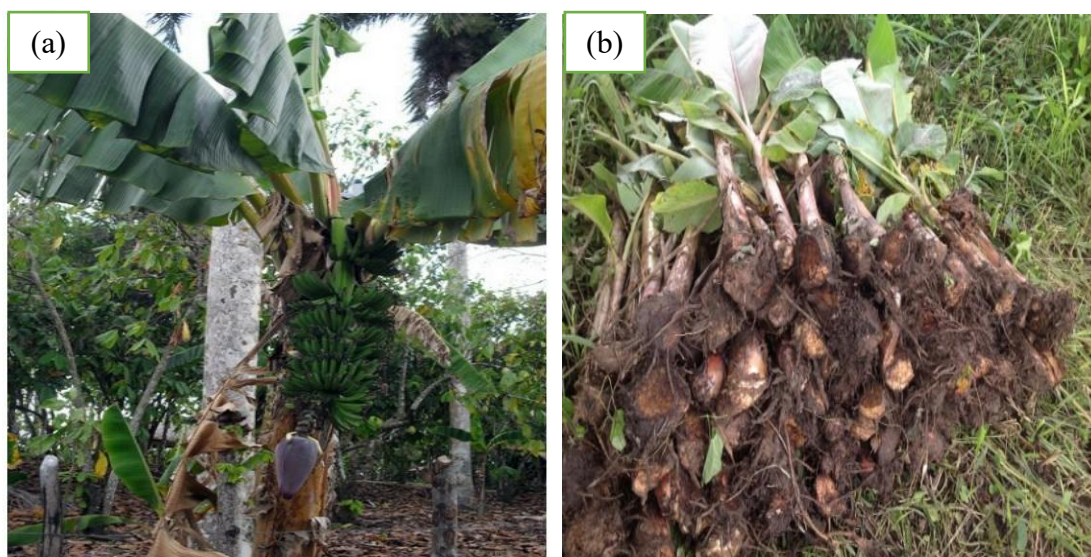


Figure 2.8: (a) Plantain plant (b) Plantain Trunk

The pseudo-stem of the plantain produces a single bunch of plantain fruit before drying and replaced by new pseudo-stem. The pseudo-stems are the stem of the plantain tree that supplies nutrients from the soil to the fruits; it becomes waste after the plantain fruit is harvested. It is estimated that each hectare of plantain plantation produces nearly 220 tons of biomass waste (Ahmad & Danish, 2018). These plantain wastes are disposed of by the cultivators into the rivers, lakes, or dump in low-lying areas; it is causing a serious threat to biosphere due to the release of greenhouse gas (Shah *et al.*, 2005). Worldwide environmental science and engineering researchers engaged in experimenting to utilize such biomass materials to convert it into useful materials to prevent environmental toxicant generated due to it, and at the same time providing affordable waste disposal techniques.

Table 2.3: Chemical Composition of Plantain Pseudo-stem (Based on Different Literatures).

Sample	Cellulose (%)	H M (%)	Lignin (%)	Extractives (%)	A C (%)	M C (%)	References
1	63.20	18.60	5.10	1.40	1.02	10.00	Li <i>et al.</i> (2015)

2	31.27	14.98	15.07	4.46	8.65	9.74	Khalil <i>et al.</i> (2007)
3	63.9	1.30	18.30	10.6	1.50	-----	Patil <i>et al.</i> (2012)
4	31.26	14.98	15.07	4.45	8.64	9.74	Bilba <i>et al.</i> (2007)
5	57	10.33	15.55	-----	-----	20.23	Basak <i>et al.</i> (2015)
Average	49.33	12.04	13.88	5.23	4.95	12.43	

Key:

H M: Hemicellulose

A C: Ash Content

M C: Moisture Content

Therefore, it is rational that commercially feasible option to this issue should include the utilization of plantain waste in new products formation for environmental remediation rather than disposal. Compared to other biomass wastes used as an adsorbent, plantain wastes have been of great importance, because various parts of the plantain tree have been extensively studied as an adsorbent against cationic, anionic, and neutral pollutants.

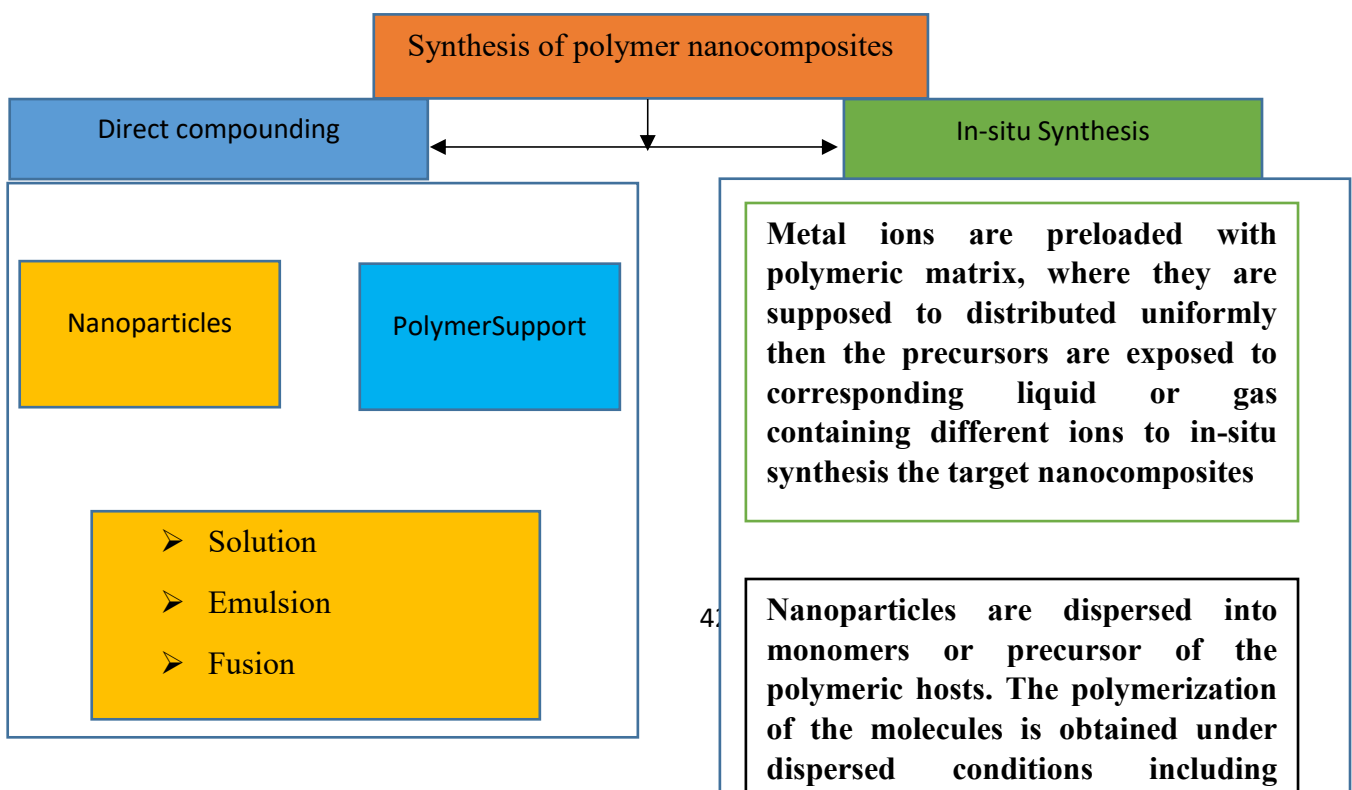
The chemical composition of constituents of plantain pseudo-stem based on different literatures are presented in Table 2.3. As shown in the table, the plantain pseudo-stem mostly consists of cellulose. Cellulose fiber can be considered as the most available natural, biodegradable, and renewable polymer that can be used in many applications (reinforcing materials, textiles, polymer matrix, and raw materials for paper) (Mukhopadhyay *et al.*, 2008).

Plantain tree wastes and pseudo-stem have gained wide interest of researcher due to abundantly available and significant adsorption capacity against water-soluble pollutants. However, it is well-known that raw/unmodified agro wastes suffer from at least two major drawbacks: Low adsorption capacity or selectivity, and poor physical

stability which can be enhanced by either through physical and/or chemical modifications of the raw adsorbents (Ibrahim *et al.*, 2010). The chemical modifications of agro wastes by various functional groups can be easily conducted due to high content of hydroxyl groups on their surfaces (Fu & Wang, 2010). Consequently, more active binding sites are provided, better ion-exchange properties are obtained, and new functional groups are formed. These modifications may include the use of different types of nanomaterials such as CNTs and silver nanoparticles to modify the plantain tress wastes to obtain biodegradable and recyclable nanomaterials for the removal of various toxic pollutant from industrial effluent.

2.8 Nanocomposites

Two or more chemically distinct materials (matrix and filler/reinforcing material), when mixed, have improved properties over the individual materials and are called composites. The reinforcing phase is in the form of fibers, sheets, or particles. A composite material where one of the phases has one, two, or three dimensions of less than 100 nm or has structures having nanoscale repeat distances between the different phases that make up the material is called a nanocomposite (Schadler, 2003).



Nanoparticles and polymers could be prepared simultaneously by blending the precursor of the polymer with an initiator in a proper solvent

Figure 2.9: Synthesis of Polymer-based Nanocomposites (Singh and Susan, 2018)

They possess unique physical, chemical, optical, mechanical, magnetic, and electric properties and have attracted much attention for a wide range of applications including water remediation. Nanocomposites are basically of two types: (i) non-polymer based nanocomposites and (ii) polymer-based nanocomposites (Singh and Agarwal, 2016). Polymer-based nanocomposites are synthesized via methods presented in Figure 2.9 (Fawaz and Mittal, 2015).

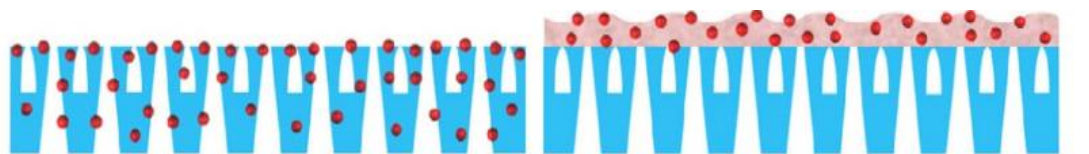
Based on the method and materials used, three types of microstructure can be obtained: unintercalated (or microcomposite), intercalated (and/or flocculated), or exfoliated (or delaminated) (Ray *et al.*, 2003).

2.8.1 Polymer membranes

Less energy requirement and easy availability of membrane materials make them to be more in demand. Polymeric membrane is currently the most widely used membrane for water treatment, but it is restricted by several challenges such as trade-off relationship between permeability and selectivity and low resistance to fouling (Singh and Susan, 2018). Nanocomposite membranes, a new class of membranes fabricated by combining polymeric materials with nanomaterials, are emerging as a promising solution of these

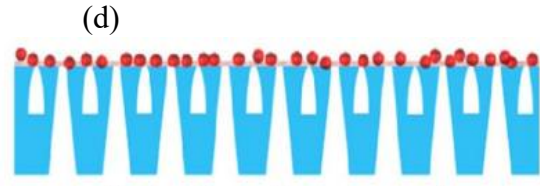
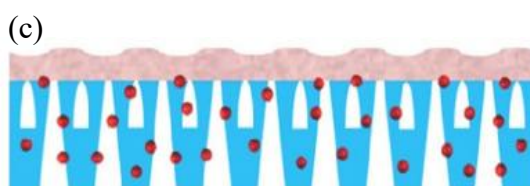
challenges. Engineered nanomaterials have the potential for the creation of membranes that are optimized to meet *all* the challenges of desalination and effluent treatment including fouling and biofouling while extending the lifetime of the membrane by enhancing their mechanical robustness and resistance to cleaning regimes (Ray *et al.*, 2003). The advanced nanocomposite membranes could be designed to meet specific water treatment applications by tuning their structure and physicochemical properties and introducing unique functionalities. There are following four types of nanocomposite membranes (Yin *et al.*, 2015): (1) conventional nanocomposite, (2) thin-film nanocomposite (TFN), (3) thin-film composite (TFC) with nanocomposite substrate, and (4) surface-located nanocomposite. The typical structures of these membranes are presented in Figure. 2.10.

The red spheres in the figure not only stand for NPs but also represent nanotubes, nanofibers, or nanosheets. The incorporation of nanomaterials provides membranes with specific properties of nanomaterials and also possibly induces new characteristics and functions based on their synergetic effects.



(a) Conventional Nanocomposites

(b) Thin-film Nanocomposites



(c) TFC with Surface Loaded Nanocomposites (d) Surface Located

Nanocomposites

Figure 2.10: Typical Types of Nanocomposite Membranes (Singh and Susan, 2018)

2.9 Characterization of the As-Synthesized Nanomaterials

Characteristic properties of the produced activated carbon such as, mineralogical phases, morphology and microstructure were examined using X-ray Diffraction (XRD) and High Resolution Scanning Electron Spectroscopy (HRSEM), High Resolution Transmission Electron Spectroscopy (HRTEM) respectively.

2.9.1 X –ray diffraction

X-ray diffraction is one of the oldest and most frequently used techniques to characterise nano-materials. It is used for the identification of bulk crystalline phases of catalysts by means of lattice structural parameter to monitor the kinetics of bulk transformations, and to obtain information on the particle sizes (Kariim *et al.*, 2016). XRD can also be used to study structural and morphological features of the as-synthesized and treated CNTs samples. From the X-ray diffractograms, one can infer whether the purification processes were effective by monitoring the carbon support as well as metal catalyst particles used (Mohamed and Robert, 2012).

2.9.2 High Resolution Transmission Electron Microscopy (HRTEM) and High Resolution Scanning Electron Microscopy (HRSEM)

High Resolution Transmission electron microscopy (HRTEM) and High Resolution scanning electron microscopy (HRSEM) are very useful tools for characterizing substances at the nanometer level. Both are used to determine the sizes and shapes of nano-materials. The main difference between HRSEM and HRTEM is that HRSEM sees contrast due to topology and composition of a surface (for instance: length, diameter, uniformity and density) whereas the electron beam in HRTEM projects all

information on the mass it encounters in a two dimensional image (such as wall structure and crystallinity) as well as length and diameter. TEM is particularly important in showing the inner cavity of the CNTs and thus distinguishes tubes from fibers (Hintsho *et al.*, 2015). High resolution Transmission electron microscopy (HRTEM) is particularly important in evaluating the quality of CNTs as this technique can view samples at higher magnifications. HRSEM technique can be coupled with an energy dispersive X-ray (EDX) spectrometer which allows for the determination of the elemental compositions of the materials (Khorrami & lofi, 2013).

2.10 Adsorption Models in Batch Tests

The Langmuir and Freundlich Isotherms as in Equations 2.1 and 2.2 are the most commonly used isotherms to describe sorption equilibrium for environmental studies (Erdem *et al.*, 2014; Kocaoba *et al.*, 2014; Oren & Kaya, 2016). The following expressions for a straight line were used, which are obtained by a mathematical transformation of isotherms:

Freundlich isotherm, linear equation

$$\text{Log}_{q_e} = \text{Log}_{K_f} + \frac{1}{n} \text{Log}_{c_e} \quad (2.1)$$

where K_f is a Freundlich constant which gives the adsorption capacity q_e and n is the heterogeneity factor. In situation where n is less than 1, the adsorption process is favourable. This isotherm gives the detail of equilibrium on heterogeneous surfaces (Gunay *et al.*, 2017). That is the energy of adsorption is not equivalent for all adsorption sites, which is a more realistic assumption than the Langmuir isotherm.

Langmuir isotherm, linear equation

$$C_e/q_e = 1/K_l Q_m + C_e/Q_m \quad (2.2)$$

where C_e is the equilibrium concentration of metal ion in solution in mg/g, Q_e is the adsorption capacity in mg/g of the metal ion adsorbed per gram of the adsorbent, Q_m is the maximum metal uptake and B is the Langmuir constant related to the affinity between the sorbent and the sorbate. This model assumes that every adsorption sites are energetically identical and have equal energies of adsorption (i.e. adsorption is a monolayer) (Gunay *et al.*, 2017). The empirical constants K_l and q_m for the Langmuir model are related to the heat of adsorption maximum (L/g) and bonding strength (L/mg) respectively (Yu *et al.*, 2013; Oren and Kaya, 2016), whereas, K_f (mg/g) and n (g/l) are the constants for the Freundlich model and are related to the adsorption capacity and intensity of adsorption (Yu *et al.*, 2013). Most industrial adsorption processes are carried out in column systems. Therefore, a laboratory batch adsorption test at equilibrium does not give sufficient data for the design of a clinoptilolite adsorption system. Batch adsorption kinetic studies give concentration decay curves in terms of C_t versus t . Where C_t is the concentration of the adsorbed metal at time t , and time t is the time taken for the adsorption. Column tests are required for design, with the kinetic adsorption information generated experimentally on a laboratory scale or pilot plant scale or theoretically by mathematical modeling. This is one advantage column systems have over the batch system approach.

2.11 Factors Affecting the Adsorption Capacity of Effluent

The efficiency of adsorption process is strongly influenced by the physicochemical characteristics of the solutions, such as contact time, pH, temperature, initial concentration and sorbent dosage (Arief *et al.*, 2008). These factors are important in evaluating the maximal sorption performance of any sorbent.

2.11.1 Effect of contact time

Generally, waste removal rate increase with an increase in contact time to a certain level. Due to deposition of the waste molecules on the available adsorption site on adsorbent material, any further increase in contact time will lead to desorption (Bharathi & Rameshsrikrishna, 2012). At this point, the amount of waste molecule desorbing from the adsorbent is in a state of dynamic equilibrium with the amount been adsorbed onto the adsorbent. The time required to attain this state of equilibrium is termed the equilibrium time and the amount of waste material adsorbed at the equilibrium time reflects the maximum adsorption capacity of the adsorbent under those operating conditions (Salleh *et al.*, 2011).

2.11.2 pH

The pH of the effluent solution has a significant impact on the uptake of metal ions, which are a major portion of the effluent discharged from a battery production plant. This is so because the pH determines the surface charge of the adsorbent, and also the degree of ionization and speciation of metal ions such as Pb^{+2} in the effluent (Boudrahem *et al.*, 2009). The average pH values at the settling tank at the final discharge point indicate that the effluent are highly acidic due to the H_2SO_4 an important raw material in the production of batteries (Akinlua & Asubiojo, 2006). However, studies by Singh *et al.* (2014) suggested that the removal of Pb^{+2} from battery effluent using agricultural waste was favoured at a $\text{pH} < 6$ therefore promoting effective removal in an acidic medium.

2.11.3 Temperature

Temperature is an important factor that serves as an indicator as to whether the adsorption is an exothermic or endothermic process. If the adsorption is an endothermic

process, the adsorption capacity of the adsorbent will increase with increasing temperature. This may possibly due to the increase in the number of active sites and the mobility of the dye molecules at higher temperature (Senthilkumaar *et al.*, 2006). In contrast, if the adsorption is an exothermic process, the adsorption capacity will decrease with increasing temperature. In this case, higher temperature may decrease the adsorptive forces between the dye molecules and the active sites on the adsorbent surface (Ofomaja & Ho, 2007). Generally, it is thought that dyes molecules diffuse more quickly as the temperature rises, resulting in more adsorption of the adsorbate by adsorbents through specific sites (Fu *et al.*, 2016).

2.11.4 Effect of initial concentration

The initial concentration provides an important driving force to overcome all mass transfer resistance of target pollutant between the aqueous and solid phases (Nuhoglu & Malkoc, 2005). This is because a given mass of sorbent material can only adsorb a fixed amount any adsorbate; hence, the initial concentration of an effluent is one of important factor to studied (Bharathi & Rameshsrikrishna, 2012).

2.11.5 Adsorbent dosage

Adsorbent dosage is an important parameter in the determination adsorbent's capacity for a given amount of the adsorbate at the operating conditions. In order to study the effect of adsorbent dosage on the adsorption process, it is necessary to prepare adsorbent-adsorbate solution with different amount of adsorbents added to fixed initial effluent concentration then shaken together until equilibrium time (Salleh *et al.*, 2011).

2.12 Kinetic Models of Adsorption

Adsorption measurements are always carried out when equilibrium is reached which has been reported to be within an hour to a day (Yu *et al.*, 1999). Under this condition of studies, the extent of adsorption continues to vary with respect to time change and frequently do not reach equilibrium, at least within the time boundaries of the experiment.

2.12.1 Pseudo first-order kinetics

Lagergren showed that the rate of adsorption of solute on the adsorption is based on the adsorption capacity and follows a pseudo-first-order equation (Kean and Thanou, 2010). The pseudo-first order rate expression of Lagergren model is generally expressed as (Lagergren, 1898):

$$\frac{dq_t}{dt} = K_{ad}(q_e - q_t) \quad (2.3)$$

Where q_e and q_t are the amount of adsorbed species (mg/g) at equilibrium and at any instant of time t (min), respectively, and K_{ad} is the rate constant of pseudo first order adsorption operation (min^{-1}). The integrated rate law after application of the initial condition of $q_t = 0$ at $t = 0$, becomes a linear equation as given by:

$$\ln(q_e - q_t) = \ln q_e - K_1 t \quad (2.4)$$

Pseudo first-order kinetic equation differs from a true first-order equation in two ways: the parameter, $(q_e - q_t)$ does not represent the number of available sites, and the parameter, $\ln(q_e)$ is an adjustable parameter and often found that it is not equal to the intercept of the plot of $\ln(q_e - q_t)$ versus t . Whereas in a true first order model the value of $\ln q_e$ should be equal to the intercept. Hence, pseudo first order kinetic model is

used for estimating K_1 alone, which is considered as mass transfer coefficient in the design calculations (Gupta & Babu, 2009).

2.12.2 Pseudo second-order kinetics

As pseudo first-order kinetic model gives only K_1 and as q_e cannot be estimated using this model, applicability of the pseudo second-order kinetics has to be tested for the estimation of q_e with the rate equation given by Ho, (2000):

$$\frac{dq}{dt} = K_2(q_e - q_t) \quad (2.5)$$

where K_2 the equilibrium is rate constant of pseudo second-order adsorption ($\text{gmg}^{-1}\text{min}^{-1}$). From the boundary conditions, $t=0$ to t and $q_t=0$ to q_t , the integrated form of the Equation (2.6) is:

$$\frac{1}{(q_e - q_t)} \frac{1}{q_e} K_2 t \quad (2.6)$$

$$\frac{1}{q_e} - \frac{1}{K_2 q_e} t \quad (2.7)$$

The plot of $\frac{t}{q_t}$ versus t should give a straight line graph with the slope and intercept which allows the computation of a second represent K_2 and q_e respectively. The pseudo-second order model is based on the assumption that the rate limiting step may be chemical adsorption involving valence forces through sharing or exchange of electrons between the adsorbent and adsorbate (Ho & Mckay, 2000).

2.12.3 Elovich model

Elovich model is applied for chemisorption processes (Okoye *et al.*, 2010). The equation is often used valid for adsorption surface that is heterogeneous. The Elovich model shown in Equation 2.8:

$$q_t = \frac{1}{b} \ln(ab) + \frac{1}{b} \ln t \quad (2.8)$$

where (a), is the initial adsorption rate (mg/gmin) and b is related to the extent of surface coverage and the activation energy for chemisorption (g/mg). A plot of q_t against $\ln(t)$ gives a straight line with a slope of $\frac{1}{b}$ and an intercept of $\frac{1}{b} \ln(ab)$ with correlation coefficient.

2.12.4 Isotherm studies

The data generated from the adsorption studies in Section 3.3, were fit into Langmuir, Freundlich, and Temkin adsorption isotherms to determine the model that best describes the adsorption studies.

2.12.5 Langmuir isotherm

The Langmuir isotherm which assumes a surface with homogeneous binding sites, equivalent sorption energies, and no interactions between adsorbed species is expressed by the Equation (2.9) (Langmuir, 1916);

$$\frac{C_e}{q_e} = \frac{1}{K_L q_m} + \frac{C_e}{q_m} \quad (2.9)$$

where C_e is the equilibrium concentration of selected heavy metals (mg/L), q_e is the quantity of heavy metal adsorbed onto the adsorbent at equilibrium (mg/g), q_m is the maximum monolayer adsorption capacity of adsorbent (mg/g) and K_L is the Langmuir adsorption constant (L/mg). The plot of $\frac{C_e}{q_e}$ against C_e gives a straight line with a slope and intercept of $\frac{1}{q_m}$ and K_L respectively. K_L is an important tool in the calculation of the dimensionless equilibrium parameters (R_L) that explains the favorability of adsorption process as shown in Equation (2.10).

$$R_L = \frac{1}{1 + K_L C_0} \quad (2.10)$$

Where c_0 is the initial concentration of each heavy metal in the battery effluent in mg/L and K_L is the Langmuir adsorption constant (L/mg).

2.12.6 Freundlich isotherm

The Freundlich isotherm that is an empirical model not limited to monolayer coverage alone but also describes multilayer adsorption (Freundlich, 1906). It is expressed mathematically as in Equation (2.11)

$$\ln q_e = \frac{1}{n} \ln C_e + \ln K_f \quad (2.11)$$

where q_e is the quantity of the selected heavy metal ion adsorbed at equilibrium (mg/g), C_e is the concentration (mg/L) of heavy metal ion in solution at equilibrium; K_f and n are Freundlich constants incorporating the factors affecting the adsorption capacity and adsorption intensity respectively. The Plots of $\log q_e$ against $\log C_e$ gives a linear graph with slope $\frac{1}{n}$ and intercept $\log K_f$ from which n and K_f can be calculated respectively.

2.12.7 Temkin isotherm

The Temkin isotherm assumes linear rather than logarithm decrease of heat of adsorption while ignoring extremely low and very high concentration. It also assumes uniform distribution of bounding energy up to some maximum bonding energy. It is expressed by Equation (2.12)

$$q_e = \beta \ln A_T + \beta \ln C_e \quad (2.12)$$

where q_e is the amount of adsorbate adsorbed at equilibrium (mg/g); C_e is concentration of adsorbate in solution at equilibrium (mg/L). β is a constant related to the heat of adsorption and it is defined Equation (2.13)

$$\beta = \frac{RT}{b} \quad (2.13)$$

b is the Temkin constant (J/mol), T is the absolute temperature (K), R is the gas constant (8.314 J/mol K), and A_T is the Temkin isotherm constant (L/g). From the plot of qe vs $\ln C_e$, β and A_T can be calculated from the slopes (β) and intercepts ($\beta \ln A_T$) respectively.

2.13 Review of Literature on the Removal of Selected Heavy Metals from Industrial Effluent by Agricultural Biomass or CNTs/Ag Modified Nanocomposites and Research Gaps

With the onset of industrialization, humanity has witnessed various environmental issues in the society. This industrialization has not only brought development and prosperity but also eventually disturbed the ecosystem. One of the impacts is visible, in form of water pollution. In the present review, various studies on the removal of heavy metal from industrial effluent by selected adsorbent were carefully examined, and the research gaps presented accordingly.

Sumesh *et al.* (2011) in their work, described the use of silver nanoparticles, protected by mercapto succinic acid (MSA) and supported on activated alumina for the removal of mercuric ions present in contaminated waters, at room temperature ($28 \pm 1^\circ\text{C}$). These nanoparticle samples were prepared by using two Ag:MSA ratios 1:6 and 1:3, respectively, were loaded on alumina at 0.5 and 0.3% by weight. The mechanism of interaction of silver nanoparticles with Hg^{2+} ions was studied using various analytical techniques such as ultraviolet–visible spectroscopy (UV–vis), Fourier transform infrared spectroscopy (FT-IR), X-ray diffraction (XRD), scanning electron microscopy (SEM), dynamic light scattering (DLS), inductively coupled plasma-optical emission

spectrometry (ICP-OES), energy dispersive analysis of X-rays (EDAX), transmission electron microscopy (TEM) and X-ray photoelectron spectroscopy (XPS). Interactions of the metal ion with the metal core, the surface head group and the monolayer functionality was investigated. Results revealed the high removal ability of 0.8 g of mercury per gram of Ag@MSA, which was achieved in the case of 1:6 Ag@MSA with the best uptake capacity of Hg^{2+} in the pH range of 5–6. The ease of synthesis of the nanomaterial by wet chemistry, capability to load on suitable substrates to create stable materials and affordable cost will make it possible to apply this approach in field applications, especially for the treatment of Hg^{2+} contaminated waters. However, the authors did not make use of real effluent whereby the Hg^{2+} ions would have to be surrounded by scavenging ions from others ions present, furthermore only Hg^{2+} were considered for removal in the study without taking into account other important ionic metals that are readily found in industrial effluent.

Sun, *et al.*, (2014) synthesized an amino-functionalized magnetic cellulose composite ($\text{Fe}_3\text{O}_4@\text{SiO}_2@\text{cellulose}@\text{GMA-EDA}$), the composite was characterized using The FT-IR spectra to determine the functional groups present. While XRD was used to investigate the crystal structure of the samples obtained, the morphology of composite was determined by TEM, whereas the magnetic properties were analyzed by Vibrating Sample Magnetometry (VSM). The surface at different pH values was measured using Zeta PALS. The Fe_3O_4 content was analyzed by inductively coupled plasma atomic emission spectrometer (ICP-OES). The organic component (cellulose or amino-modified cellulose) content of composite was determined by thermo- gravimetric analysis (TGA), the specific surface area, total pore volume and average pore diameter were measured by nitrogen adsorption at 77 K using an automated gas sorption analyzer.

Consequently, the composite was tested for its ability to remove Cr (VI) from an aqueous solution in batch experiments. The results demonstrated that Cr (VI) adsorption was highly pH dependent. The optimized pH value was 2.0. The adsorption isotherms of the adsorbent fit the Langmuir model, with the maximum adsorption capacity of 171.5 mg/g at 25 °C. The adsorption rate was considerably fast, and the adsorption reached equilibrium within 10 min. The obtained thermodynamic parameters showed that the adsorption of Cr (VI) onto the adsorbent was an exothermic and spontaneous process. In addition, the Cr (VI) ions could be effectively desorbed using a 0.1 mol/L NaOH solution and the adsorbent exhibited a good reusability. The composite material should be a promising adsorbent for Cr (VI) removal, with the advantages of high adsorption capacity, rapid adsorption rate and convenient recovery under magnetic field. Yet, real industrial waste containing Cr (IV) ions was seldom used in the study, therefore only Cr (IV) was considered in the study. More so, only the pH was optimized for the batch adsorption studies and the effect of adsorbent dosage, contact time, and metal ion concentration were left unexplored.

Luo *et al.* (2015) developed recyclable magnetic chitosan/cellulose hybrid microspheres (MCCM) by sol-gel method. Achieved by embedding magnetic $\gamma\text{-Fe}_2\text{O}_3$ nanoparticles in chitosan/cellulose matrix drops in NaOH/urea aqueous solution, it combined renewability and biocompatibility of chitosan and cellulose as well as magnetic properties of $\gamma\text{-Fe}_2\text{O}_3$ to create a hybrid system in heavy metal ions removal. The prepared (MCCM) adsorbent was characterized by XRD, SEM VSM and TGA and tested for their ability to remove Cu^{+2} , Cd^{+2} and Pb^{+2} ions from samples of modelled pollutants. Results obtained from adsorption kinetics analysis indicated that a period of 60–80 min was sufficient to attain equilibrium for all three metals. The order of selectivity for competitive conditions in a multi-metal solution was as follows:

$\text{Pb}^{2+} > \text{Cd}^{2+} > \text{Cu}^{2+}$. The highest efficiency of desorption (92%) was obtained with Cu^{2+} , followed by Cd^{2+} (89%) and Pb^{2+} (85%). Again, the authors did not make use of real industrial effluent in their study, nor did they establish the amount of cycles the prepared adsorbent would be used for before it loses its potency.

Zhan *et al.* (2016) prepared amino functionalized Fe_3O_4 /multi-walled carbon nanotubes hybrid by a facile and efficient one-pot solvothermal process. The 3-aminophenoxyphthalonitrile which was regarded as phthalonitrile monomer was introduced into the solvothermal process and promoted the phthalocyanine cyclization reaction, finally forming the amino functionalized hybrid. The structure, composition, and morphology were characterized by FTIR, XRD, XPS, SEM, and TEM. It was found that the monodispersed amino functionalized Fe_3O_4 spheres with diameters of 180–220 nm were uniformly attached on the surface of multi-walled carbon nanotubes. Owing to the synergistic effect between the amino groups and magnetic carbon nanotubes, the as-prepared hybrid exhibited the high separation efficiency when used to remove Cu (II) from aqueous solutions. The adsorption isotherms of the as-prepared hybrid for Cu (II) removal fitted the Langmuir model, the maximum adsorption capacity of our amino-functionalized Fe_3O_4 /MWCNTs hybrid calculated from the isotherm model is 30.49 mg g^{-1} . This work demonstrated that the amino functionalized Fe_3O_4 /multi-walled carbon nanotubes hybrid was promising as efficient adsorbent for heavy metal ions removal from effluent in low concentration. However, the authors made use of simulated effluent and the effect of other metallic ions present in a real effluent system could not be examined. Furthermore, no toxicity or biodegradability studies were carried out on this so-called novel nanoadsorbents.

Manjuladevi and Sri (2017) investigated activated carbon produced from *Cucumis Melo* peel (CM) used as adsorbent to remove Cr^{6+} , Cd^{2+} , Ni^{2+} and Pb^{2+} ions from battery

industry and electroplating industrial effluent. Scanning electron microscope (SEM) (5910LV SEM model) machine was used to characterize the surface morphology of activated carbon produced, and revealed the presence of cracks, ridges and adequate facets for interaction with the metal ions. Batch adsorption experiment was conducted to examine the effects of adsorbent dosage, contact time, pH and metal ion concentration on adsorption of Cr^{6+} , Cd^{2+} , Ni^{2+} and Pb^{2+} ions from the effluent. The obtained results showed that, the adsorption of the metal ions was dependent on some factors such as, adsorbent dosage, contact time, pH and metal ion concentration. The optimum adsorbent dosage, metal ion concentration and pH, were found to be at 250 mg, 100 mg/L and pH 3 to 6 respectively. The study also showed that activated carbon prepared from *Cucumis Melo* peel can be efficiently used as low cost alternative for removal of metal ions. Nevertheless, this study did not produce nanocomposites between the biomass *Cucumis Melo* peel and a nanomaterial, which could facilitate higher removal capacity amongst other advantages. Moreover, the produced carbon material was not characterized using important techniques such as; Fourier transform infrared spectroscopy (FT-IR), X-ray diffraction (XRD), scanning electron microscopy (SEM), inductively coupled plasma-optical emission spectrometry (ICP-OES), energy dispersive analysis of X-rays (EDAX), transmission electron microscopy (TEM) and X-ray photoelectron spectroscopy (XPS) and would provide very useful information about adsorbent.

In this study, Baysal *et al.* (2018) developed a starch-coated TiO_2 NPs nanosorbent, which was characterized by FTIR, Zeta potentials and DLS and found application for the sequestration of cadmium, cobalt, copper, nickel, and lead ions from samples of simulated effluent. The heavy metal concentration was analysed by graphite furnace atomic absorption spectrometry (GFAAS). Results obtained in sorption experiments

showed that optimum conditions were investigated for quantitative sorption by using the mentioned technique, the analyte elements were determined in spiked tap-water samples in the range of 95% confidence level. Limit of detection (3δ) were 0.05, 0.28, 1.90, 3.10 and 0.11 $\mu\text{g/L}$ (3σ , $N = 10$) for cadmium, cobalt, copper, nickel and lead, respectively. The optimized technique was fast, easy handled, simple and environmental friendly. Nevertheless, the surface morphology of the prepared starch-coated TiO_2 NPs was not examined using either SEM or TEM analysis. Furthermore, real effluent sample was not used during the study.

Bankole *et al* (2019) investigated the removal of heavy metals (As, Pb, Cr, Cd, Ni, Cu, Fe, and Zn) via batch adsorption process from industrial electroplating effluent using two different nano-adsorbents; purified carbon nanotubes (P-CNTs) and polyhydroxybutyrate functionalized carbon nanotubes (PHB-CNTs), both produced through catalytic chemical vapour deposition (CCVD) method. HRSEM, HRTEM, XRD, DLS, BET, FTIR, XPS, TGA, pH drift and Raman spectroscopy were used to characterize the developed nano-adsorbents. In the batch adsorption process, the effects of contact time, dosage, temperature and pH were studied. Both nano-adsorbents gave optimum contact time, equilibrium time, optimum dosage, and pH of 10 minutes, 70 minutes, 20 mg, and 5.63–5.65 respectively. The heavy metals removal efficiencies by the nano-adsorbents followed the order of PHB-CNTs > P-CNTs based on ion exchange and electrostatic forces mechanism. For P-CNTs and PHB-CNTs, the equilibrium sorption isotherm suits temkin model, kinetic data fitted to pseudo-second order based on the linear regression correlation coefficient, and the thermodynamic study established spontaneity and endothermic nature of the adsorption process. The authors concluded that both nano-adsorbents have exceptional capacity to remove heavy metals from the adsorbate, with PHB-CNTs possessing better quality and the treated adsorbate

meets the standard for industrial or irrigation re-use. However, the authors did not carry out toxicity and biodegradability studies on the nanomaterials produced during the study.

Lucaci *et al.* (2019) investigated the removal of Co (II) ions from aqueous media using three types of biochars obtained from algae waste biomass, mustard waste biomass, and soy waste biomass. The biochar samples were obtained by pyrolysis of waste biomass resulted from biofuels production, at relative low temperature (600–650°C), and this procedure can be considered a suitable alternative to reduce the volume of such waste. FTIR spectra recorded for each type of biochar reveal the presence of several functional groups that can be used as binding sites for Co (II) retention. The batch biosorption experiments were performed as a function of initial Co (II) ions concentration and contact time, at constant solution pH (5.0), sorbent dose (8.0 g/L), and room temperature ($25 \pm 1^\circ\text{C}$). The sorption experiments showed that the Co (II) ions retention reaches the equilibrium in maximum 60 min, and the maximum sorption capacity follows the order: Mustard biochar (MBC—24.21 mg/g) < soy biochar (SBC—19.61 mg/g) < algae biochar (ABC—11.90 mg/g). The modeling of experimental data proved that the retention of Co (II) ions from aqueous solution occurs through electrostatic interactions, and that the sorption process takes place until a monolayer coverage is formed on the outer surface of the biochar. The desorption results showed that by treating the biochar samples loaded with Co(II) ions with 0.1 mol/L HNO₃ solution, over 92% of Co(II) ions are desorbed and can be recovered, and the biochar samples can be used in at least three sorption/desorption cycles. However, complete characterization of the biochar was neither carried out, nor was the biochar incorporated with nanomaterials to build composites.

Ahmaruzzaman *et al.* (2019) described a biogenic, additive free, eco-friendly synthesized SnO₂-CNTs nanohybrid as an efficient, re-collectable and reusable material

for onsite water remediation. The authors demonstrated that the SnO₂-CNTs can provide a one stop solution for water remediation as it effectively accomplished the major treatment tasks like adsorption, catalytic transformation/degradation and disinfection. The structural, morphological, surface chemical compositions of the nanocomposite and the adsorption, catalytic and antimicrobial properties were investigated using common characterization and instrumental techniques. The results revealed the brilliant efficiency of SnO₂-CNTs nanoadsorbent towards As (III) and a maximum Langmuir adsorption capacity of 106.95 mg/g was observed at high arsenite concentration ($c_0 = 1$ mg/L). The nanoadsorbent was also found to be equally efficient in low arsenite concentration ranges ($c_0 = 100$ µg/L) as it could bring down the arsenic concentration below maximum permissible limit. Moreover, using model pollutants like p-nitrophenol, Alizarin red S, Metronidazole, bacterial strains (*Bacillus subtilis*, *Escherichia coli*, *Streptococcus pneumonia* among others.), and fungal strains (*Aspergillus niger* and *Candida albicans*), the multifunctional capability of SnO₂-CNTs towards water decontamination has been established. The results suggested the promising potential of hierarchical nano-heterojunctions for engineering efficient water treatment processes. Nevertheless, the authors did not make use of real effluent and the biodegradability of the produced composite was yet to be established according to the studies.

In another study, Rodríguez and Leiva (2020) assessed the capacity of oxidized and double-oxidized multiwalled carbon nanotubes (MWCNTs) to remove heavy metals ions from acidic solutions. The MWCNTs were tested for copper (Cu), manganese (Mn), and zinc (Zn) removal, which showed an increment of 79%, 78%, and 48%, respectively, with double-oxidized MWCNTs compared to oxidized MWCNTs. Moreover, the increase in pH improved the sorption capacity for all the tested metals, which indicates that the sorption potential is strongly dependent on the pH. The kinetic

adsorption process for three metals can be described well with a pseudo-second-order kinetic model. Additionally, in multi-metallic waters, the sorption capacity decreases due to the competition between metals, and it was more evident in the removal of Zn, while Cu was less affected. Besides, XPS analysis showed an increase in oxygen-containing groups on the MWCNTs surface after oxidation. Finally, these analyses showed that the chemical interactions between heavy metals and oxygen-containing groups are the main removal mechanism. Overall, these results contribute to a better understanding of the potential use of CNTs for water treatment. This study was limited to the use of oxidized CNTs and did not exploit the possibilities of forming composites between the modified CNTs and natural biomass or other nanoparticles such as zinc and silver.

2.14 Chapter Summary

Different studies that have utilized various nanoparticles, such as, silver (Ag) (prince *et al.*, 2014), titania (TiO₂) (Shi *et al.*, 2012), zinc oxide (ZnO) (Balta *et al.*, 2012), carbon nanotubes (CNTs) (Celik *et al.*, 2017), graphene oxide (GO) (Xia *et al.*, 2015), alumina (Al₂O₃) (Arsuaga *et al.*, 2013), silicon oxide (SiO₂) (Yu *et al.*, 2009), iron oxide (Fe₃O₄) (Alam *et al.*, 2016), cobalt (Co) (Gzara *et al.*, 2016), zirconium oxide (ZrO₂) (Maximous *et al.*, 2010), clay nanoparticles (Mierzwa *et al.*, 2013) and zeolite (NaX) (Fathizadeh *et al.*, 2011), in the development of novel nanocomposite polymer membranes for water treatment applications. Likewise, several new types of nanocomposite membranes have been recently commercialized for a variety of filtration applications. In particular, membranes containing silver based NPs are used for RO, as reported by Sterlitech (Sterlitech, 2018) and for water filtration by Lenntech (Lenntech, 2018).

However, after a careful review of some related literature as discussed in the section above, there is a need to develop a cost-effective, recyclable, operation-convenient and highly efficient natural polymer-based adsorbent for their biodegradability, biocompatibility, and non-toxicity. This study attempt to fill the research gap by via a facile synthetic route by embedding Ag-CNTs composites into cellulosic matrix extracted from the trunk of plantain shrub in an ionic solution. This is because the combined renewability and biocompatibility of cellulose, tremendous adsorption capacity of modified CNTs for heavy metal ions such as, Cd^{2+} , Cu^{2+} , Pb^{2+} , and Zn^{2+} from aqueous media. As well as the antimicrobial properties of Ag NPs that would create an improved hybrid system for the removal of the aforementioned heavy metal ions commonly found in battery effluent even at the industrial scale. This study also intends to characterize the produced adsorbent using appropriated techniques and optimize process conditions such as, contact time, adsorbent dosage, as well as carry out kinetic studies during the batch adsorption system.

CHAPTER THREE

3.0 MATERIALS AND METHODS

3.1 Materials, Reagents and Equipment

The grade of materials, chemicals and equipment used in this study are provided in Tables 3.1 and 3.2, respectively.

Table 3.1: List of reagents used

Reagent/chemicals	Name	Purity (%) / Grade	Supplier
C ₉ H ₁₈ NO	Tempo	98.0, ACS reagent	Merck
NaClO	Sodium hypochlorite	95.0, technical	BDH poole, England
HCl	Hydrochloric acid	37.0, reagent	BDH poole, England
H ₂ SO ₄	Tetraoxosulphate (IV) acid	98.0, ACS reagent	BDH poole, England
HNO ₃	Nitric Acid	70.3, reagent	BDH poole, England
CH ₃ COOH	Acetic acid	98.0, ACS reagent	BDH poole, England
C ₂ H ₅ OH	Ethanol	98.8, ACS reagent	Sigma-Aldrich
NaOH	Sodium hydroxide	97.0, ACS reagent	BDH poole, England
AgNO ₃	Silver nitrate	99.99, analytical	Sigma-Aldrich
C ₃ H ₆ O	Acetone	99.8, ACS reagent	BDH poole, England
Ar	Argon gas	99.9, analytical	BOC Gases Nigeria Plc, Lagos
C ₂ H ₂	Acetylene gas	99.9, analytical	BOC Gases Nigeria Plc, Lagos

Fe(NO ₃) ₃ ·9H ₂ O	Iron (III) nitrate nanohydrate	99.9, ACS reagent	Sigma-Aldrich
Ni(NO ₃) ₃ ·6H ₂ O	Nickel (II) nitrate hexahydrate	99.9, ACS reagent	Sigma-Aldrich
C ₄ H ₉ NO	Dimethyl acetamide	99.5, ACS reagent	Sigma-Aldrich
NaBr	Sodium bromide	99.0, ACS reagent	Parchem

Table 3.2: List of Equipment and Apparatus

	Equipment/Apparatus	Location	Model
1	Furnace	Federal University of Technology, Minna Chemistry lab.	Gallenkamp, PSE-621-010L, Germany
2	Magnetic Stirrer/Hot plate	Federal University of Technology, Minna Chemistry lab.	Gallenkamp, 78HW-1, England
3	Mechanical shaker	Federal University of Technology, Minna Chemistry lab.	Stuart Lab-Scale Model SSL1, Staffordshire, UK
4	Freeze dryer	Federal University of Technology, Minna STEP B.	LGJ-10, Lyophilizer, Denmark
5	Thermostat oven	Federal University of Technology, Minna Chemistry lab.	Gallenkamp, PI09334, Germany
6	Electronic weighing balance	Federal University of Technology, Minna Chemistry lab.	T-scale Precision, SP601, China
7	Sieve (250 µm)	Federal University of Technology, Minna Chemistry lab.	Bilson, ASTM No. 100, USA
8	Agate Mortar and Pestle	Federal University of Technology, Minna Chemistry lab.	Porcelain, China

9	Atomic Absorption Spectrometer (AAS)	Multi-Users Research Laboratory, ABU Zaria	Varian AA 240 FS, California, United States
10	Digital pH meter	Federal University of Technology, Minna Chemistry lab.	Vantakool Digital pH meter, Germany
11	CVD reactor	STEP B, Federal University of Technology, Minna.	XD-1200NT, Zhengzhou, China
12	Ceramic boat	SEDI, Minna	Porcelain, China
13	Centrifuge	STEP B, Federal University of Technology, Minna.	GallenKamp, GR100, Germany
14	HRSEM	University of Western Cape, South-Africa	Zeiss Auriga, Germany
15	HRTEM	University of Western Cape, South-Africa	Zeiss Auriga, Germany
16	XRD	University of Western Cape, South-Africa	XRD-6000, Japan
17	Ultrasonicator	STEP B, Federal University of Technology, Minna.	SB25-12DT, Japan
18	UV-Visible Spectrometer	STEP B, Federal University of Technology, Minna.	UV-1800, Shimadzu. Japan

3.2 Methods

3.2.1 Collection of sample and pre-treatment of plantain trunk

The plant was obtained from the Suleja, Niger state, Nigeria and was not subjected to any post-harvest treatment. Dried plantain trunk (DPT) was prepared from the trunk of plantain of the variety *Musa paradisiaca*. The harvested plantain trunk was washed with distilled water to remove sand and debris. Subsequently, they were arranged in aluminum trays and dried in an oven at 60°C for 24 h. The dried samples were then

pulverized into powder using mortar and pestle to representative samples. These was washed with ethanol to remove lipid fractions, and dried again in an oven at 60°C for 8 h to remove excess solvents. The resulting material was sieved through a 200-mesh sieve, which afforded (DPT) for the production of cellulose nanocrystals CNCs (Happi *et al.*, 2008).

3.2.2 Preparation of cellulose nanocrystals (CNCs)

CNCs were prepared via 2,2,6,6-tetramethylpiperidine-1-oxyl radical TEMPO-mediated oxidation of dried plantain trunk (DPT) following the method described by Isogai *et al.* (2011) with some modifications. About 2 g of DPT in dry weight was stirred in 200 cm³ deionized water in a 500 cm³ conical flask where 32 mg TEMPO and 200 mg sodium bromide were already dissolved. There was no large DPT aggregates formed in the suspension, TEMPO mediated oxidation was initiated by adding dropwise 7.45 g of the sodium hypochlorite solution. The pH of the oxidation system was kept at 10.0-10.5 by adding 0.5 M sodium hydroxide aqueous solution. After oxidation at room temperature under mild magnetic stirring (~250 rpm) for 4 h, the oxidation reaction was terminated by adding 15 cm³ ethanol as presented in Figure 3.1. The TEMPO-oxidized DPT (O-DPT) was thoroughly washed three times with deionized water and then was dried by a freeze dryer (LGJ-10, China) for 3 days. A known mass of freeze-dried O-DPT was re-dispersed in deionized water and disintegrated to cellulose nanocrystals by ultrasonication (Scientz, SB25-12DT) for 30 min.

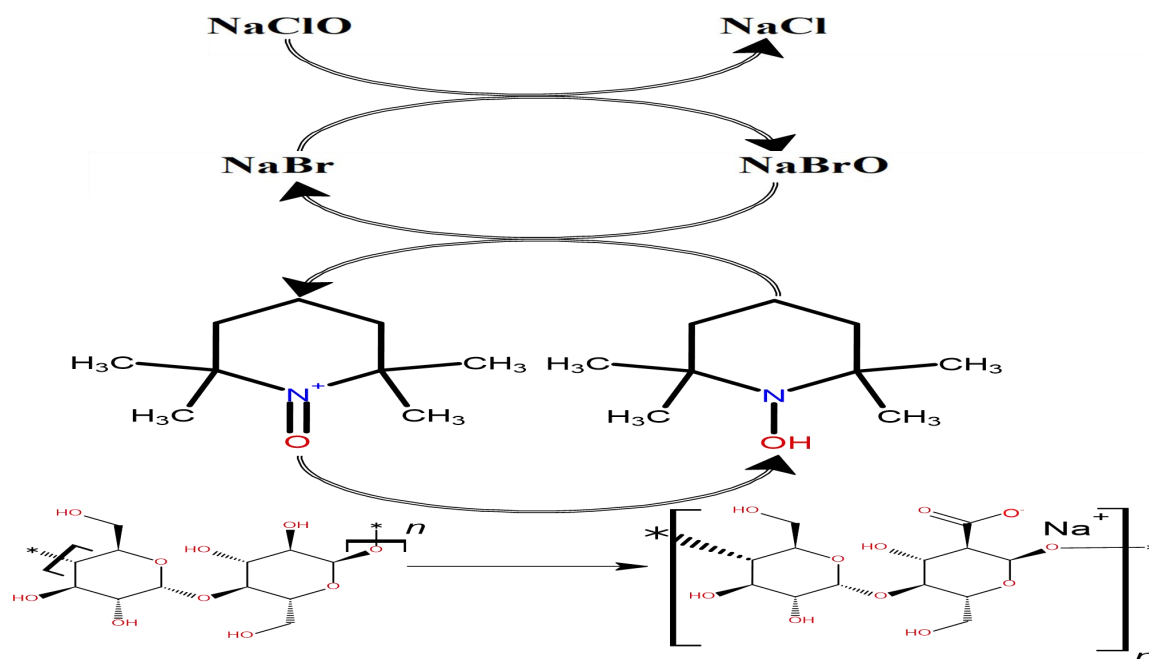


Figure 3.1: Reaction Scheme for the TEMPO-mediated Oxidation of Cellulose (Isogai *et al.*, 2011)

3.2.3 Green synthesis of silver nanoparticles

The green synthesis of Ag NPs was carried out according to the method reported by Sharmila *et al.* (2019) with little modifications. Fresh tea leaves (*Camellia sinensis*) were collected from Bida, Niger state, and the leaves were cleaned with tap water, shade dried and powdered. 5 g of the leaf powder was added to 100 cm³ of distilled water and kept in water bath for 15 min at 70°C. The mixture was stirred using a magnetic stirrer for about 20 min and extract was collected by filtering the solution using the Whatman paper. About 1 mM AgNO₃ precursor solution and (plant extract) were mixed in 4:1 ratio and the mixture was incubated at room temperature for complete synthesis of Ag NPs. The formation of Ag NPs was observed by measuring the absorbance in the wavelength range of 200–700 nm using UV–Vis spectrophotometer (Shimadzu UV-1800, England) at regular intervals. After completion of Ag NPs synthesis, the solution was centrifuged at 5000 rpm for 10 min, dried at 80°C and stored for further studies.

3.2.4 Synthesis of carbon nanotube

Catalytic vapour deposition method was employed in this research for the synthesis of carbon nanotubes. Carbon nanotubes was synthesized by the decomposition of acetylene (C_2H_2) in a tubular quartz reactor placed horizontally in a furnace. The furnace was electronically controlled such that the heating rate, reaction temperature and gas flow rates could be accurately maintained as desired. The catalyst (Fe-Ni/kaolin) was loaded into a quartz boat ($120 \times 15 \text{ mm}^2$) at room temperature and the boat was placed in the centre of the quartz tube. The furnace was then heated at $10 \text{ }^\circ\text{C min}^{-1}$ while argon was flowing over the catalyst at 300 ml min^{-1} . Once a temperature of $750 \text{ }^\circ\text{C}$ was attained, the argon flow rate was reduced to 230 ml min^{-1} and C_2H_2 was then introduced at flow rate 200 ml min^{-1} for a period of 60 min. The C_2H_2 flow was stopped after this reaction period and the furnace was allowed to cool to room temperature under a continuous flow of argon. The boat containing the CNTs was removed from the reactor and weighed to know the deposited synthesized CNTs (Bankole *et al.*, 2019). The percentage yield of CNTs produced was determined using Equation 3.1

$$CNTs \text{ Yield (\%)} = \frac{W_{Product} - W_{catalyst}}{W_{catalyst}} \times 100 \%$$

(3.1)

3.2.4.1 Purification of the synthesized CNTs

Acid treatment method was employed to remove residual Fe, Ni, amorphous carbon from the as-synthesised CNTs according to Bankole *et al.* (2019). A known weight (1.0 g) of CNTs was washed in 100 cm^3 of 30 % H_2SO_4 and 300 cm^3 of 30 % HNO_3 mixture (v/v 1:3) to remove residual Ni and Fe impurities originating from the (Fe-Ni/kaolin) catalyst. The mixture was then sonicated for 90 min at 40°C in an ultrasonic bath

(Scientz, SB25-12DT, England) to introduce oxygen to the surface of the CNTs (Kumar & Ando, 2010). The CNTs were cooled to room temperature and thereafter washed with distilled water and filtered until the pH of 7 was obtained. The wet CNTs were oven dried at about 120 °C for 12 h.

3.2.5 Preparation of Ag-CNTs nanocomposites

The experimental procedure for the synthesis of Ag-CNTs was adopted from Singh *et al.* (2020) with slight modifications. About 0.36 g of purified CNTs were dispersed in 100 cm³ of ethanol and sonicated by an ultrasonicator (Scientz, SB25-12DT, England) for 60 min. Then 0.15 g of the above prepared Ag NPs were added to this solution. The resulting mixture was again sonicated for another 80 min with simultaneous magnetic stirring for 4 h. The sonicated solution was then centrifuged at 5000 rpm for 30 min and the precipitates were oven-dried at temperatures not exceeding 100°C to obtain Ag/CNT nanocomposite, and stored in an air tight container.

3.2.6 Preparation of CNCs-Ag-CNTs nanocomposite

The preparation of CNCs-Ag-CNTs nanocomposites in the combining ratio of (3:1:1) for CNCs, Ag NPs and CNTs respectively was carried out as follow: About four 4 g of CNCs was dissolved in a 250 cm³ beaker labeled A, containing 50 cm³ of acetone/dimethyl acetamide (DMAC) in the ratio of 2:1 v/v % and placed in an ultrasonicator Scientz, SB25-12DT, England) for 30 min at room temperature 25°C. Then, 1.33 g of Ag-CNTs was weighed and dispersed in 25 cm³ of acetone/water in the ratio of 9:1 in a separate 100 cm³ beaker labelled B. Subsequently, the solutions in beaker B was transferred into beaker A, stirred to attain a homogenous constituency and further ultra-sonicated for 2 h. The resultant dense colloid was dried in an electric oven

at 120 °C for 6 h. All the samples were then pulverized and stored in sterile air tight containers and labeled appropriately.

3.2.7 Characterisation of the as-synthesized nanomaterials

The prepared nanomaterials were characterized for their crystalline phases and surface morphology, using XRD, HRSEM-EDS and HRTEM-SAED respectively. All analysis was done for Ag NPs, CNTs, CNCs and CNCs-Ag-CNTs nanocomposites.

3.2.7.1 X-Ray diffraction (XRD)

X-ray diffractometer (XRD, 6000, Shimadzu, Japan) was used to evaluate the crystalline or mineralogical phases present in the as-synthesized nanomaterials such as Ag NPs, CNTs, CNCs and CNC-Ag-CNTs. Scans were run with a step size of 0.02°/s of 2 θ , typically in the angle range between 10° and 90°.

Debye Scherrer Equation (3.2) was used to calculate the particle size of the nanomaterials

$$d = \frac{K\lambda}{\beta \cos\theta} \quad (3.2)$$

where, D is the crystallite size in nanometers, K is the shape factor (0.89), λ is the wavelength of CuK α radiation ($\lambda = 1.54056 \text{ \AA}$), β is full width at half maximum (FWHM) of the particular peak and θ is the Bragg's angle (Mohanta & Nath, 2019).

3.2.7.2 High resolution scanning electron microscope / electron dispersive x-ray spectroscopy (HRSEM/EDS)

High Resolution Scanning Electron Microscope (HRSEM) (Polaron SC515, Zeiss Auriga, Germany) was employed in this study. Prior to the analysis, 0.05 g of each sample was sprinkled on a sample holder with a carbon adhesive tape on it. This was sputter-coated with Au-Pd Quorum T150T for 5 min and the samples were

subsequently, characterized at different magnifications. The microscope was operated at Electron High Tension (EHT) of 5 kV for imaging. Other operating parameters are presented in Table 3.3

Table 3.3: HRSEM Operating Settings

Operating Parameters	Conditions
Current	10 Ma
Magnification	Varies
Aperture	0.4 mm
Resolution	1 nm, but sometimes varies
Emitter	Thermal field emission type
Working distance	4-10.4 mm
Voltage	5 Kv
Signal A	In-lens

For the determination of the elemental composition of the samples using Energy Dispersive Spectroscopy (EDS) measurements, the secondary electron mode was activated for the imaging. A homogenous region of the sample was identified and the microscope operated using electron high tension (EHT), of 20 kV for about 30 min at 150°.

3.2.7.3 High resolution transmission electron microscope / selected area electron diffraction spectroscopy (HRTEM/SAED)

The structure and morphology of as-synthesized nanomaterials were studied using high resolution transmission electron microscopy/selected area electron diffraction (HRTEM/SAED) (JEM2100F, Zeiss Auriga, Jena Germany). A trace amount (10 mg) of the sample was placed in a tube and vibrated ultrasonically in 10 cm³ methanol and thereafter subjected to ultrasonication. The suspension of the sample was subsequently spread on a copper grid with lacy carbon thin film and allowed to dry. The dried sample was loaded onto the single tilt sample holder and mounted thereafter onto the shaft of

the electron microscopy. The detailed instrument parameters and conditions settings are provided in Table 3.4. Through the utilization of the magnification knob, clear pictures were achieved. The copper was disembarked from the HRTEM after the pictures of the desired images were taken.

Table 3.4: HRTEM experimental conditions

Operating parameters	Conditions
Illumination angle	15 °
Magnification	Varied
Emissioncurrent	54 μ A
Resolution	0.24 nm
Extraction voltage	3950 V
Spot size	3 nm
Electron high tension	200 kV
Gun lens	1 nm
Condenser aperture	3 mm
Objective aperture	2 nm

3.2.8 Sampling and sample pre-treatment for battery effluent

About 500 cm³ of battery effluent was collected from Forgo Battery Industry Taiwo Road Ilorin, Kwara State Nigeria, and stored in clean polythene bottles. Sample bottles were washed with 10% nitric acid and thoroughly rinsed with de-ionized water. 500cm³ of battery standard methods were used for determination of physico-chemical parameters in the effluent. The effluent was stored at 4°C during a storage period of about one month to avoid any change in its characteristics.

3.2.8.1 Digestion of the battery effluent for the determination of heavy metal

A known volume (10 cm³) of the battery effluent was measured into a 100 cm³ beaker followed by addition of 5cm³ of conc. HNO₃ and 2cm³ of conc. HCl and thereafter

covered with a watch glass. The mixture was digested in a fume cupboard to final volume of 5 cm³ followed by the addition of the resultant mixture to 15cm³ of deionized water, and then filtered using Whatman filter paper (No. 42). The filtrate was made to 50 cm³ with deionized water according to Udo and Ogunwale, (1986). The residual concentrations of heavy metals in the solution were determined using atomic absorption spectrometer (Varian AA-240 FS, Shimadzu Corporation, Japan).

3.2.9 Determination of selected heavy metals in the battery effluent

The heavy metals (Fe, Zn, Cu, Ni and Pb) concentrations in all the samples were determined by atomic absorption spectrophotometer (AAS) (Varian AA-240 FS, Shimadzu Corporation, Japan) at an oxidant rate of 4.5 L/min and the fuel rate (C₂ H₂) of 1.5 L/min with digital read-out system. Iron (wavelength 248.3 nm), Zn (wavelength 213.19 nm), Copper (wavelength 324.8 nm), Ni (wavelength 232.0 nm) and Lead (wavelength 283.3 nm) specific hollow cathode lamps were used to analyze the samples. The light sources of the different elements were hollow-cathode lamps from Cathoden, UK. The instrument has a minimum detection limit of 0.006 mg/L for Fe, 0.001 mg/L for Zn, 0.003 mg/L for Cu, 0.004 mg/L for Ni and 0.001 mg/L for Pb in the flame method. Samples were aspirated through nebulizer and the absorbance was measured with a blank as a reference. The correlation coefficient was found for Fe 0.999, for Zn 0.996, for Cu 0.994, for Ni 0.999 and for Pb 0.994. The sample had to be diluted many folds to keep the results in the analytical range (Islam *et al.*, 2016). Calibration curves obtained for each of the metals (Fe, Zn, Cu, Ni and Pb) using standard samples are shown in the Appendix B section.

3.2.9 Physicochemical characterisation of battery effluent sample

After the effluent was collected from Forgo battery industry, it was subjected to physicochemical characterisation. Physicochemical parameters such as pH, Biochemical oxygen demand (BOD), Chemical Oxygen Demand (COD), Total Dissolved Solid (TDS) and Total Suspended Solid (TSS) were determined. The procedures for the determination of these parameters are as follows:

3.2.9.1 Determination of pH of the effluent

The pH meter was standardized by immersing it in different buffer solutions (acetate pH 4 and ammonium pH 10) respectively. It was then rinsed and inserted into 20 cm³ of the effluent sample in a 100 cm³ beaker. After it has stabilized, the reading on the meter was taken and recorded. This was repeated thrice for the water samples (Amadi *et al.*, 2015).

3.2.9.2 Determination of total dissolved solid and total suspended solid

The standard procedure of APHA, (2005) and Sawyer *et al.* (2000) were used to determine the total suspended solid (TSS) and total dissolved solid (TDS) in the water samples. A known amount of the effluent sample was emptied into the previously weighed glass fibre strainer that has a detailed pore size just before commencing the vacuum filtration procedure. The filter was then detached after completing the filtration procedure and then positioned in a stainless bowl in an oven for 2-3 h at 100°C to totally dry off the left over water. The filter was weighed, and the increase in filter weight denoted as the TSS contents, represented in mass per volume of sample filtered (mg/L). The TDS of the water samples was obtained by the gravimetric method. After the filtration for the TSS analysis was concluded, the deposit was heated in an oven at 105°C for 20 min. The left over mass of the deposit signified the quantity of TDS in a sample in (mg/L).

3.2.9.3 Determination of the biochemical oxygen demand (BOD)

BOD was determined according to APHA, (2005). Specialized 300 cm³ BOD bottles designed to allow full filling with no air space were filled with the sample of the effluent to be tested or dilution water. One bottle was filled only with dilution water to act as a control or “blank.” A dissolved oxygen (DO) meter was used to measure the initial dissolved oxygen concentration (mg/L) in each bottle. Each bottle was then placed into a dark incubator at 20°C for five days. After the fifth day (± 3 h), the DO meter was used again to measure a final dissolved oxygen concentration (mg/L). The final DO reading was then subtracted from the initial DO reading and the result is the BOD concentration (mg/L). Mathematically, biochemical oxygen demand is given by Equation 3.3

$$\text{BOD}_5 = \text{DO}_5 - \text{DO}_1 \quad (3.3)$$

where BOD_5 is the biochemical oxygen demand in mg/L, DO_5 is the amount of dissolved oxygen after an incubation period of five days, DO_1 is the amount of dissolved oxygen in the water sample the first day, both also measured in mg/L.

3.2.9.4 Determination of the chemical oxygen demand (COD)

Following the method of APHA (2005), about 2 cm³ of water sample was added to vial. In the case of the “blank,” 2 cm³ of deionized water was added with 2 cm³ of a standard prepared from KHP (potassium hydrogen phthalate) to the corresponding vials. Each vial was mixed well and placed into the reactor block for 2 h. Afterwards, the vials were removed from the block to a cooling rack for about 15 min. Finally, a calibrated colorimeter was used to measure the wavelength of the solution in the vial, and the value recorded as the chemical oxygen demand (COD) concentration in mg/L.

3.2.9.5 Determination of turbidity

The turbidity of the battery effluent was measured by turbidity meter. The turbidity meter was first calibrated by cal 800NTU, cal 200NTU and cal 100NTU and the sample cell was then filled with the effluent connected to a sample holder. The turbidity meter machine was then switched on to read the turbidity.

3.2.9.6 Determination of the concentration of sulphate

The concentration of sulphate in the effluent was determined by spectrophotometric method. Conditional reagents were prepared by mixing appropriate amount of chloride compound, alcohol, concentrated acid and distilled water. 100 mg/L of standard sulphate solution was prepared by dissolving 4.438 g of anhydrous sodium sulphate in 500 cm³ of distilled water and diluting the solution to 1. Series of standards, blank and known volume of the effluent sample was prepared separately in flat bottom flasks. 5 cm³ of the conditioning reagent was added to each of the flat bottom flask and topped up to 100 cm³ after which 10 mg of barium chloride was added. The resultant solutions were measured with a UV-Visible spectrometer (Shimadzu UV-1800, England) at 420 nm. The sulphate concentration in the effluent sample was determined with reference to the graphical representation obtained for the standard solutions, with the calibration curve presented in Appendix B.

3.2.9.7 Determination of the concentration of Chloride

The concentration of chloride ions in the effluent was determined using Mohr's method. The Mohr method uses chromate ions as an indicator in the titration of chloride ions with a silver nitrate standard solution. A known volume of effluent sample was titrated against a known concentration of silver nitrate. After all the chloride has been precipitated as white silver chloride, the first excess of titrant resulted in the formation

of a brownish red silver chromate precipitate, indicating the end point. The reactions are given in Equations 3.4 and 3.5:



The concentration of chloride in the effluent was determined from the stoichiometry and moles consumed at the end point.

3.2.9.8 Determination of dissolved Oxygen (DO)

Measurement of DO in the collected effluent samples were determined with Winkler's method. The Winkler method involves 'trapping' the DO in the water sample by reacting it with series of reagents resulting in the formation of an acid compound in the presence of iodine. The iodide solution was then titrated with an appropriate neutralising reagent. The change in colour signifying the end point is equivalent to the quantity of DO in the water sample (USEPA, 2021).

3.2.9.9 Determination of the concentration of Fluoride

Fluorides in the effluent was determined by Colorimetric SPADNS method. Under acidic conditions fluorides (HF) react with zirconium SPADNS solution and the lake (colour of SPADNS reagent) was bleached due to formation of ZrF_6 . Since bleaching is a function of fluoride ions, it is directly proportional to the concentration of fluoride. It obeys Beers law in a reverse manner. The colour becomes progressively lighter as the concentration fluoride increases, and absorbance was measured at 570 nm by the colorimeter (USEPA, 2021). The standard calibration curve is presented in Appendix B.

3.2.9.10 Determination of the concentration of cyanide

APHA (2005) approved methods for the determination of total cyanide in waste water was adopted. Distillation was first carried out followed by the addition of pyridine-barbituric acid to give a red-blue coloured complex and the absorbance was measured in a UV spectrophotometer (Shimadzu UV-1800, England) at 578 nm, with the standard calibration curve is presented in Appendix B. This method has very low detection limits, making it ideal for the analysis of cyanide in waste water. Quality control was carried out using blank determination and recovery study.

3.2.9.11 Determination of the concentration of ammonium

Ammonium was determined according to the modified Nessler Method as reported by Jeong *et al.* (2013). All the experiments were carried out as follows. Firstly, 25 cm³ effluent sample was placed in a 100 cm³ graduated cylinder and three drops of a solution (MS) (prepared by dissolving 250 g of sodium citrate and 300 g of sodium potassium tartrate (NaKC₄H₄O₆) in 1 dm³ deionized water) were added to the cylinder, which was subsequently covered and shaken to obtain a homogenous solution. Afterwards, three drops of polyvinyl alcohol (PVA) reagent were also added to the solution. Then, the solution was again covered and mixed. Lastly, 1.0 cm³ of Nessler reagent was added into the cylinder with mixture. Once the final solution was prepared, its portion was transferred into a spectrophotometer (Shimadzu UV-1800, England) cell and the UV light absorbance was measured. The wavelength for the light used in the measurement was set at 425 nm and the standard calibration curve is presented in Appendix B. Prior to the measurement of each water sample, a blank solution was prepared for reference. When only the MS was added to the blank solution with the Nessler reagent and without NH₄⁺, the absorbance did not increase.

3.3 Batch Adsorption of Selected Heavy Metals Using the Prepared Nanomaterial

3.3.1 Effect of contact time on adsorption

The effect of contact time on the adsorption of selected heavy metals by the samples was carried out at the time interval of 30, 60, 90, 120 and 150 min. 0.03 g of each nanomaterial samples (Ag-CNTs, and Ag-CNTs-CNCs,) was mixed with 50 cm³ of the battery effluent in a different 100 cm³ beaker and shaken constantly on an electric stirrer for the period of 30, 60, 90, 120 and 150 min at 300 rpm respectively. Samples were taken at appropriate time and filtered using whatman filter paper and the residual fraction was transferred into sample bottles prior to analysis. The residual concentration of the metal ion in the filtrate was determined by atomic adsorption spectrophotometer (Varian AA-240 FS, Shimadzu Corporation, Japan) (Hameed, 2007).

3.3.2 Effect of adsorbent dosage

The effect of adsorbent dosage on adsorption of selected heavy metals was carried out using 50 cm³ each of the battery effluent placed in a 250 cm³ volumetric flask. Adsorbent dosages of 0.01, 0.02, 0.03, 0.04 and 0.05 g were then added differently to the 50 cm³ of battery effluent. The mixture was shaken for the period of 90 min using an electric stirrer at a speed of 300 rpm, after which the mixture was filtered separately using Whatman filtered paper. The residual concentration of the metal ion in the filtrate was determined by atomic adsorption spectrophotometer (Varian AA-240 FS, Shimadzu Corporation, Japan) (Hameed, 2007).

3.3.3 Adsorption data analysis

The adsorption capacity of the different prepared adsorbent was determined as follows $\% \text{ removal} = \frac{C_0 - C_e}{C_e} \times 100$

(3.6)

The adsorption capacity, q_e , was calculated using the relationship described in equation 3.7:

$$q_e = \frac{(C_0 - C_e)}{m} V \quad (3.7)$$

where C_0 and C_e are the initial and equilibrium adsorbate concentrations in solution (mg/L), respectively; V is a known volume of effluent (L), and m is a known mass of dry adsorbent (g).

3.4 Adsorption Kinetics

For kinetic studies, about 0.02 g adsorbents were contacted with the battery effluent and shaken at 300 rpm at $25^\circ\text{C} \pm 2$. At respective contact time, the solution was filtered and analysed for the final concentrations using AAS. The adsorption capacity at time t , q_t (mg/g) was calculated as:

$$q_t = \frac{(C_0 - C_t)}{m} V \quad (3.8)$$

where q_t (mg/g) is the adsorptive capacity at time t

In order to analyze the adsorption kinetics of the heavy metal ions, the pseudo-first and pseudo second order were applied to the data.

3.4.1 Pseudo first-order kinetic model

The linearised form of the pseudo first-order kinetic model was applied to the experimental data to describe the kinetics of selected heavy metals. The equation is given as:

$$\log (q_e - q_t) = \log q_e - \frac{K_1}{2.303} t \quad (3.9)$$

where q_e is the mass of metal adsorbed at equilibrium (mg/g), q_t is the mass of metal adsorbed at time t (mg/g), k_1 is the first-order reaction rate constant (min^{-1}) and t is the time in (min). Hence the amount of solute sorbed per gram of sorbent at equilibrium (q_e) and the first-order sorption rate constant (k_1) can be evaluated from the slope and the intercept of $\log (q_e - q_t)$ against t .

3.4.2 Pseudo second-order kinetic model

The Lagergren pseudo second-order kinetic model was applied to the experimental data to describe the kinetics of selected heavy metals. The model is represented in Equation 3.10

$$\frac{t}{q_t} = \frac{1}{k_2 q_e^2} + \frac{t}{q_e} \quad (3.10)$$

Where k_2 is the second order reaction rate equilibrium constant (g/mg min). A plot of $\frac{t}{q_t}$ against t should give a linear relationship for the applicability of the second-order kinetic.

3.4.3 Elovich kinetic model

The Elovich kinetic model is expressed as Equation 3.11.

$$q_t = \frac{1}{\beta} \ln (\alpha \beta) + \frac{1}{\beta} \ln t \quad (3.11)$$

where q_t is the quantity of adsorbate adsorbed at time t (mg/g), α is a constant related to chemisorption rate and β is a constant which depicts the extent of surface coverage. The two constants (α and β) can be calculated from the intercept and slope of the plot of q_t versus $\ln t$ respectively (Inyinbor *et al.*, 2016).

CHAPTER FOUR

4.0

RESULTS AND DISCUSSION

4.1 Characterisation of Nanomaterials

4.1.1. UV-Vis Analysis of Ag NPs

The results obtained from the UV spectroscopy of the synthesized silver nanoparticles prepared by the reduction of AgNO_3 by aqueous plant extract showed the surface Plasmon resonance peak wavelength maximum at 413.50 nm indicating the presence of spherical or roughly spherical Ag NPs as shown in Figure 4.1. The wavelength (413.50) proved the samples are Ag NPs because it falls within the silver nanoparticles surface Plasmon resonance (SPR) peak wavelength (400nm-530nm) (Sharmila *et al.* (2019)).

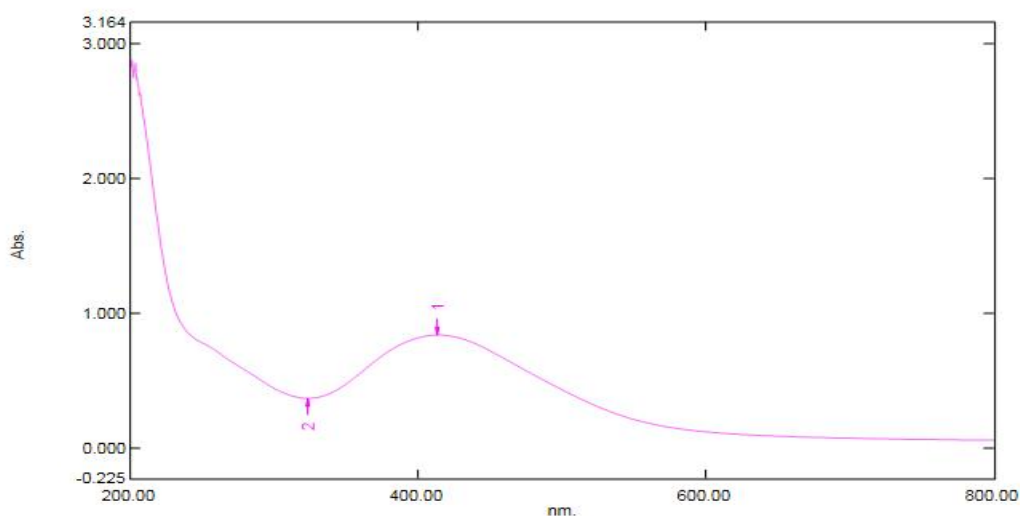


Figure 4.1: UV-Vis Absorption Spectrum of Biosynthesized Ag NPs

4.1.2 HRSEM analysis

Surface morphologies and structures of the Ag NPs, CNTs, CNCs, Ag-CNTs and Ag-CNTs-CNCs nanocomposites obtained from HRSEM analysis were presented in Plate I (a-e). The HRSEM in image in Plate I (a) indicate the presence of spherically shaped

clusters of Ag nanoparticles. A close inspection of the HRSEM micrographs confirms that the silver nanoparticles have well defined grain boundaries with soft surfaces forming slight agglomeration. Typically, the poly-dispersed Ag NPs with an average diameter of 14 nm were observed without strong aggregation indicating the role the plant extract as a capping agent during the formation of nanoparticles (Hamid *et al.*, 2013). Elumalai, *et al.* (2016) and Khan *et al.* (2019) who worked independently have reported identical spherically clusters of Ag NPs structures obtained with via green synthesis with the aid of plant extracts as reduction and stabilization agents. The HRSEM image in Plate I (b) showed purified CNTs with a clear defined long tubular morphology displaying less agglomeration, which confirms the effectiveness of the adopted purification process (Abdulrahman *et al.*, 2017). The CNCs image shown in Plate I (c) revealed structures with a smooth surface, crumpled edges and particle sizes between 20.50 nm to 27.54 nm as similarly observed by Abu-Danso *et al.* (2017). The uniform distribution Ag-CNTs of nanocomposites is shown in Plate I (d),

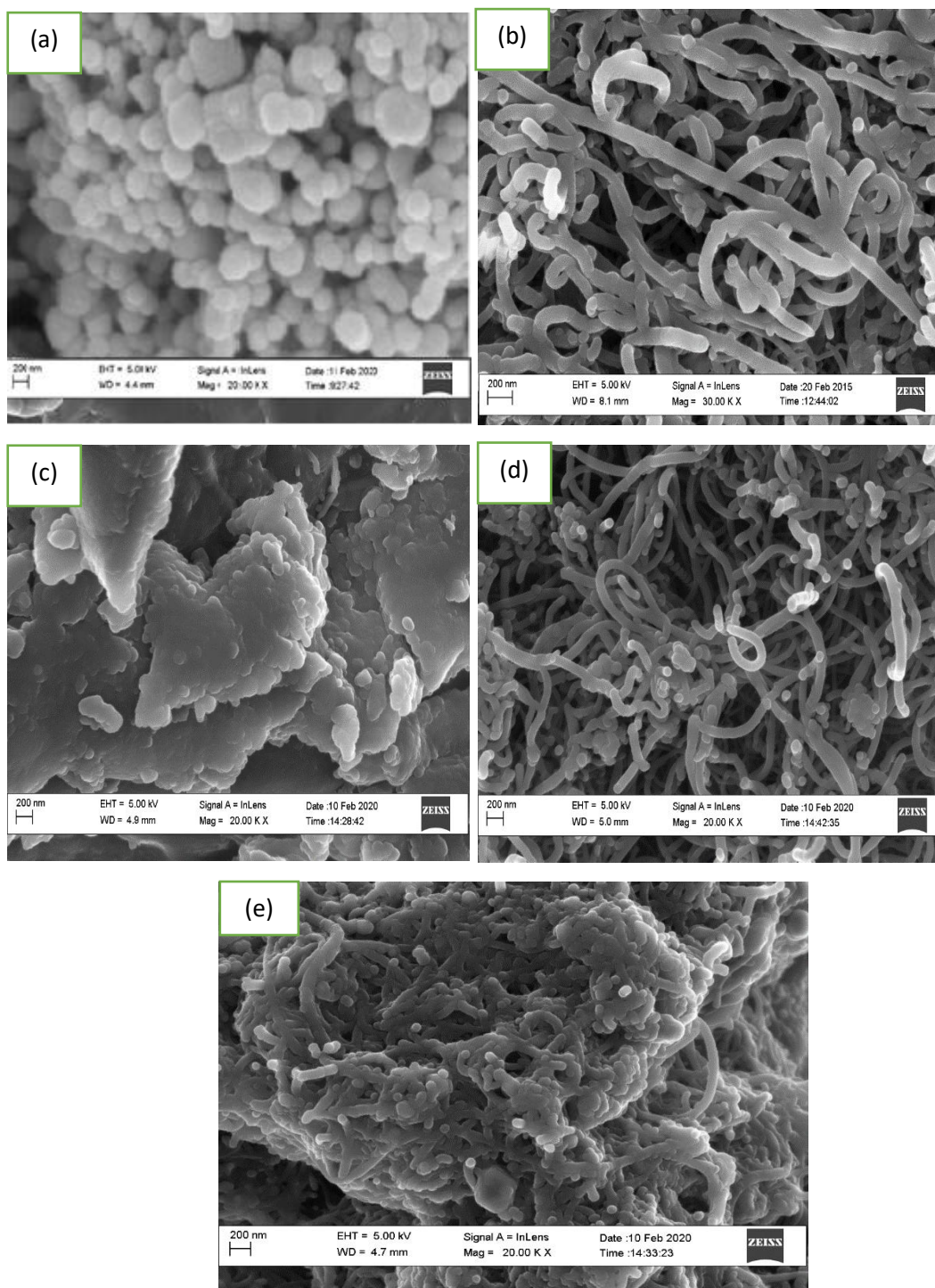


Plate I: HRSEM Micrographs of (a) Silver Nanoparticles (Ag NPs), (b) Carbon Nanotubes (CNTs), (c) Cellulose Nanocrystals (CNCs), (d) Ag-CNTs composites, (e) Ag-CNTs-CNCs composite

with the Ag NPs embedded in the cylindrical structures of the CNTs to create a network of Ag-CNTs nanostructures which may provide more binding sites for improved

adsorption. Plate I (e) shows the HRSEM image of Ag-CNTs-CNCs nanocomposite with very different morphology compared to individual CNCs, CNTs and Ag nanoparticles. Overall, the CNCs sheets were intercalated within the CNTs matrix, which is embedded, with Ag NPs. This translated to several ridges, wrinkles, micro and nano-pores throughout the entire surface and constitutes active sites for adsorption processes. Furthermore, from the HRSEM image of Ag-CNTs-CNCs, the surface morphology differed on comparison with Ag-CNTs giving evidence that the formation of Ag-CNTs-CNCs composite gave rise to a conspicuous nano-membrane morphology with availability of more pores for adsorption area and sites on the surface of the adsorbent for the removal of heavy metal ions (Radhakrishnan *et al.*, 2020).

4.1.3 EDS profile of synthesized silver nanoparticles

The synthesized silver nanoparticles Ag NPs were further characterised by EDS analysis, which gives additional evidence for the reduction of silver nitrate precursor to silver nanoparticles Ag NPs. In Figure 4.1 illustrates the optical absorption peak at approximately 3 keV, which is typical of the absorption of metallic silver nanocrystals due to surface plasma resonance (Dimitrijevic' *et al.*, 2013). This confirms the presence of Ag NPs, typical for the absorption of metallic silver nanocrystals due to surface plasma resonance. The spectrum in Figure 4.1 also shows weak oxygen and carbon peaks, which may have originated from the biomolecules (such as polyphenols and tannins) that are bound to the surface of the silver nanoparticles from the plant extract. Thus, the EDX provides information about the elemental composition and chemical purity of the synthesized nanoparticles (Suman *et al.*, 2015).

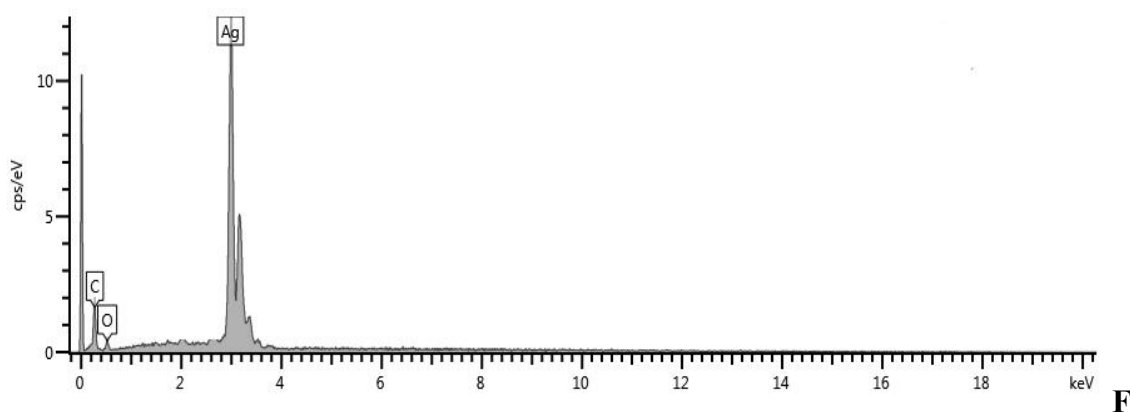


Figure 4.2: EDS Spectrum of Green Synthesized Ag NPs

The percentage by atomic weight of elemental constituents present in the nanoparticles and nanocomposites are shown in Table 4.1

Table 4.1: Elemental composition from EDS of Ag, CNCs, CNTs, Ag-CNTs and Ag-CNTs-CNCs

Sample	Ag Nps		CNCs		CNTs		Ag-CNTs		Ag-CNTs-CNCs	
Element	Wt (%)	At (%)	Wt (%)	At (%)	Wt (%)	At (%)	Wt (%)	At (%)	Wt (%)	At (%)
Ag	92.97	65.50	---	---	---	---	17.81	2.45	8.34	1.06
C	0.68	4.33	55.11	62.05	71.60	77.67	71.23	88.18	72.40	83.07
O	6.35	30.17	44.89	37.95	27.08	22.03	9.71	9.06	18.12	15.59
Ni	---	---	---	---	0.74	0.17	0.73	0.18	0.68	0.16
Fe	---	---	---	---	0.58	0.13	0.52	0.13	0.46	0.12
Total	100	100	100	100	100	100	100	100	100	100

As expected the Ag NPs consisted of Ag (65.50%), C (4.33%) and O (30.17%) by atomic percent, corroborating with the result presented in Figure 4.1 with indication of Ag as the major constituent (Muthukumar, and Karuppan, 2016). Whereas CNCs

comprised solely of C (62.05 %) and O (37.95 %) indicating a high purity for the nanoparticles which could be ascribed to the synthesis method adopted by this research. Hence 2,2,6,6-tetramethyl-1-piperidinyloxy TEMPO-mediated oxidation of dried plantain trunk (DPT) gave a high level of pristine CNCs. Conversely, the CNTs consisted of C (71.60%), O (27.08%), Fe (0.58%) and Ni (0.74%) by atomic percentage, while Ag-CNTs comprised of Ag (2.45%), C (88.18%), O (9.06%), Ni (0.68%) and (0.13%) atomic percentage respectively, with O from the plant origin whereas Fe and Ni possibly originated from the (Fe-Ni/kaolin) catalyst used during the catalytic vapor deposition (CVD) synthesis. Furthermore, the composite Ag-CNTs-CNCs consisted of Ag (1.06%), C (83.07 %), O (15.59 %), Ni (0.16 %) and Fe (0.12 %), indicating that the composite obtained is a hybrid of the three nanoparticles Ag, CNCs and CNTs.

4.1.4 XRD values of the samples

The crystalline structure of the Ag NPs, CNTs, CNCs, Ag-CNTs, and Ag-CNTs-CNCs samples were analyzed by XRD and presented in Figure 4.3. The Ag NPs peak corresponds to Ag nanoparticles having face centered cubic (FCC) crystal structure (JCPDS no. 04-0713) via exposing the crystallographic planes of (111), (200), (220) and (311) corresponding to 2θ values of 38.2° , 44.2° , 64.3° and 77.4° , respectively. In XRD, the size of coherently diffracting domains is measured and it does not necessarily agree with the crystalline grain size (Larrude *et al.*, 2014). The XRD peaks could be attributed to the nanocrystalline nature of the Ag-NPs, which is consistent with the result from the UV-vis spectra in Section 4.1.1.

The average crystallite size of the as-synthesized Ag NPs was obtained as 14.0 nm. This corroborates the average particle size obtained via High-Resolution Transmission Electron Microscopy (HRTEM) (14.64 nm). The XRD results are in agreement with

reports by Adibzadeh and Motakef-kazemi (2018), and Al-Namil, and Patra (2019), who worked independently to obtain spherically shaped and face cubic centred Ag NPs with sizes ranging from (12-15 nm). The X-ray diffraction (XRD) patterns of the CNTs exhibit major peaks around $2\theta = 26.55^\circ$ and 44.56° , which correspond to the crystal planes (002) and (100), respectively. These two diffraction peaks, are the characteristic planes of a typical graphitized carbon of the CNTs. The other peaks appearing at 39.20° , 51.68° , 59.23° and 67.98° with crystal planes of (110), (107) (220), and (211) respectively, may indicate the presence of kaolin or catalytic bimetallic oxide (NiFe_2O_4) (Aliyu *et al.*, 2017).

The diffraction pattern of CNCs revealed a single diffraction peak at 22.2° which corresponds to the (200) plane of cellulose type I, with an average particle size of 24.02 nm (Lin and Dufresne, 2014). The crystallinity index (CrI) of CNCs was calculated to be 52.3% according to Segal's method using Equation (4.1) (Segal, 1959):

$$Crl(\%) = \left(\frac{I_{200} - I_{am}}{I_{200} \times 100} \right) \quad (4.1)$$

Where I_{200} is the maximum intensity of the (200) lattice diffraction peak at $2\theta \approx 22^\circ$ - 25° and I_{am} is the lowest intensity at $2\theta \approx 18^\circ$, representing the amorphous part of the sample.

The peak Ag-CNTs in Figure 4.3 with an average particle size of 48.96 nm shows one weak peak at about $2\theta = 26.0$ originating from CNTs while the crystallographic peaks at 38.2° , 44.2° , 64.3° and 77.4° can be assigned respectively to (111), (200), (220), and (311) crystalline planes originating from silver nanoparticles (Dhibar and Das, 2014; Xu *et al.*, 2019). It was further observed that the nano-crystalline silver coating has a strong (111) orientation along the nanotube's axial direction because the specific free energy of silver is minimum on (111) planes of the face center cubic structure (Peng, and Chen, 2012).

Ag-CNTs-CNCs revealed characteristic diffraction peaks at 2θ values of 26.5° , 38.2° , 44.2° , 64.3° , and 77.4° which corresponds to, (002) of CNTs, and (111), (200), (220) and (311) crystal planes of Ag NPs with an average particle size of 52.14 nm with a shift in the diffraction peak originating from CNCs origin 22.2° to 26.5° . This is attributable to the polar- π interactions between the C-H in cellulose and carbon rings of CNTs (Shariatnia *et al.*, 2020). Over all, the crystallinity value of pristine CNCs was 52.3% and decreased to 49.86% after modification with Ag NPs and CNTs to form Ag-CNTs-CNCs nanocomposites. It could be seen that the modification resulted in no change in the crystallinity of CNTs, and slight decrease in the crystallinity of CNCs. Previous studies by Lin *et al.* (2018) had established a decrease in the crystallinity of CNCs when modified with hydrophobic agents.

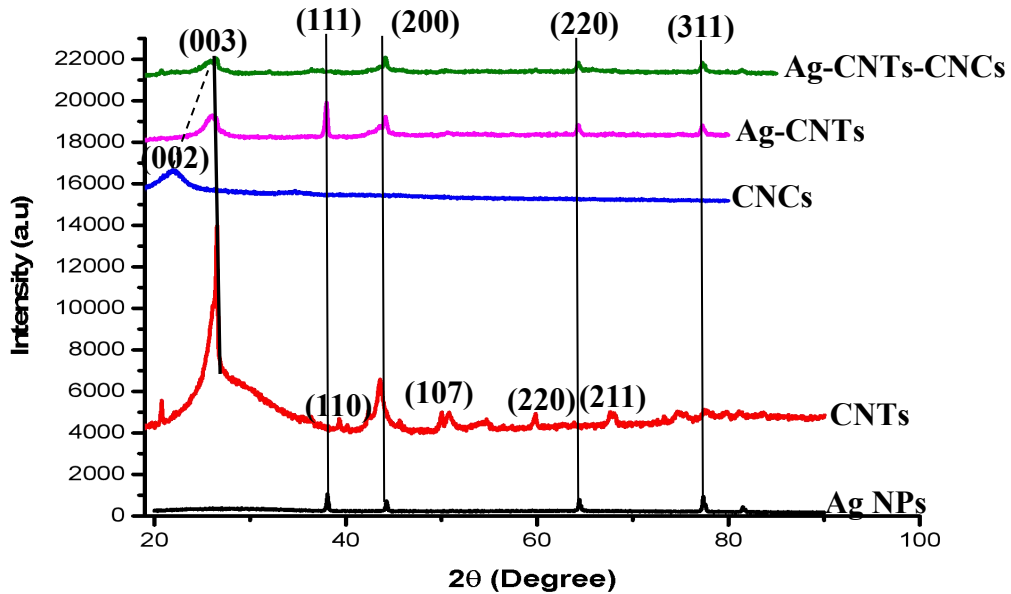


Figure 4.3: XRD Graph of Ag-NPs, Carbon Nanotubes (CNTs), Cellulose Nanocrystals (CNCs), Ag-CNTs and Ag-CNTs-CNCs Composites

However, diffraction peaks in CNTs with planes such as (110), (107) (220), and (211) were absent in the Ag-CNTs-CNCs nanocomposite, this may be due to the fact that

these planes corresponded to residual metallic catalyst (Ni and Fe) that were substituted by Ag NPs during ultrasonic cavitation.

4.1.5 High Resolution Transmission Electron Microscopy (HRTEM) of the sample

HRTEM result was explored for further insight into the microstructure (shape) and crystallinity of the as-prepared Ag-NPs, CNTs, CNCs, Ag-CNTs and Ag-CNTs-CNCs nanomaterials. Plate II (a-e) displays the HRTEM images of the prepared nanomaterials respectively. According to Plate II (a) the HRTEM images of Ag NPs shows that Ag nanoparticles were uniformly distributed with a quasi-spherical morphology over the surface with an average diameter of 12–14 nm, as similarly reported by Dhibar and Das in 2014. From Plate II (b) the average external diameter and length of synthesized CNTs are 44.3 nm and 6.15 μm respectively. Dark spots were observed inside the tubes, which denoted the presence of bi-metallic Fe-Ni from the catalyst. The HRTEM images of the CNTs also revealed the multi walled nature of the nanoparticles with high crystallinity (Larrude *et al.*, 2014). In addition, the CNTs showed open ends due to the higher oxidation on the CNTs tips, which indicates C=C bond breakages (Gómez *et al.*, 2016). A closer inspection of the CNCs obtained from HRTEM analysis in Plate II (c) revealed two dimensional sheet-like structure of CNCs with smooth surfaces that gave rise to a loose surface and porous nano- membrane that improved the hydrophilicity of the composite (Radhakrishnan *et al.*, 2020). Plate II (d) shows the HRTEM micrograph of CNTs decorated with Ag-NPs. The silver nanoparticles are the spots on the CNTs surfaces. The HRTEM image shown in Plate II (d) exhibits silver particles with sizes ranging from 10 to 14 nm attached on the outer layers of CNTs. Almost no free particles were observed in the morphology of Ag-CNTs, which confirms that most of the formed Ag NPs were firmly anchored to the nanotubes (Larrude *et al.*, 2014). HRTEM was also

used to determine how silver nanoparticles were attached to the surface of the nanotubes. The shape and crystallographic structure of the silver nanoparticles with respect to the graphite planes in the tubes were also examined. Accordingly, the nanocrystals growing on the tube surface apparently did not damage the nanotube wall structures. In fact, the (002) graphitic planes (0.33 nm interplanar distance) and (111) silver planes (0.23 nm interplanar distances) were found to be perpendicular to each other. The overall synergy between Ag NPs and CNTs composite resulted in an improved nanocomposite with denser convolutions pertinent for the sequestration of heavy metal ions from industrial effluent.

In the case of the Ag-CNTs-CNCs composite as presented in Plate II (e), both Ag and CNCs approached the CNTs and infiltrated into it due to their smaller length scales. Although there are CNCs aligned along the CNT sidewalls, it appears that CNCs mainly tends to attach to CNTs by their tips as shown in Plate II (e). This implies that a stronger C-H- π interactions took place between the tip of CNCs and sidewalls of CNT rather than an interaction between the hydrophobic (200) crystalline plane of CNCs because of a lower curvature associated with MWCNTs compared to SWCNTs (Mougel *et al.*, 2016). It is worthy of note that CNCs are more concentrated in some regions which suggests that these more concentrated regions might be due to defects on the sidewalls of CNTs.

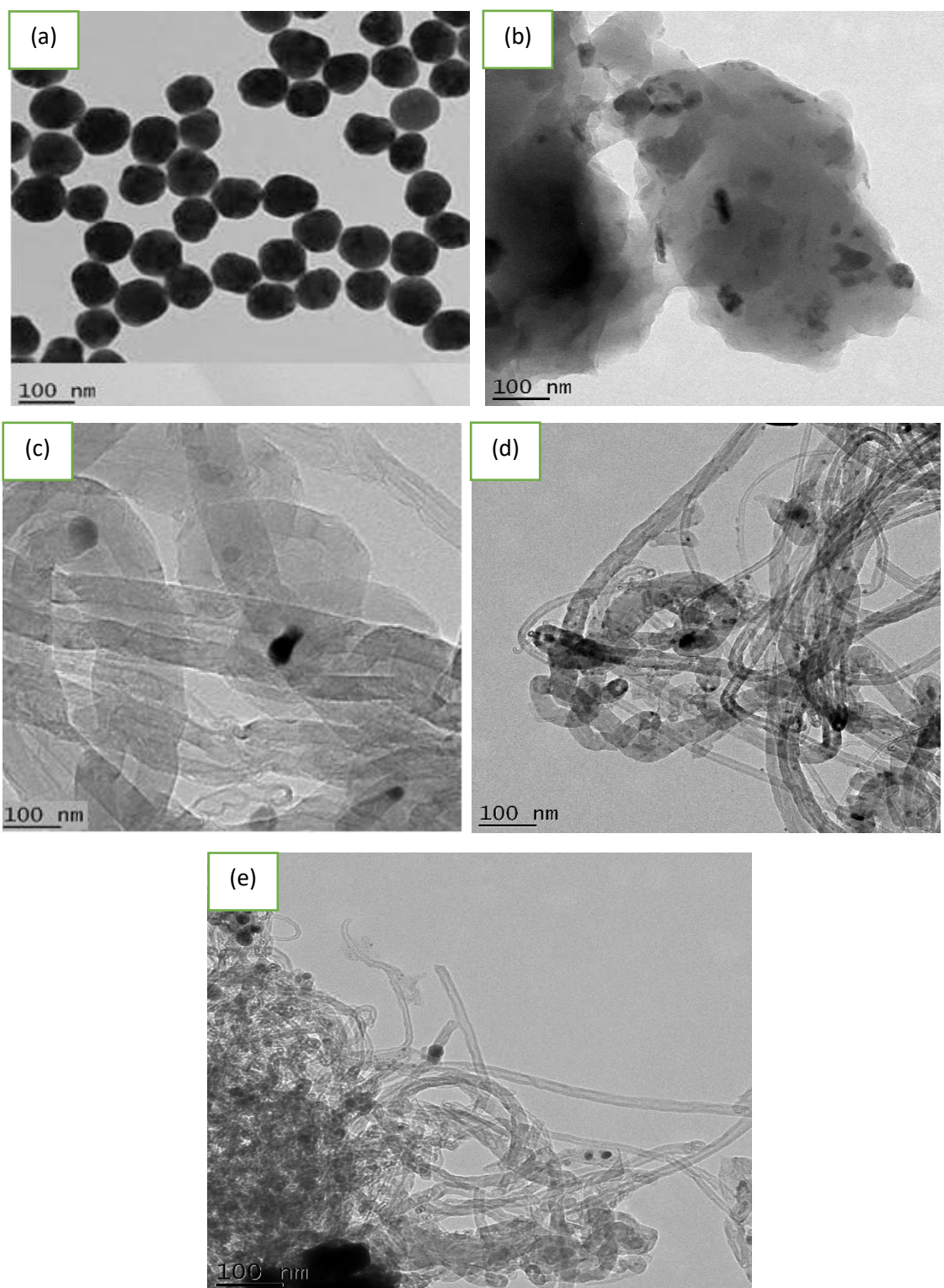


Plate II: HRTEM Micrographs of (a) Silver Nanoparticles (Ag NPs), (b) Cellulose Nanocrystals (CNCs), (c) Carbon Nanotubes (CNTs), (d) Ag-CNTs composites, (e) Ag-CNTs-CNCs composite

Overall, CNCs formed nano-membrane framework with CNTs, signifying that the binding between CNCs and MWCNTs is stronger compared to that of individual CNCs (Shariatnia *et al.*, 2020).

Hence, CNCs-CNTs matrix provided an excellent site for the incorporations of Ag NPs since CNCs acts a dispersing agent improving the dispersion of CNTs in aqueous media as well as disrupting bulk aggregation between the nanoparticles by decreasing the surface energy of the system. This resulted to a more uniform distribution of Ag NPs in the Ag-CNTs-CNCs composite as compared with Ag-CNTs composite in Plate II (d). Similarly, Zamudio *et al.* (2006) have reported that nitrogen-doped MWCNTs nanocomposites exhibited uniform coverage with Ag nanoparticles whereas; pristine MWCNTs resulted in non-homogeneous coverage of Ag clusters that tend to agglomerate with other Ag particles. HRTEM from this study shows that this agglomeration could be eliminated due to the polar- π interactions between the C-H in cellulose from CNCs and carbon rings of MWCNT as well as lowering the number of O-H bonds in cellulose after interaction with TEMPO, which enhanced the dispersion and stabilization of the Ag-CNTs-CNTs matrix in the system (Shariatnia *et al.*, 2020).

4.1.6 Selected Area Electron Diffraction Pattern (SAED)

The SAED pattern for Ag-NPs in Plate III (a) showed ring like diffraction patterns characteristic of crystalline Ag nanoparticles. The diffraction rings were indexed on the basis of the face cubic crystals (FCC) structure of Ag (Dhibar and Das, 2014). The rings originated due to reflections from (111), (200), (220), and (311) lattice planes of (FCC) in Ag NPs as corroborated by XRD results in Section 4.1.4.

CNTs presented in Plate III (b) exhibits the strong diffraction rings for the (002) and (110) diffractions, and a pair of weak rings for the (111) and (211) diffractions. The

presence of diffuse haloes and sharp rings might originate from the amorphous carbon film on the

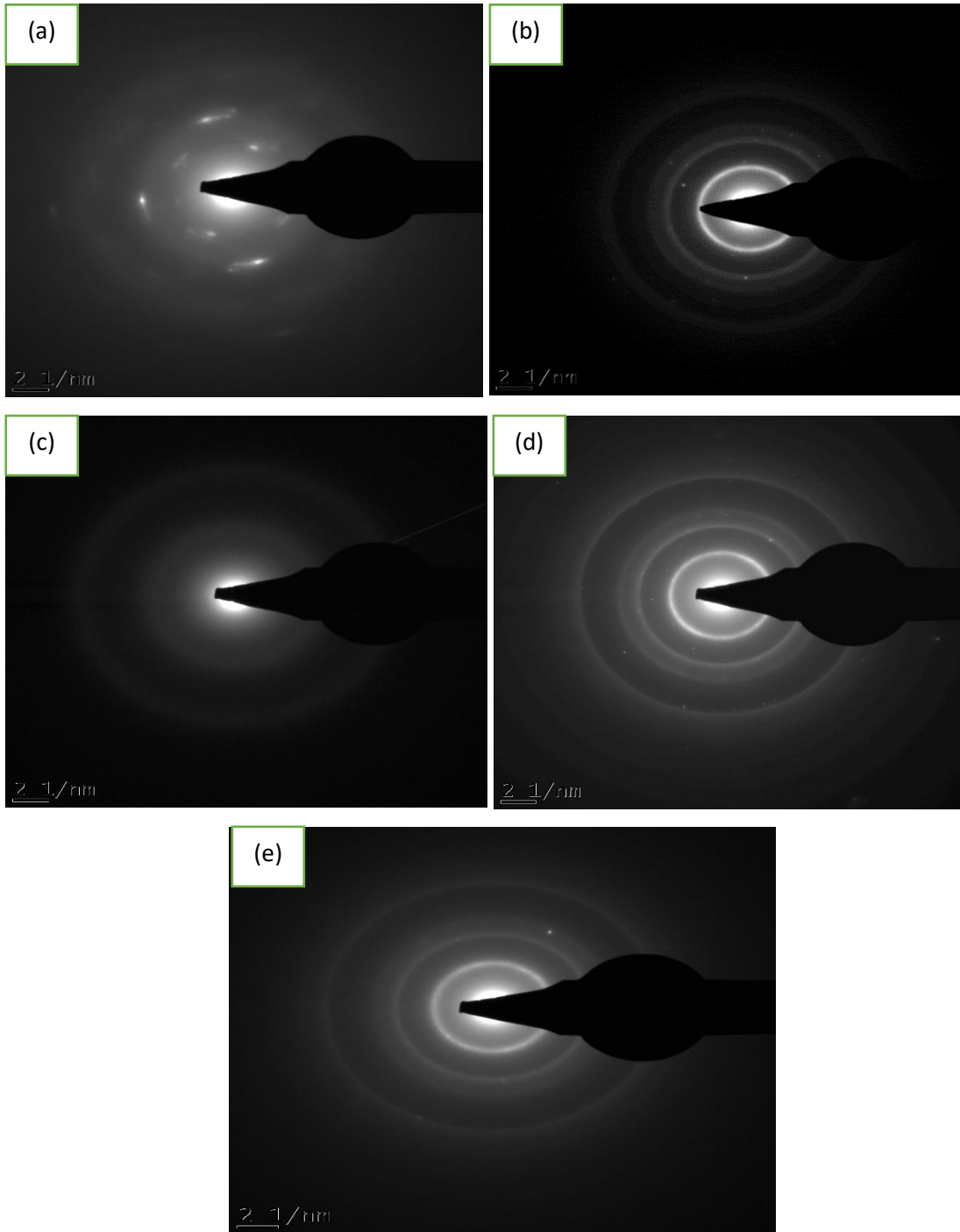


Plate III: SAED Micrographs of (a) Silver Nanoparticles (Ag NPs), (b) Carbon Nanotubes (CNTs), (c) Cellulose Nanocrystals (CNCs), (d) Ag NPs-CNTs composites, (e) Ag NPs-CNTs-CNCs composite

copper grid and the MWCNTs. Using the reciprocal lattice spacing ($\frac{1}{d}$) measured from the ring occurrences, the interplanar distance (d) was determined. The interplanar

spacing values (d) were calculated with the Image J software using the diffraction ring diameter and the camera length of the SAED images. The calculated interlayer spacing of approximately 0.33 nm, which corresponds to the (002) distance of the graphite carbon, and agrees with values reported by Aliyu *et al.* (2017). The resultant selected-area electron diffraction (SAED) pattern for CNCs (Plate III (c)) consists of a strong diffraction ring for (200) which is characteristic of type I cellulose, with a lattice spacing of 0.33 nm similar to that of polycrystalline graphite suggesting a well-crystallized structure (Lin, 2014). The SAED image in Plate III (d) evidences the presence of diffraction bright spots or lattice fringes with interplanar spacings of 0.33 and 0.23 nm due to (002) and (111) diffraction planes of graphitic carbon and Ag nanoparticles respectively, supporting the results obtained from XRD investigation. Other less obvious ring patterns belonging to the, (200), (220), and (311) planes of Ag indicated the polycrystalline nature of Ag NPs as established by Kim *et al.* (2020).

While the (SAED) pattern in Plate III (e) for the Ag-CNTs-CNCs composite is representative of (002), (111) and (110) diffraction rings originating from CNTs characteristic of graphite, Ag and from CNCs, which is distinct of type I cellulose respectively (Lin, 2014, Lin *et al.*, 2018). These values were substantiated and further confirmed by the XRD results in the next Section 4.1.4.

4.2 Physiochemical Characterization of Effluent before Batch Adsorption

The battery effluent was characterized to determine the initial concentration of the five selected heavy metals and contaminants present before treatment.

Table 4.2 shows initial concentration of heavy metals in battery effluent while Table 4.3 shows physicochemical characteristics of battery effluent before treatment.

Table 4.2: Initial Concentration Metals ion in Battery Effluent

Heavy metal	Initial concentration (mg/L)	National discharge standard (mg/L)	Reference
Nickel	1.665	0.25	NESREA, 2011
Iron	23.647	0.3	WHO, 2017
Copper	2.309	0.01	NESREA, 2011
Lead	7.575	0.01	WHO, 2017
Zinc	1.084	0.2	WHO, 2017

Table 4.3: Physicochemical Characteristics of Battery Effluent before Adsorption

Parameter	Raw	NESREA (2011)
pH	1.1	6.5-8.5
TDS (mg/L)	8,146	--
Conductivity (μS/cm)	12,231	--
Dissolved Oxygen (mg/L)	4.83	4.0
Ammonium (mg/L)	4.00	2.0
Chloride (mg/L)	4.30	350
Cyanide (mg/L)	0.80	0.05
Fluoride (mg/L)	3.21	----
Sulphate (mg/L)	112	500
COD (mg/L)	720	30
BOD ₅ (mg/L)	17.0	6.0
Total Bacteria Count (cfu/ml)	0.00	----

Table 4.2 revealed the presence of the five selected heavy metals in battery effluent at different concentrations. The selected heavy metals were found to be beyond the maximum acceptable levels. Zinc (Zn) had the least concentration (1.084 mg/L) and Iron (Fe) with the highest concentration (23.647 mg/L). Nickel (Ni) and lead (Pb) are listed as category 1 carcinogenic metals by International Agency for Research on

Cancer (Debasree, 2014). In Table 4.2 the pH is 1.1 and not within the range of acceptable limits for effluents discharge (6.5 – 8.5) set by NESREA (NESREA, 2011), showing that the effluent sample is highly acidic and the acidity is due to the presence of the electrolyte (H_2SO_4) (Feglian, 2011). There is no WHO nor NESREA guidelines for the Total Dissolved Solids (TDS). However, drinking- water becomes significantly and increasingly unpalatable at TDS level greater than 1000 mg/L (WHO, 2011). The TDS value is greater than 1000 mg/l which is above the permissible limit. The sulphate concentration falls within the NESREA (2011) guideline values (<500) in contrast with Ammonia, Nitrate, Cyanide, DO, COD and BOD_5 which exceeds the permissible limit set by NESREA (2011). WHO (2011) health base guidelines for chloride value in national drinking water standard (including Nigeria) must not exceed 0.3 mg/l. However, in this study the chloride ion is 4.30 mg/l indicating it goes beyond acceptable limit. High chloride content may harm metallic pipes and structures as well as growing plants (Emeka, 2015). The total bacteria count is zero, which is expected because the pH of the battery effluent is too acidic and no living organism can survive under this condition.

From Tables 4.2 and 4.3 the concentration of the selected heavy metal and prominent physicochemical characteristics in the effluent sample and revealed that most of these exceeded their standard permissible limits. Hence, there is a need to either completely remove or reduce the level of these contaminants in the effluent before final discharge into the water bodies.

4.3 Adsorption Parameters

In this study, the influence of parameters such as contact time and adsorbent dosage on the removal efficiency of the selected heavy metals by the developed nano-adsorbents (Ag-CNTs and Ag-CNTS-CNCs) were investigated. These parameters were optimized

by varying one parameter and keeping the other constant. Though the pH also plays an important role in adsorption process of heavy metals from aqueous solution but in this case, the pH was not varied due to the fact that the study was conducted on real battery effluent.

4.3.1 Effect of contact time

The contact time in adsorption plays an important role on the adsorptive kinetics irrespective of the other experimental parameters. The effect of contact time on the removal of copper, iron, lead, nickel and zinc ions onto Ag-CNTs and Ag-CNTs-CNCs nanocomposite are shown in Figures 4.4 and 4.5

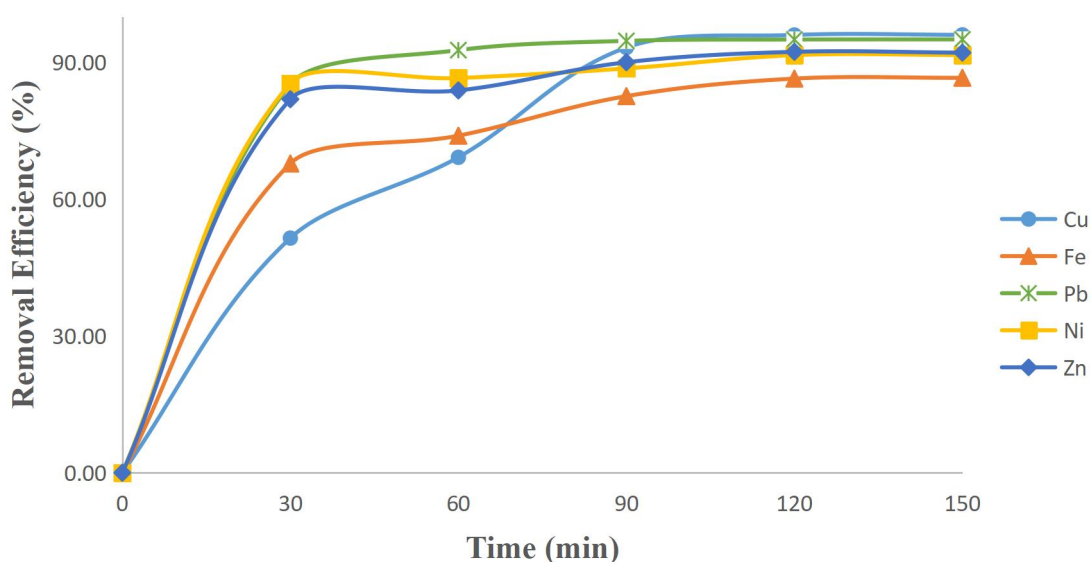


Figure 4.4: Effect of Contact Time on Percentage Removal of Heavy Metal using Ag-CNTs (Experimental Conditions: Stirring Time (90 min Stirrer Speed (180 rpm), Volume of Effluent (50 cm³) and Temperature (27 °C))

In Figure 4.4, the effect of contact time on the removal of Cu, Fe, Pb, Ni and Zn ions from battery effluent using Ag-CNTs composite showed that the adsorption of the metal ions onto the nanoadsorbent increases gradually in the beginning of the reaction until equilibrium was attained at 90 min for copper, iron, zinc, nickel and lead. At optimum

contact time, 90.94%, 82.57%, 94.68%, 88.64% and 90.90% of Cu, Fe, Pb, Ni and Zn were removed respectively by Ag-CNTs composite.

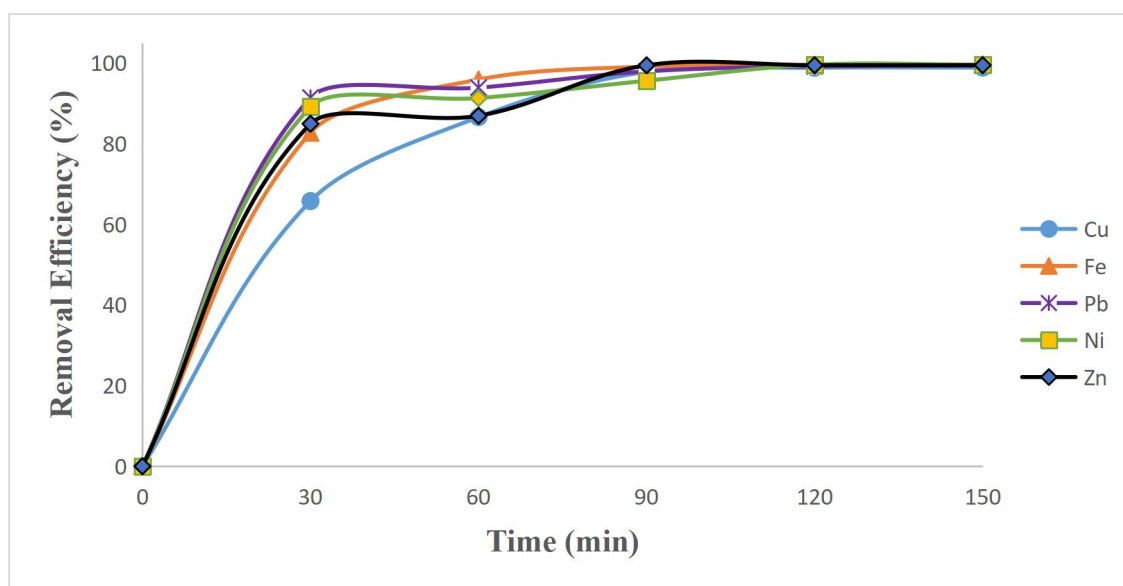


Figure 4.5: Effect of Contact Time on Percentage Removal of Heavy Metal using Ag-CNTs-CNCs (Experimental Conditions: Stirring Time (90 min Stirrer Speed (180 rpm), Volume of Effluent (50 cm³) and Temperature (27 °C))

From Figure 4.5, it can be observed that the adsorption of the metal ions onto Ag-CNTs-CNCs was rapid for the first 30 min for the metals and thereafter, gradually attained equilibrium at 90 min for copper, iron, nickel, lead and zinc. After which adsorption no longer changed with further increase in contact time. Equilibrium removal of Cu, Fe, Pb, Ni and Zn ions were achieved at 97.82%, 99.13%, 97.93%, 95.82 and 99.43% respectively.

The fast adsorption observed for Ag-CNTs and Ag-CNTs-CNCs might be attributed to the availability of a large number of active binding sites on the surfaces of both nanocomposites. Therefore, heavy metal ions occupied most of the vacant active surface area within the first 30 min of the reaction time. The low adsorption rate observed after 30 min of contact time might be due to the progressive decrease in adsorption binding sites on the adsorbent and/or slow diffusion of metal ions into the inner pores (Kumar *et*

al., 2019). Thus, the optimum contact time was fixed at 90 min for the rest of the adsorption experiments. The decrease in the percentage removal of each metal ion below the optimum time could be due to the competition for the decreasing availability of active sites intensified by the metal ions remaining in the solution. This is in agreement with the results obtained by Farghali *et al.* (2017) for removal of Ni (II), Pb (II) and Cu from effluent using O-modified MWCNTs, as well as the findings of Ma *et al.*, 2016 for the removal of Pb (II), Cu (II) and Zn (II) from industrial effluent using MWCNTs. The Ag-CNTs-CNCs successfully removed more of the metal ions than Ag-CNTs suggesting greater interaction between the adsorbent and the adsorbate in the former than the later. This could be attributed to improved dispersibility of Ag in CNTs-CNTs (Plate II (e)) when compared to Ag-CNTs Plate II (d) due to the electrostatic interaction in water when CNCs interacts with the carbon atoms in CNTs and induce local surface charges that enhances the dispersion of the composite water (Shariatnia *et al.*, 2020).

Therefore, good dispersibility of materials in water which allow facile manipulation could be responsible for shorter better adsorption efficiency of Ag-CNTs-CNCs compared to Ag-CNTs. Alternatively, a plausible reason for high adsorption efficiency of Ag-CNTs-CNCs may be due to an increased level of chemical functional groups which translated to more binding sites for chemisorption as described in the mechanism of adsorption in Section 4.7. The metal-ion adsorption rate and mechanism could be described using different kinetic models such as, intra-particle diffusion, pseudo-first-order, and pseudo-second-order kinetic models as discussed in Section 4.6.

4.3.2 Effect of dosage

The effect of adsorbent dosage on the removal of Ni, Cd and Cr ions was studied by varying dosage from 0.01 to 0.05 g. The results obtained using Ag-CNTs and Ag-CNTs-CNCs nanocomposites are presented in Figures 4.6 and 4.7.

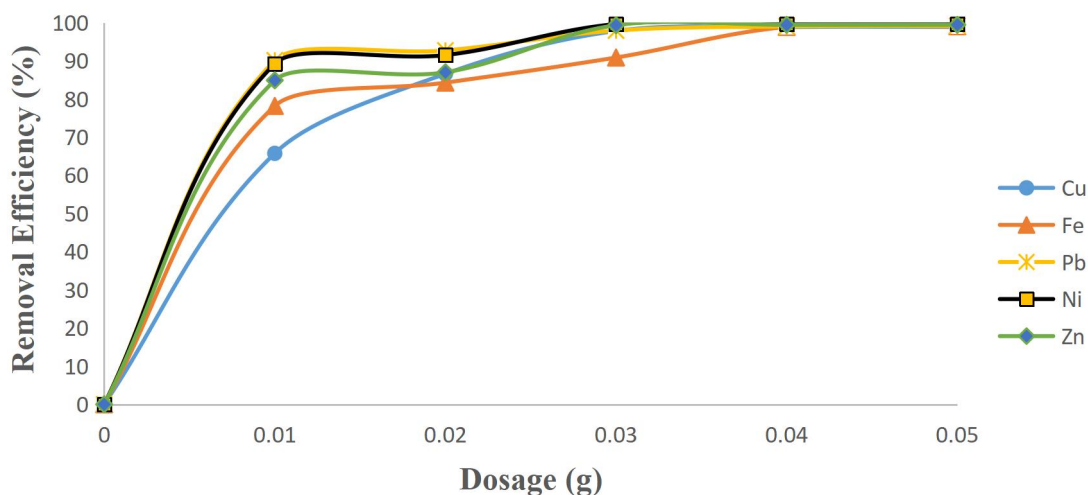


Figure 4.6: Effect of Dosage on Percentage Removal of Heavy Metal using Ag-CNTs (Experimental Conditions: Stirring Time (90 min Stirrer Speed (180 rpm), Volume of Effluent (50 cm³) and Temperature (27 °C))

Figure 4.6 revealed a definite increase in the adsorption capacity of the adsorbent with dosage. After 90 min of adsorption, the remaining concentrations of Cu, Fe, Pb, Ni, and Zn were measured in battery effluent. About 93.67% Pb (II), and 93.89% Fe (II) were adsorbed within 90 min on using a dose of 0.02 g of Ag-CNTs nanocomposite, whereas, 86.79% Zn (II), 89.87% Ni (II) and 93.59% Cu (II) could be removed on using 0.03 g dosage of Ag-CNTs nanocomposite in the battery effluent. Further increase in adsorbent dosage did not improve the adsorption efficiency of metal ions to any significant level. This might be because at large concentration of adsorbent in the solution, the adsorbent begins to agglomerate and the active sites cannot be properly explored for the adsorption of metal ions. In addition, the diffusion paths for contaminants increases when the optimum dosage of the adsorbent is exceeded as explained by Gusain *et al.*

(2109). Therefore, the optimal concentration of Ag-CNTs nanocomposite for further study was determined to be 0.03 g.

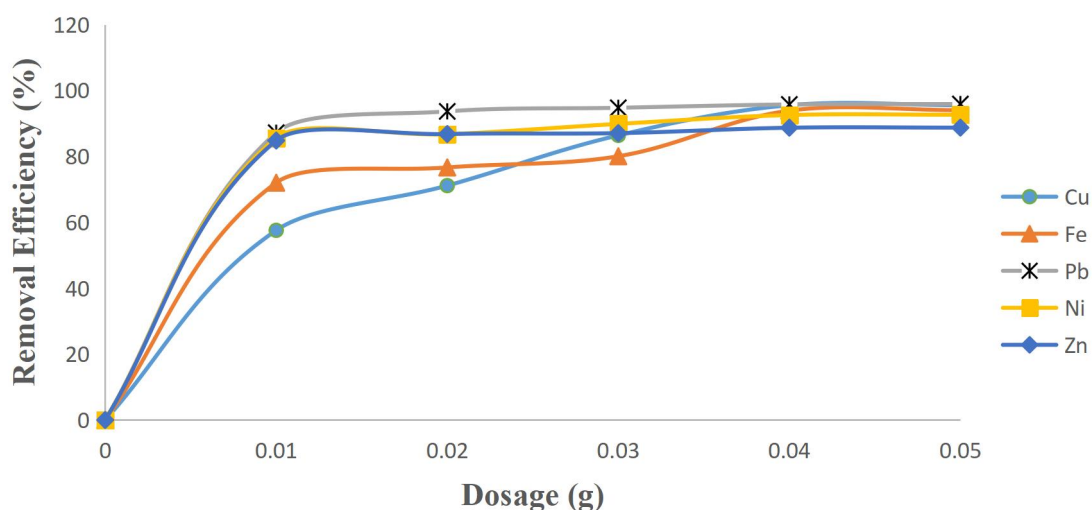


Figure 4.7: Effect of Dosage on Percentage Removal of Heavy Metal using Ag-CNTs-CNCs (Experimental Conditions: Stirring Time (90 min Stirrer Speed (180 rpm), Volume of Effluent (50 cm³) and Temperature (27 °C))

The effect of the Ag-CNTs-CNCs dosage is shown in the Figure 4.7. The removal efficiency was found to increase proportionally with the amount of the Ag-CNTs-CNCs until equilibrium was established and afterwards; the removal efficiency remained constant despite the increment in the dosage of Ag-CNTs-CNCs. Figure 4.7 shows that increasing in the Ag-CNTs-CNCs mass from 0.01 g to 0.02 g sharply enhances the percentage adsorption of Pb from 90.12%-99.01%, Ni from 89.27 to 99.62 % and Zn from 84.89 to 99.62 %. A plateau was observed between 0.03 g to 0.05 g for these three metals, hence increasing the mass of Ag-CNTs-CNCs above 0.02 had a negligible effect on the increase in removal efficiency of the heavy metals in battery effluent. Nevertheless, increasing Ag-CNTs-CNCs mass from 0.02 to 0.03 g increased the percentage adsorption of Cu (II) from 66.76 to 99.68 %, and Fe (II) from 78.17 to 99.07 %.

Relatively, from the results in Figures 4.5 and 4.7 Ag-CNTs-CNCs nanocomposites may adsorb heavy metal ions better than Ag-CNTs due to polar- π interactions between the C-H in cellulose from CNCs and carbon rings of CNTs providing uniform dispersion of Ag in the CNTs-CNCs matrix translating to a high surface area of the former as similarly reported by Shariatnia *et al.*, (2020). Therefore, the maximum dosage for the removal of the metal ions from the battery effluent is 0.02 g for Ag-CNTs-CNCs.

The findings agree with the observation made by Ramana *et al.*, (2013) and Gusain *et al.*, (2019) who worked independently on the removal of heavy metals from effluents using Ag-CNTs and MoS₂/SH-MWCNT respectively. The authors established that increase in adsorption by an increase in adsorbent dose is due to the availability of more number of active binding sites on the surface of the adsorbent, whereas decrease in efficiency at a higher concentration of an adsorbent is due to the decrease in surface active sites by consequence of partial aggregation and agglomeration of the adsorbent leading to an increase in the diffusion path of the metal ions.

4.4 Physicochemical Parameters of Battery Effluent at Batch Adsorptions

The effluent was characterized for their physicochemical properties after adsorption. Table 4.4 shows the result of physicochemical characteristics of battery effluent after adsorption compared with standard limits for effluents discharge.

Table 4.4: Physicochemical characteristics of battery effluent after adsorption process with Ag-CNTs and Ag-CNTs-CNCs

Parameter	Nano-adsorbent			NESREA (2011)	WHO (2017)
	Raw	Ag-CNTs	Ag-CNTs-CNCs	Limit	Limit
pH	1.1	6.43	7.07	6.5-8.5	5.5-8.5
TDS (mg/L)	8,146	174	118	--	600
Conductivity (μ S/cm)	12,231	203	199	--	1000
Dissolved Oxygen (mg/L)	3.83	4.21	4.08	4.0	5.6
Ammonium (mg/L)	4.00	2.83	0.98	2.0	1.5
Chloride (mg/L)	4.30	0.64	0.43	350	250
Cyanide (mg/L)	0.80	0.00	0.00	0.05	0.05
Fluoride (mg/L)	3.21	0.65	0.44	----	1.5
Sulphate (mg/L)	112	26.12	7.28	500	200
COD (mg/L)	720	24.34	13.00	30	40.0
BOD ₅ (mg/L)	37.0	3.14	1.86	6.0	10
Total Bacteria Count (cfu/ml)	0.00	0.00	0.00	-----	-----

According to Table 4.4, the pH of the effluent which was 1.1 (very acidic) improved significantly to 6.43-7.07 depending on the nano-adsorbents. The improved value

closely agrees with the standard. The pH of effluent needs to be maintained between 6.5-8.5 to protect and be beneficial to organisms (NESERA, 2011).

Aquatic organisms are sensitive to the pH changes in its environment because their metabolic activities are pH dependent. Hence, the pH of the treated battery effluent will pose no threat to the aquatic organisms. The investigation of other physico-chemical parameter revealed high concentrations of TDS, BOD, COD, ammonium, cyanide, chloride, fluoride and sulphate as being all within the permissible standard concentrations recommended by either NESREA (2011) or World Health Organization, (2017), The total bacterial count was zero because of the acidic nature of the effluent. As can be seen in Table 4.4, the adsorption of the effluent by Ag-CNTs-CNCs significantly reduced the indicator parameters to fall within the threshold concentrations permissible by the standards. The observed reduction could be attributed to the attachment of the pollutants to the functional groups and massive adsorption sites on the nano adsorbents (Qu *et al.*, 2020). In view of the results, the obtained treated water of both Ag-CNTs and Ag-CNCs-CNCs could be recommended for reuse for various household and industrial purposes.

4.5 Adsorption Isotherms

In the present study, the equilibrium data were analysed using Langmuir, Freundlich and Temkin isotherms to establish which of the isotherms that best described the adsorption process. The Langmuir model supposes that the adsorption happens on a monolayer surface at the specific sites of the adsorbent (Balouch *et al.*, 2013). A well-known linear form of Langmuir model is presented in Tables 4.5 and 4.6, where q_m is the maximum amount of the adsorption capacity (mg/g) of each ion, which is adsorbed to form a complete monolayer covered on the surface at the equilibrium. C_e is the equilibrium

concentration (mg/L), q_e is the amount of each metal ion adsorbed at the equilibrium (mg/g), and K_L is the Langmuir constant (L/mg), which is related to the surface affinity of the respective metal ion to the nanomaterial adsorbent. The crucial characteristics of the Langmuir isotherm may be expressed in terms of the equilibrium parameter R_L , which is known as the separation factor or the equilibrium parameter (see Equation (3.13)).

The R_L values indicate the type of adsorption as to whether it is unfavorable ($R_L > 1$), linear ($R_L = 1$), favorable ($0 < R_L < 1$), or irreversible ($R_L = 0$) (Yuan *et al.*, 2015). A plot of $\frac{1}{q_e}$ against $\frac{1}{C_e}$ yielded a straight-line graph with the values of Q_m and K_L calculated from the slope and intercept, respectively.

The Freundlich isotherm model describes the adsorption on the heterogeneous surfaces with the interaction between the adsorbed molecules and is not limited to the formation of a monolayer (Balouch *et al.*, 2013; Boujelben *et al.*, 2013). This model presumes that as the adsorbate concentration increases, its concentration on the surface of adsorbent also increases. Correspondingly, the sorption energy exponentially decreased on the completion of the sorption centers of the adsorbent. The well-known expression for the Freundlich model are also provided in Tables 4.5 and 4.6 where q_e is the amount of the respective metal ion adsorbed on the Ag-CNTs or Ag-CNTs-CNCs nanocomposite at equilibrium (mg/g) and K_F and nF are the Freundlich constants and the intensity of adsorption, respectively, the constant K_F approximately gives adsorption capacity, $\frac{1}{n}$ is a function of the adsorption strength in the adsorption process. The slope $\frac{1}{n}$ ranging between 0 and 1 is a measure of adsorption intensity or surface heterogeneity. The surface becomes more heterogeneous as its value gets closer to 0 (Farghali *et al.*, 2017).

K_f and n are derived from the intercept and slope of the plot of $\ln Q$ against $\ln C_e$ respectively.

The Temkin adsorption isotherm contains a factor that considers the interaction between adsorbates (Dada *et al.*, 2012). The model assumes that the heat of adsorption of all molecules in the layer will decrease linearly rather than logarithmically with coverage at average concentrations (Temkin 1940, Foo and Hameed, 2010). The heat of adsorption is characterized by a uniform distribution of binding energies up to some maximum binding energy (Foo and Hameed, 2010). The linearized model of the Temkin equation is presented in Tables 4.5 and 4.6, where A_T is the Temkin isotherm equilibrium binding constant (L/g), b_T is the Temkin isotherm constant, R is the universal gas constant (8.314 J/mol/K), T is temperature at 298 K, and β is the constant related to heat of sorption (J/mol).

Table 4.5: Isotherm Parameters for the selected heavy metal removed from battery effluent using Ag-CNTs

Isotherms	Fe	Cu	Ni	Zn	Pb
Langmuir					
$\frac{C_e}{q_e} = \frac{1}{K_L q_m} + \frac{C_e}{q_m}$					
q_m (mg/g)	105.263	238.095	166.667	121.951	119.048
K_L (mg/g) (L/mg) ^{1/n}	0.0419	0.0097	0.0238	0.0326	0.0329
R_L	0.398	0.741	0.539	0.460	0.458
R^2	0.932	0.990	0.994	0.984	0.994
Freundlich					
$\ln q_e = \frac{1}{n} \ln C_e + \ln K_f$					
$1/n$	0.766	0.653	0.718	0.744	0.599
K_f	1.762	2.044	2.126	1.934	1.984
R^2	0.983	0.913	0.991	0.977	0.950
Temkin					

$q_e = \beta \ln A_T + \beta \ln C_e$					
A_T	0.175	0.595	0.358	0.798	1.100
β	38.098	20.962	30.349	18.826	12.744
R^2	0.960	0.854	0.922	0.926	0.954

A_T and β were respectively determined from the intercept and slope of the plot of q_e against $\ln C_e$. The fitting plots of Langmuir, Freundlich and Temkin adsorption of Fe, Cu, Ni, Zn and Pb ions onto Ag-CNTs or Ag-CNTs-CNCs nanocomposites are presented in the Appendix C.

Table 4.5 displays the relevant parameters of Cu (II), Ni (II), Zn (II) and Pb (II) adsorption isotherms on Ag-CNTs. The results show that the correlation coefficients were fitted much better with Langmuir model with R^2 0.984-0.994 than the Freundlich model R^2 0.913-0.983 or Temkin models R^2 0.854-0.954 which suggests that all sites of adsorption on the Ag-CNTs nano-adsorbent have equal affinity to adsorbates and monolayer adsorption process is homogeneous. The result predicts the homogeneity of the adsorption sites and more likely the monolayer coverage of adsorbent surface by the Pb^{2+} , Cu^{2+} , Ni^{2+} Zn^{2+} and Pb^{2+} ions. The results also indicate that all the adsorption sites on the adsorbent are energetically identical (Kanthapazham *et al.*, 2016). Maximum adsorption capacity of q_m mg/g of Fe (II), Cu (II), Ni (II) and Zn (II) ion were given as 105.26, 238.09, 166.67, 121.95 and 199.05 mg/g respectively which suggests a high level of interaction between each metal ions and the Ag-CNTs nanoadsorbent.

The Langmuir isotherm constant (K_L) and R_L were also determined to be in the range of 0.0097-0.419 L/mg and 0.398-0.741, respectively (Table 4.5). The R_L value was less than 1, for each metal ion, indicating that the adsorption of individual metal ions onto the surface of the Ag-CNTs nano-adsorbent was a favorable process as similarly reported by Desta (2013). It also describes monolayer sorption where each metal ion

molecule is adsorbed on distinct localized sorption sites with no transmigration of the adsorbate in the plane of the surfaces giving uniform energies of monolayer sorption onto the adsorbent surface (Wang *et al.*, 2018).

Although the metal ion adsorption favored multiple adsorption isotherms, since the R^2 values for both Langmuir, Freundlich and Temkin were observed to be $R^2 > 0.9$ as observed in Table 4.5. Tofighy and Mohammadi (2015) have earlier established that metal ions sorption onto CNTs based binary composites can be described by both the Langmuir and the Freundlich isotherms. This could be ascribed to metal ions being adsorbed on the adsorbents by multiple mechanisms, including electrostatic attraction and surface complexation, that causes the occurrence of multilayer sorption in the case of Freundlich or Temkin, as well as adsorption by complexation with the surface groups of the adsorbents resulting in a monolayer adsorption as in the case of Langmuir.

However, the regression results in the case of Fe (0.983) indicate that the Freundlich isotherm fitted the experimental results a little better than the Langmuir isotherm, as given in Table 4.5. Overall, the values of $\frac{1}{n}$ were in the range of (0.599-0.756) which being less than 1, indicates that respective metal ions were favorably adsorbed onto the surface of Ag-CNTs adsorbent (Lasheen *et al.*, 2013). Generally, from Table 4.5, the K_f values indicated that Ni had the highest adsorption capacity of (2.126), with Fe (1.762) having the least, indicating that Ag-CNTs nano-adsorbent have a good affinity for Fe (II), Cu (II), Ni (II) Zn (II) and Pb (II) ions.

Furthermore, Temkin isotherm parameter provided in Table 4.5 showed positive heat of adsorption β with values between 12.744-38.098 J/mol while A_T (Temkin isotherm equilibrium binding constant (L/g)) is in the range of (0.175 -1.100). With positive heat of adsorption (β) and binding constant (A_T) values, Temkin isotherm parameters

supports the endothermic behavior of adsorption process. This could be attributed to the high mobility of the heavy metal ions in the battery effluent solution at the ambient temperature (27°C), which further supports the diffusivity of metal ions from the external layer to the internal pores of binary Ag-CNTs composites (Gusain, *et al.*, 2019).

Adsorption isotherm experiments were equally performed to quantitatively analyse the adsorption characteristics of the selected metal ions on the Ag-CNTs-CNCs nanostructures and to gain a deeper understanding of the adsorption mechanism. The experimental adsorption isotherm data were fitted to all the commonly used models, viz. the Langmuir, Freundlich and Temkin models and the obtained results presented in Table 4.6.

Table 4.6: Isotherm Parameters for the selected heavy metal removed from battery effluent using Ag-CNTs-CNCs

Isotherm	Fe	Cu	Ni	Zn	Pb
Langmuir					
$\frac{C_e}{q_e} = \frac{1}{K_L q_m} + \frac{C_e}{q_m}$					
q _m (mg/g)	200.000	263.158	232.047	169.492	181.818
K _L (mg/g) (L/mg) ^{1/n}	0.0410	0.0351	0.0193	0.0411	0.0474
R _L	0.404	0.441	0.589	0.404	0.370
R ²	0.864	0.910	0.725	0.983	0.860
Freundlich					
$\ln = \frac{1}{n} \ln C_e + \ln K_f$					
$\frac{1}{n}$	0.534	0.648	0.711	0.766	0.685
K _f	3.237	2.353	2.804	2.372	2.700
R ²	0.992	0.994	0.995	0.999	0.999
Temkin					
$q_e = \beta \ln A_T + \beta \ln C_e$					
A _T	1.356	1.145	1.220	1.196	2.110
β	28.518	21.025	30.196	23.670	22.923
R ²	0.812	0.848	0.819	0.892	0.800

The experimental data for the Ag-CNTs-CNCs nanostructures were the best fit with the Freundlich isotherm, which had a much higher value of R^2 (0.9917-0.990) compared to other isotherms such as, Langmuir R^2 (0.7252-0.9098), and Temkin R^2 (0.8002-0.8924). Therefore, the adsorption of Fe (II), Cu (II), Ni (II), Zn (II) and Pb (II) ions occurred in a multilayer fashion with non-uniform distribution of heat of adsorption and affinities over the heterogeneous surface of Ag-CNTs-CNCs. The $\frac{1}{n}$ values were <1 and in the range of (0.534-0.766) indicating favorable adsorption for all the heavy metal ions while, K_f values were between 2.363-3.237 suggesting a higher level of affinity between the same set of selected heavy metals with Ag-CNTs-CNCs, as compared to Ag-CNTs, with a lower range of (1.762-2.126) K_f values. This could be attributable to the presence of more binding or active sites on the surface of Ag-CNTs-CNCs, that are responsible for the interaction of the heavy metal ions.

From the Langmuir isotherm the calculated maximum adsorption capacities for Fe (II), Cu (II), Ni (II), Zn (II), and Pb (II) on the Ag-CNTs-CNCs nanostructures were 200.00, 263.156, 232.047, 169.492 and 181.818 mg/g, respectively. The high adsorption capacity of Ag-CNTs-CNCs could be ascribed to its excess more carbon functionality and enhanced metal ion complexation as illustrated in the mechanism of the adsorption in Figure 4.8. Additionally, the obtained Langmuir, K_L was between 0.0193-0.0474 while the separation factor R_L for the Ag-CNTs-CNCs nanostructures was in the range of 0.370-0.589, which was less than 1 for each metal ion, and suggested monolayer adsorption also took place in the system.

In the same vein, Wang *et al.* (2018) had reported that the q_m values calculated from the Langmuir model for Cd(II), Cu(II) and Ni(II) adsorption on γ -PGA-Fe₃O₄-GO-(O-

MWCNTs) were 625.00, 574.71 and 384.62 mg/g, respectively. Which were significantly higher than the adsorption capacity of Fe₃O₄-GO-(O-MWCNTs) for Cd(II), Cu(II) and Ni(II) (94.33, 78.00 and 59.52mg/g), respectively. These was ascribed to the improved negative zeta potential and additional functionalities in the γ -PGA-Fe₃O₄-GO-(O-MWCNTs) nanocomposite.

The Temkin isotherm also showed a good fit with the experimental data for all isotherms studied with R^2 values in the range of 0.8002-0.8924 as presented in Table 4.6. A_T and β values were also in the range 1.145-2.110 L/mg, and 22.923-30.196 J/mol respectively as shown in (Table 4.6). The positive value of A_T and β means that the adsorption was endothermic, confirming the result of the kinetic study.

The adsorption of heavy metal ions is influenced by many factors (related to the properties of the ions in aqueous solutions), such as accessibility centers or interactions and surface binding, which are linked to the size of adsorbed species. From the isothermal results, the adsorption capacity of Cu and Ni is higher than for Fe, Zn and Pb though the ionic radii of Zn (II)_(aq) (74 pm), and Pb (II)_(aq) (119 pm) are larger than Cu(II)_(aq) (73 pm) and Ni (II) _(aq) (70 pm). Previous studies on Cu (II) and Ni (II) revealed that high copper and nickel adsorption can be attributed to their ability to be reduced by the carbonaceous surface (Gupta *et al.*, 2017). However, the relatively lower adsorption of Pb and Zn might be attributed to the lower tendency to form hydrolysis products and its ions do not compete effectively for variable charge surfaces, such as carbonaceous materials (Srivastava *et al.*, 2005; Gao *et al.*, 2009). In this work nevertheless, it is imperative to note that adsorption does not depend clearly on the ionic radius of metal ions, but depends on the properties of the modified binary Ag-CNTs and ternary Ag-CNTs-CNCs nanocomposites. In addition, it is clear that some metal ions tend to interact effectively with some functional groups. Hence, the nature and

concentration of functional groups present in each nanoadsorbent is related to its adsorptive capacity for different metal ions. Consequently, the adsorptive capacity and morphology of Ag-CNTs and Ag-CNTs-CNCs nanocomposites could be attributed to their preparation process and precursors.

4.6 Kinetic Studies

The adsorption kinetics of the selected heavy metal ions onto Ag-CNTs and Ag-CNTs-CNCs was investigated using the pseudo-first-order, pseudo-second-order, and Elovich kinetic models. The pseudo-first-order kinetic model explains the relationship between the sorption sites of the adsorbents that are occupied and the number of unoccupied sites. It is defined using the Lagergren equation (Zhou *et al.*, 2011) as presented in Tables 4.7 and 4.8, where q_e and q_t are the amounts of metal ions adsorbed at equilibrium and at time t (min), respectively, and k_1 is the rate constant of adsorption (min^{-1}). The linear plot of $\ln(q_e - q_t)$ against time was used to determine the rate constant k_1 . The pseudo-second-order kinetic model describes the dependency of the adsorption capacity of the adsorbent on time and was determined from the pseudo-second-order equation as represented in Tables 4.7 and 4.8. where q_e and q_t are the amounts of respective metal ion that is adsorbed at equilibrium and at time t (min), respectively, and k_2 is the pseudo-second-order rate constant (g/mg/min). The linear plot of $\frac{t}{q_t}$ against time is used to determine q_e and k_2 from the slope and intercept, respectively.

The Elovich kinetic model has been used for the chemisorption of gases onto heterogeneous surfaces and solid systems and has found an application for the study of the removal of pollutants from aqueous solutions (Yuan *et al.*, 2015). It describes the second-order kinetics assuming that the solid surface has heterogeneous energy but does not propose any mechanism for adsorption (Mezenner *et al.*, 2009). The Elovich kinetic

model is represented in both Tables 4.7 and 4.8 accordingly, where q_t is the amount of the corresponding metal ion adsorbed at time t , α is the initial rate of adsorption (mg/g/min) and β is related to the extent of surface coverage and activation energy for chemisorption (g/mg). A plot of q_t against $\ln t$ yields a straight line with α and b determined using the slope and intercept, respectively and presented in the Appendix D.

Table 4.7: Pseudo First, Second, and Elovich Diffusion Kinetic Parameters for Adsorption of Selected Heavy Metals on Ag-CNTs

Model	Fe	Cu	Ni	Zn	Pb
Pseudo first order					
$\log(q_e - q_t) = \log q_e - \frac{K}{2.303}t$					
q_{exp} (mg/g)	71.04	51.02	53.33	40.03	28.99
q_{cal} (mg/g)	1.805	2.875	1.875	2.942	3.302
K_1	0.0068	0.0066	0.0052	0.0034	0.0076
R^2	0.685	0.558	0.587	0.258	0.506
Pseudo second order					
$\frac{1}{q_t} = \frac{1}{k_2 q_e^2} + \frac{t}{q_e}$					
q_{cal} (mg/g)	71.412	51.813	52.356	41.152	29.940
K_2	0.0272	0.0103	0.0219	0.0078	0.0067
R^2	1.000	0.999	0.999	0.999	0.999
Elovich model					
$q_t = \frac{1}{\beta} \ln(\alpha\beta) + \frac{1}{\beta} \ln t$					
α (mg/g/min)	22.760	15.246	15.282	10.189	6.750
β (g/min)	0.0614	0.0852	0.0901	0.1189	0.1652
R^2	0.923	0.951	0.929	0.971	0.987

From Table 4.7, the correlation coefficients (R^2) for the pseudo-first order, pseudo-second-order and Elovich were in the range of 0.258-0.6585, 0.999-1.000 and 0.923-0.987, respectively for the Ag-CNTs adsorbent. The adsorption data fit the pseudo-second-order model better than the pseudo-first-order model, and the q_e values ($q_{e,cal}$) calculated from the pseudo-second-order model were more consistent with the experimental q_e values ($q_{e,exp}$). These facts indicated that the adsorption data for the

Ag-CNTs adsorbent was better represented by the pseudo-second-order model (Elmi *et al.*, 2017).

Therefore, it can be concluded that pseudo second-order model could be used to express the adsorption kinetics for the Ag-CNTs adsorbent. This model is based on the assumption that the rate-limiting step may be chemisorptions, which involves the valence forces through sharing or the exchange of electrons between the Ag-CNTs and the respective heavy metal ions. In chemisorption, the heavy metal ions may have possibly adhered to the Ag-CNTs surface by forming chemical bonds and tend to find sites, which can maximize the coordination (Atkins 2014; Elmi *et al.*, 2017). Similar, pseudo-second-order adsorption have been reported for many adsorbents such as acid-chitosan modified carbon nanotubes sheets (Tofighy and Mohammadi, 2015), sodium alginate/hydroxyapatite/CNT (NaAlg-HAp-CNT), nanostructures (Karkeh-abadi *et al.*, 2016), and MoS₂-CNTs nanocomposite (Gusain *et al.*, 2019) for the removal of Cu (II), Pb(II), Zn (II) and Ni (II) metal ions.

Furthermore, since the pseudo-second-order model assumes that each heavy metal ion is adsorbed onto two adsorption sites which allows a stable binuclear bond to form. The rate constant (k_2) was in the range of 0.5143-3.0985, and was larger when compared to the (k_1) (0.0034-0.0076) for pseudo first order and α (0.0614-0.1652) for Elovich at 27°C. This could be attributed to the fact that the propensity of metal ions to migrate from the battery effluent to the bulk phase (Ag-CNTs) is best explained by the second-order kinetics.

The parameters of the adsorption kinetics models for the ternary nanocomposite is presented in Table 4.8. As expected, the correlation regression coefficients (R^2) of the pseudo-second-order kinetics model ($R^2=0.99$) are higher than those of the pseudo-first-

order kinetics model in the range of (0.671-0.755) and Elovich kinetic model with R^2 between 0.931-0.951. In addition, the experimental q_e values are closer to the q_e values calculated using the pseudo-second order kinetics model.

Table 4.8: Pseudo First, Second, and Elovich Diffusion Kinetic Parameters for Adsorption of Selected Heavy Metals on Ag-CNTs-CNCs

Model	Fe	Cu	Ni	Zn	Pb
Pseudo first order					
$\log(q_e - q_t) = \log q_e - \frac{K}{2.303}t$					
q_{exp} (mg/g)	76.15	54.04	55.66	42.74	32.29
q_{cal} (mg/g)	6.039	2.085	2.017	2.731	2.246
K_1	0.0176	0.0073	0.0068	0.0089	0.0073
R^2	0.755	0.724	0.751	0.716	0.671
Pseudo second order					
$\frac{1}{q_t} = \frac{1}{k_2 q_e^2} + \frac{t}{q_e}$					
q_{cal} (mg/g)	71.943	60.606	51.631	45.872	35.088
K_2	0.1973	0.0240	0.0077	0.0167	0.0161
R^2	0.999	0.999	0.999	0.999	0.999
Elovich model					
$q_t = \frac{1}{\beta} \ln(\alpha\beta) + \frac{1}{\beta} \ln t$					
α (mg/g/min)	19.095	17.171	14.427	12.635	9.334
β (g/min)	0.0680	0.0795	0.0951	0.1057	0.1383
R^2	0.951	0.931	0.932	0.941	0.951

The consistency of the experimental data with the pseudo-second-order kinetics model indicates that the rate-limiting step may be chemical adsorption (chemisorption) involving valence forces through sharing or exchanging electrons between corresponding heavy metal ions and the Ag-CNTs-CNCs nanocomposite. In chemical adsorption, it is assumed that the adsorption capacity is proportional to the number of

active sites (functional groups) incorporated on the adsorbent surface (Figaro *et al.*, 2015; Tofighy and Mohammadi 2015).

In tandem to this study, are the reports from Lasheen *et al.* (2014) who used pristine and acid oxidized multi-walled carbon nanotubes (MWCNTs) to establish a second-order kinetics for the removal of Pb^{2+} , Cu^{2+} , Cd^{2+} , Ni^{2+} and Cr^{+6} ions. Since the correlation coefficients of the pseudo-second-order equation for the linear plots are very close to one and calculated q_e values agreed very well with the experimental data, the pseudo-second-order kinetics was a pathway to reach the equilibrium and the rate-limiting step in adsorption is chemisorption. Gusain *et al.* (2019) also reported that the removal of Pb (II) and Cd (II) from industrial mine water by ternary hierarchical molybdenum sulfide (MoS_2)/thiol-functionalized multi-walled carbon nanotube $\text{MoS}_2/\text{SH-MWCNT}$ nanocomposite was best described using the pseudo second-order-kinetics. More recently, Tao *et al.* (2020) had recounted that the use of cellulose nanocrystals-graphene oxide composite in the removal of levofloxacin hydrochloride antibiotic from aqueous solution was also followed the pseudo second-order-kinetics.

4.7 Adsorption Mechanism

A close examination of the HRSEM results in Section 4.1.1, suggests that a possible adsorption mechanism for Fe(II), Cu(II), Ni(II), Zn(II) and Pb(II) ions adsorption by Ag-CNTs-CNCs as illustrated in Figure 4.8 was principally controlled simultaneously by supportive parameters including surface adsorption/diffusion, electrostatic interaction and surface complexation. From HRSEM information, the porous surface of Ag-CNTs-CNCs enhanced the mass transfer and provided adsorption routes and area responsible for Fe(II), Cu(II), Ni(II), Zn(II) and Pb(II) ions removal via diffusion to available defects, and subsequent attachment to the surface of the adsorbent. However,

the occurrence of electrostatic interaction was clearly evident between the positively charged heavy metal ions and negatively charged carboxylate ions (COO^-) attached to Ag-CNTs-CNCs nanocomposite after purification. In addition, Isotherm studies revealed that the adsorption follows the Freundlich adsorption isotherm and hence obeys multilayer adsorption of Fe(II), Cu(II), Ni(II), Zn(II) and Pb(II) ions) on Ag-CNTs-CNCs nanocomposites.

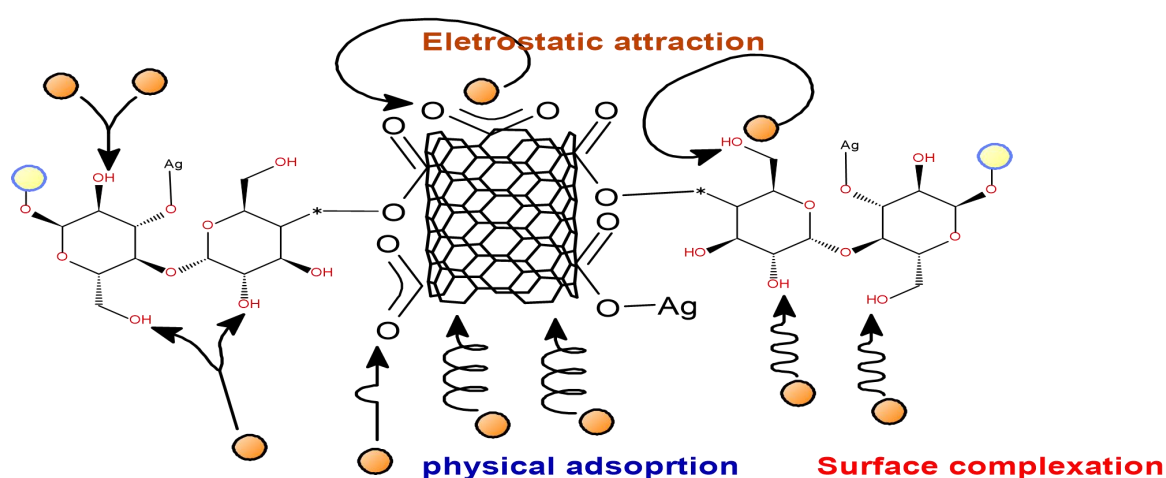



Figure 4.8: Possible Adsorption Mechanism of Fe(II), Cu(II), Zn(II), Ni(II), and Pb(II) Ions Adsorption by Ag-CNTs-CNCs

Key

 is a metal ion such as Fe^{2+} , Cu^{2+} , Ni^{2+} , Zn^{2+} , or Pb^{2+}

Furthermore, inner layer adsorption of metal ions on Ag-CNTs-CNCs nanocomposite can be attributed to the formation of the metal-oxygen complex between the Fe(II), Cu(II), Ni(II), Zn(II) and Pb(II) ion and oxygen present on the Ag-CNTs-CNCs in the aqueous solution through the exchange of H^+ ions. More so, ion exchange and surface complexation were obvious in the combination of the positively charged metal ions and the active sites of negatively charged Ag-CNTs-CNCs through electrostatic attraction, and subsequent removal via the carboxyl and hydroxyl groups (Bo *et al.*, 2020). This

shows that the bonding of the heavy metal ions with the adsorbent was multilayered adsorption and associated with the electrostatic interaction between the respective metal ions and the negatively charged functional groups (such as COO^- , and OH^-) on the adsorbent. Therefore, hydroxyl/deprotonated groups could form complexes with Fe(II), Cu(II), Ni(II), Zn(II) and Pb(II) ion. Hence, the surface complexation mechanism occurred via metal ions deposition on the adsorbent-adsorbate interface and intermolecular interaction between the metal ions and the adsorbent (Zhang *et al.*, 2020). Finally, from the kinetic studies, since the adsorption process for each selected heavy metal is best described by pseudo-second-order kinetics model. This implies that the rate-limiting step is chemical adsorption (chemisorption), which involves valence forces through sharing or exchanging electrons between corresponding heavy metal ions and the Ag-CNTs-CNCs nanocomposite indicating that electrostatic attraction placed a major role in the adsorption mechanism (Tofighy & Mohammadi 2015).

CHAPTER FIVE

5.0 CONCLUSIONS AND RECOMMENDATIONS

5.1 Conclusion

This study, bimetallic Fe-Ni supported on kaolin was synthesized using a wet impregnation method for the production of carbon nanotube (CNTs) by the catalytic chemical vapour deposition method. CNCs was synthesized via TEMPO-mediated oxidation of dried plantain trunk (DPT), while Ag nanoparticles was prepared by the reduction of $\text{Ag}(\text{NO}_3)$ via green synthesis. Subsequently, the as-synthesized CNTs were purified using 30% (v/v) $\text{HNO}_3/\text{H}_2\text{SO}_4$ and modified with CNCs and Ag nanoparticles via an environmental friendly and facile route.

The Ag-CNTs, and Ag-CNCs-CNTs modified CNTs were characterised using standard analytical techniques. The adsorption potentials of Ag-CNTs, and Ag-CNCs-CNTs for the removal of selected heavy metals from battery effluent was studied. The effects of contact time and adsorbent dosage on the removal efficiency of the selected metals were investigated. The generated equilibrium data were fitted to different isotherms and kinetic models.

The acid treatment of as-synthesized CNTs with $\text{HNO}_3/\text{H}_2\text{SO}_4$ removed residual catalyst and amorphous carbon. TEMPO-mediated oxidation of dried plantain trunk (DPT) gave a high level of pristine CNCs. Ag nanoparticles was successfully prepared by the bio-reduction of AgNO_3 with aqueous tea extract. XRD, EDS, SAED provided uniform evidence that CNCs and Ag nanoparticles were successfully grafted into the CNTs matrix resulting to Ag-CNTs-CNCs nanocomposites, due to polar- π interactions

between the C-H in cellulose from CNCs and carbon rings of CNTs matrix with the Ag metal ions.

The Ag-CNTs-CNCs possessed better-defined ridges, wrinkles, micro and nano-pores throughout the entire surface, which are believed to be due to the synergistic interaction between Ag, CNCs and CNTs in the nanocomposite, derived from the protection of junction and entanglement points in the continuous CNTs network by the closely packed CNCs matrix. It was established that optimum contact time and adsorbent dosage for the removal of the selected heavy metal from the battery effluent was 90 min and 0.03 g for Ag-CNTs and 90 min 0.02 g for Ag-CNTs-CNCs respectively.

The maximum % removal efficiency of the heavy metals from battery effluent by the Ag-CNTs-CNCs nano-adsorbents, is Fe (99.13 %), Cu (97.82 %), Zn (99.43 %), Ni (95.62 %), and lastly Pb (97.93 %). Compared to Ag-CNTs with Fe (86.64 %), Cu (90.94 %), Ni (88.64 %), Zn (90.90 %), and lastly Pb (94.68 %). Ag-CNTs-CNCs was more efficient than Ag-CNTs in removal of selected heavy metals due to improvement in adsorption capacity and removal efficiency. The adsorption isotherm for the Fe, Cu, Ni, Zn and Pb ions using Ag-CNTs were best fitted by the Langmuir model. With respect to Ag-CNTs-CNCs isothermal model for Fe, Cu, Ni, Zn and Pb, were better fitted for Freundlich than Langmuir due to the high regression correlation coefficient of the former. Both Ag-CNTs and Ag-CNTs-CNCs obeyed pseudo-second order model indicating chemisorption in relationship with the removed heavy metal ions. The proposed mechanism of the adsorption process recounts that the removal of the selected heavy metal from the battery effluent occurred via a combination of , physical adsorption, and chemical interactions such as, electrostatic attraction and surface complexation.

5.2 Recommendations

Research in heavy metal removal from industrial effluent using nanocomposites as adsorbents is a continuous process.

1. The Usage of Ag-CNTs-CNCs composite for the treatment of other pollutants present in other effluents such as dye effluent and oil spills is recommended
2. There should be further studies on the characterization of the as-synthesized nanocomposite before and after adsorption by analytical techniques such as, BET, FTIR and XPS would help to further understand the interaction between the nanocomposite and respective metal ion.
3. The peak adsorption capacity and best-fit conditions for the batch adsorption should be investigated using response surface response methodology.
4. The Maximum adsorption capacity of Fe, Cu, Ni, Zn and Pb can also be determined using a fixed column bed (Column adsorption).
5. Detailed investigation of desorption of heavy metal ions and regeneration of the spent Ag-CNTs, and Ag-CNTs-CNCs nanocomposite needs to be considered.

5.3 Contribution to Knowledge

1. CNCs was produced using inexpensive plantain trunk waste and was subsequently modified with CNTs and Ag NPs by a simple and efficient method to produce novel Ag-CNTs nanoadsorbents with a high adsorption capacity.
2. The optimum batch adsorption parameters for the novel Ag-CNTs-CNCs nano adsorbent were established and the adsorption capacity was determined for the removal of metal ions Fe^{2+} , Cu^{2+} , Ni^{2+} , Zn^{2+} and Pb^{2+} from battery effluent.

3. The adsorption studies confirmed that adsorption of selected metal ions takes place via physical adsorption, and metal coordination by electrostatic interactions and surface complexation between adsorbent and the heavy metal ions.

REFERENCES

- Abbasi, E., Sedigheh, F. A., Abolfazl, A., Morteza, M., Hamid T. N, Younes, H., Kazem, N-K., & Roghiyeh, P.A. (2014). Dendrimers: synthesis, applications, and properties. *Nanoscale Research Letters*, 9(1), 247–255.
- Abdul-Khalil, H. P. S., Davoudpour, Y., Islam, M. N., Mustapha, A., Sudesh, K., Dungani, R., & Jawaaid, M. (2014). Production and modification of nanofibrillated cellulose using various mechanical processes: a review. *Carbohydrate Polymer*, 99, 649–655. <https://doi.org/10.1016/j.carbpol.2013.08.069>
- Abdulrahaman, M. A., Abubakre, O. K., Abdulkareem, S. A., Tijani, J. O., Aliyu, A., & Afolabi, A. S. (2017). Effect of coating mild steel with CNTs on its mechanical properties and corrosion behaviour in acidic medium. *Advances in Natural Sciences: Nanoscience and Nanotechnology*, 8, 1-14.
- Abu-danso, E., Srivastava, V., Sillanpää, M., & Bhatnagar, A. (2017). Pretreatment Assisted Synthesis and characterization of cellulose nanocrystals and cellulose nanofibers from absorbent cotton. *International Journal of Biology and Macromolecules*, 102, 248–257. <https://doi.org/10.1016/j.ijbiomac.03.172>.
- Adibzadeh, P. & Motakef-kazemi, N. (2018). Preparation and characterization of curcumin-silver nanoparticle and evaluation of the effect of poly ethylene glycol and temperature. *Journal of Nanoanalysis*, 5, 156–162.
- Agency for Toxic Substances and Disease Registry (ATSDR). (2017). Agency for Toxic Substances and Disease Registry. Retrieved from <https://www.atsdr.cdc.gov/index.html>.
- Ahmad, T., & Danish, M. (2018). Prospects of banana waste utilization in effluent treatment: A review Prospects of banana waste utilization in wastewater treatment: A review. *Journal of Environmental Management*, 206, 330–348. <https://doi.org/10.1016/j.jenvman.2017.10.06.1>.
- Ahmed, F., Santos, C. M., Mangadlao, J., Advincula, R., & Rodrigues, D. F. (2013). Antimicrobial PVK: SWNT nanocomposite coated membrane for water purification: performance and toxicity testing. *Water Resources*, 47, 3966–3975.
- Ahmed, S., Ahmad, M., Swami, B. L., & Ikram, S. (2016). Review A review on plants extract mediated synthesis of silver nanoparticles for antimicrobial applications: A green expertise. *Journal of Advanced Research*, 7(1), 17–28. <https://doi.org/10.1016/j.jare.2015.02.007>.
- Ajayan, P. M., & Ebbesen, T. W. (1997). Nanometre-size tubes of carbon. *Report on Progress in Physics*, 60(10), 1025.

- Akinlua, A., & Asubiojo, O. I. (2006). Physico-Chemical and Trace Metal Characterization of Battery Factory Waste. *Journal of Applied Science*, 6(7), 1456-1462. <https://doi.org/10.3923/jas.2006.1456.1462>.
- Alam, J., Alhoshan, M., Dass, L.A., Shukla, A. K., Muthumareeswaran, M. R., Hussain, M., Aldwayyan, A. S. (2016). Atomic layer deposition of TiO₂ film on a polyethersulfone membrane: Separation applications. *Journal of Polymer Resources*, 23, 183-185
- Alina, M., Azrina, A., Mohd-Yunus, A. S., Mohd-Zakiuddin, S., Mohd-Izuan, E, & Muhammad, R. R. (2012). Heavy metals (mercury, arsenic, cadmium, plumbum) in selected marine fish and shellfish along the Straits of Malacca. *International Food Research Journal*. 19(1), 5-11.
- Aliyu, A., As, A., As, K., Ok, A., Jo, T., & Kariim, I. (2017). Synthesize Multi-Walled Carbon Nanotubes via Catalytic Chemical vapour deposition method on Fe-Ni bimetallic catalyst supported on kaolin. *Carbon Letters*, 21, 33–50.
- Al-Namil, D.S. & Patra, D. (2019) Green solid-state based curcumin mediated rhamnolipids stabilized silver nanoparticles: Interaction of silver nanoparticles with cysteine and albumins towards fluorescence sensing. *Colloids and Surfaces. B Biointerfaces*, 173, 647–653.
- Alves, B. M. A. & Pinho, D. N. M. (2000). Ultrafiltration for colour removal of tannery dyeing wastewaters. *Desalination*, 1303, 147-154.
- Alzahrani, S. & Wahab, A. (2014). Journal of water process engineering challenges and trends in membrane technology implementation for produced water treatment: A review. *Journal of Water Processing Engineering*, 4, 107–133.
- Amadi, A. N. & Nwankwoala, H. (2015). Evaluation of heavy metal in soils from Enyimba dumpsite in Aba, south eastern Nigeria using contamination factor and geo-accumulation index. *Energy and Environment Research*, 3(1), 125-134.
- Anusha, K.J. (2020). History and Future of Nanotechnology. *Nano Research & Applications*, 6(24), 1–2.
- APHA (American Public Health Association) (2005). Standard methods for the examination of Water and Wastewater (21st Edition). New York, 75 – 86.
- Appenroth, K. J. (2010). *Definition of “heavy metals” and their role in biological systems, in soil heavy metals*. Springer Berlin Heidelberg, Berlin, 19–29.
- Arief, V. O., Trilestari, K., Sunarso, J., Indraswati, N. & Ismadji, S. (2008). Recent progress on biosorption of heavy metals from liquids using low cost biosorbents: Characterisation, biosorption parameters and mechanism studies. *CLEAN – Soil, Air, Water*, 36, 937-962.
- Arsuaga, J. M., Sotto, A., del Rosario, G., Martínez, A., Molina, S., Teli, S. B. & De Abajo, J. (2013). Influence of the type, size, and distribution of metal oxide particles on the properties of nanocomposite ultrafiltration membranes, 428, 131–141.
- Atkins P.W (2014). Physical chemistry, 10th edn. Oxford University Press, Oxford.
- Baby, R., & Saifullah, B. (2019). Carbon Nanomaterials for the Treatment of Heavy Metal-Contaminated Water and Environmental Remediation. *Nanoscale Research Letters*, 14, 341-358.

- Balouch, A., Kolachi, M., Talpur, F.N., Khan, H., Bhanger, M. I (2013). Sorption Kinetics, Isotherm and Thermodynamic Modeling of Defluoridation of Ground Water Using Natural Adsorbents. *American Journal of Analytical Chemistry*, 4, 221–228.
- Balta, S., Sotto, A., Luis, P., Benea, L., van der Bruggen, B., & Kim, J. (2012). A new outlook on membrane enhancement with nanoparticles: The alternative of ZnO. *Journal of Membrane Science*, 389, 155–161.
- Bankole, M. T., Abdulkareem, A. S., Mohammed, I. A., Shaibu, S., Tijani, J. O., & Abubakre, O. K. (2019). Selected heavy metals removal from electroplating wastewater by purified and polyhydroxylbutyratefunctionalized carbon nanotubes adsorbents, *Scientific Reports*. <https://doi.org/10.1038/s41598-018-37899-4>.
- Baruah, A., Chaudhary, V., Malik, R., & Tomer, V.K. (2019). Nanotechnology Based Solutions for Wastewater Treatment. In *Nanotechnology in Water and Wastewater Treatment: Theory and Applications*, Elsevier: Amsterdam, The Netherlands, 337–368.
- Basak, S., Samanta, K. K., Saxena, S., Chattopadhyay, S., Narkar, R., & Mahangade, R. (2015). Flame resistant cellulosic substrate using banana pseudo-stem sap. *Polish Journal of Chemical Technology*, 17, 123-133.
- Baysal, A., Kuznek, C., & Ozcan, M. (2018). Starch coated titanium dioxide nanoparticles as a challenging sorbent to separate and preconcentrate some heavy metals using graphite furnace atomic absorption spectrometry. *International Journal of Environmental Analytical Chemistry*, 00(00), 1–11. <https://doi.org/10.1080/03067319.2018.1427741>.
- Bernholc, J., Roland, C., & Yakobson, B. I. (1997). Nanotubes. *Current Opinion Solid State Material Science*, 2(6), 706–715.
- Bharathi, K. S., & Rameshsrikrishna, P. (2012). Equilibrium, thermodynamic and kinetic studies on adsorption by of a basic dye by *Citrullus lanatus* rind. *Iranica Journal of Energy & Environment*, 3(1), 23-34.
- Bhatnagar, A., & Sillanp, M. (2010). Utilization of agro-industrial and municipal waste materials as potential adsorbents for water treatment-A review. *Chemical Engineering Journal*, 157, 277–296.
- Bilba, K., Arsene, M. A., & Ouensanga A (2007). Study of banana and coconut fibers: Botanical composition, thermal degradation and textural observations. *Bioresource Technology*, 98, 58-68.
- Bo, S., Luo, J., An, Q., Xiao, Z., Wang, H., Cai, W., Zhai, S., Li, Z. (2020). Efficiently selective adsorption of Pb(II) with functionalized alginate-based adsorbent in batch/column systems: Mechanism and application simulation. *Journal of Cleaner Production*, 250, 119-185.
- Boudrahem, F., Aissani-Benissad, F., & Ait-Amar, H. (2009). Batch sorption dynamics an equilibrium for the removal of lead ions from aqueous phase using activated carbon developed from coffee residue with zinc chloride. *Journal of Environmental Management*, 90, 3031-3039.
- Boujelben, N., Bouhamed, F., Elouear, Z., Bouzid, J., & Feki, M. (2013). Removal of phosphorus ions from aqueous solutions using manganese-oxide-coated sand and brick. *Desalination Water Treatment*, 52, 2282–2292.

- Brinchi, L., Cotana, F., Fortunati, E., & Kenny, J. M. (2013). Production of nanocrystalline cellulose from lignocellulosic biomass: technology and applications. *Carbohydrate Polymer*, 94, 154–169.
- Brita, T. A. D. S., Muysen, Karel, A. C., Janssen, Colin, R. (2006). Mechanisms of chronic waterborne Zn toxicity in *Daphnia magna*. *Aquatic Toxicology*, 77(4), 9.
- Cannon, V. T., Zalups, R. K., & Barfuss, D. W. (2016). Molecular homology and the luminal transport of Pb in the renal tubule. *Journal of Hazardous Materials*, 33, 402–509.
- Castro-Muñoz, R., Barragán-Huerta, B. E., Fila, V., Denis, P. C., & Ruby-Figueroa, R. (2018). Current Role of Membrane Technology: From the Treatment of Agro-Industrial by-Products up to the Valorization of Valuable Compounds. *Waste Biomass Valorization*, 9, 513–529.
- Castro-Muñoz, R., Yáñez-Fernández, J., & Fila, V. (2016). Phenolic compounds recovered from agro-food by-products using membrane technologies: An overview. *Food Chemistry*, 213, 753–762.
- Celik, E., Park, H., Choi, H., & Choi, H (2011). Carbon nanotube blended polyethersulfone membranes for fouling control in water treatment. *Water Resources*, 45, 274–282.
- Chaloupka, K., Malam, Y., & Seifalian, A. M. (2018). Nanosilver as a new generation of nanoparticle in biomedical applications. *Trends Biotechnology*, 28, 580–588.
- Chang, T. H., Liu, F. K., Chang, Y. C., & Chu, T. C. (2008). *Chromatographia*, 67, 723–725
- Chico, L., Crespi, V. H., Benedict, L. X., Louie, S. G., & Cohen, M. L. (1996). Pure carbon nanoscale devices: nanotube heterojunctions. *Physics Review Letters*, 76(6), 971–974.
- Chihoon, K., Beom, J. E., Soyoun, J., Taeksoo, J. (2016). Detection of organic compounds in Water by an optical absorbance method. *Sensors*, 16, (61), 12–25. (Doi:10.3390/S16010061 Http://Www.Mdpi.Com/Journal/Sensor).
- Dada, A., Olalekan, A., Olatunya, A., & Dada, O (2012). Langmuir, Freundlich, Temkin and Dubinin-Radushkevich isotherms studies of equilibrium sorption of Zn^{2+} onto phosphoric acid modified rice husk. *Journal of Applied Chemistry*, 3, 38–45.
- Dai, H., & Huang, H. (2017a). Synthesis, characterization and properties of pineapple peel cellulose-G-acrylic acid hydrogel loaded with kaolin and sepia ink. *Cellulose*, 24, 69–84. <https://doi.org/10.1007/s10570-016-1101-0>.
- Dai, H., & Huang, H. (2017b). Enhanced swelling and responsive properties of pineapple peel carboxymethyl cellulose-Gpoly(acrylic acid-co-acrylamide) superabsorbent hydrogel by the introduction of carclazite. *Journal of Agriculture and Food Chemistry*, 65, 565–574.
- Dai, H., & Huang, H. (2016). Modified pineapple peel cellulose hydrogels embedded with sepia ink for effective removal of methylene blue. *Carbohydrate Polymer*, 148:1–10. <https://doi.org/10.1016/j.carbpol.2016.04.040>.
- Daraei, P., Madaeni, S. S., Ghaemi, N., Khadivi, M. A., Astinchap, B., & Moradian, R (2013). Enhancing antifouling capability of PES membrane via mixing with various types of polymer modified multi-walled carbon nanotube. *Journal of Membrane Science*, 444, 184–191.

- Das, R., Ali, M. E., Hamid, S. B. A., Ramakrishna, S., & Chowdhury, Z. Z. (2014). Carbon nanotube membranes for water purification: A bright future in water desalination. *Desalination*, 336, 97–109. <https://doi.org/https://doi.org/10.1016/j.desal.2013.12.026>.
- Debasree, P., Umesh, M., & Swarup, B. (2014). A comprehensive review on Cd (II) removal from aqueous solution. *Journal of chemistry and material*, 4, 2223–2249.
- Deng, S., Huang, R., Zhou, M., Chen, F., & Fu, Q. (2016). Hydrophobic cellulose films with excellent strength and toughness via ball milling activated acylation of microfibrillated cellulose. *Carbohydrate Polymers*, 154, 129–138.
- Dervishi E, Li Z, Xu Y, Saini V, Biris AR, Lupu D, & Biris A. S. (2009). Carbon nanotubes: synthesis, properties, and applications. *Particulate Science and Technology*, 27(2), 107–125.
- Desta, M. B. (2013). Batch Sorption Experiments: Langmuir and Freundlich isotherm studies for the adsorption of textile metal ions onto teff straw (*Eragrostis tef*) Agricultural Waste. *Journal of Thermodynamics*, 71 (1), 1–6.
- Dhermendra, K.T., Behari, J., & Prasenjit, S. (2008). Application of nanoparticles in waste water treatment. *World Applied Sciences Journal*, 3 (3) 417–433.
- Dhibar, S., & Das, C. K. (2014). Silver Nanoparticles decorated polyaniline / multiwalled carbon nanotubes nanocomposite for high-performance supercapacitor electrode. *Industrial and Engineering Chemistry Research*, 53, 3495–3508.
- Dhuper, S., Panda, D., & Nayak, P. L. (2012). Green synthesis and characterization of zero -valent iron nanoparticles from the leaf extract of *Mangifera indica*. *Nano Trends: Journal of Nanotechnology Applications*, 13(2), 16–22.
- Dimitrijevic', R., Cvetkovic', O., Miodragovic', Z., Simic', M., Mano-jlovic', D., Jovic', V. (2013). SEM/EDS and XRD characterization of silver nanocrystalline thin film prepared from organometallic solution. *Journal of Mining and Metallurgy, Section B: Metallurgy*, 49 (1), 91 - 95.
- Du-Bois, R.M., Holroyd, K.J., Saltini, C., & Crystal, R.G. (1991). Granulomas process. In: The Lung, R.G. Crystal, J. B. West, P. J. Barnes, N. S. Cherniack, E. R. (Eds) Weibel, Published by Raven Press, NY, USA, 1925 – 1938.
- Eatemadi, A., Daraee, H., & Karimkhanloo, H. (2014). Carbon nanotubes: properties, synthesis, purification, and medical applications. *Nanoscale Research Letters*, 9, 393. <https://doi.org/10.1186/1556-276X-9-393>.
- Ebbesen T. W., & Ajayan, P. M. (1992). Large-scale synthesis of carbon nanotubes. *Nature*, 358(6383), 220–222.
- Ejazul, X. Y., Zhen, L., & Qaisar, M. (2007). Assessing Potential dietary toxicity of heavy metals in selected vegetables and food crops. *Journal of Zhejiang University of Science*, 8, 1–13.
- Elanthikkal, S., Gopalakrishnapanicker, U., Varghese, S., & Guthrie, J. T. (2010). Cellulose microfibrils produced from banana plant wastes: Isolation and characterization. *Carbohydrate Polymers*, 80 (3), 852–859. <https://doi.org/https://doi.org/10.1016/j.carbpol.2009.12.043>,

- Elmi, F., Hosseini, T., Taleshi, M. S., Taleshi, F. (2017). Kinetic and thermodynamic investigation into the lead adsorption process from wastewater through magnetic nanocomposite Fe₃O₄/CNT. *Nanotechnology for Environmental Engineering*, 2(1), 13.
- Elumalai, D., Kaleena, P. K., Ashok, K., Suresh, A., & Hemavathi, M. (2016). Green synthesis of silver nanoparticle using *Achyranthes aspera* and its larvicidal activity against three major mosquito vectors. *Engineering in Agriculture, Environment and Food*, 9(1), 1–8. <https://doi.org/10.1016/j.eaef.2015.08.002>.
- Emeka, D. D. (2015). Comparative Analysis of Effluent Discharge from Emene Industrial Area of Enugu, Nigeria, With National and International Standards. *Civil and Environmental Research*, 7, 84-90.
- Emongor, V., Nkegbe, E., Kealotswe, B., Koorapetse, I., Sankwase, S. & Keikanetswe, S. (2005). Pollution indicators in Gaborone industrial effluent. *Journal of Applied Science*, 5, 147-150.
- Erdem, E, Karapinar, N., & Donat, R. (2014). The removal of heavy metal cations by natural zeolites. *Journal of Colloidal Interface and Sciences*, 280 (2), 309-314.
- Fakayode, S. O. (2005). Impact assessment of industrial effluent on water quality of the receiving Alaro River in Ibadan Nigeria. *African Journal of Environmental Assessment and Management*, 10, 1- 13
- Farghali, A., Tawab, H.A., Moaty, S.A., & Khaled, R. (2017). Functionalization of acidified multi-walled carbon nanotubes for removal of heavy metals in aqueous solutions. *Journal of Nanostructure in Chemistry*, 7(2), 101–111.
- Fathizadeh, M., Aroujalian, A., & Raisi, A. (2011). Effect of added NaX nano-zeolite into polyamide as a top thin layer of membrane on water flux and salt rejection in a reverse osmosis process. *Journal of Membrane Sciences*, 375, 88–95.
- Fawaz, J., & Mittal, V. (2015). Synthesis of polymer nanocomposites: review of various techniques. In: Mittal V, editor. *Synthesis techniques for polymer nanocomposites*. 1st ed. Weinheim: Wiley-VCH, 45-48
- Fedorov, M. P., Makarova, E. I., Titova, T. S. (2017). Recycling of spent battery electrolytes for construction material production. *Magazine of Civil Engineering*, 3, 3-9
- Fenglian, F., & Qi, W. (2011). Removal of heavy metal ions from wastewaters: A review. *Journal of Environmental Management*, 92, 407-418.
- Figaro, S., Avril, J.P., Brouers, F., Ouensanga, A., Gaspard, S. (2009). Adsorption studies of molasse's wastewa- ters on activated carbon: Modelling with a new fractal kinetic equation and evaluation of kinetic models, *Journal of Hazardous Materials*, 161, 649–656.
- Flauzino, N. W. P., Silve´rio, H. A., Dantas, N. O., & Pasquini, D. (2013). Extraction and characterization of cellulose nanocrystals from agro-industrial residue-Soy hulls. *Industrial Crops and Productions*, 42, 480–488. <https://doi.org/10.1016/j.indcrop.2012.06.041>.
- Fontananova, E., Grosso, V., Aljlil, S. A., Bahattab, M. A., Vuono, D., Nicoletta, F. P., Curcio, E., Drioli, E., & di Profio, G. (2017). Effect of functional groups on the properties of multiwalled carbon nanotubes/polyvinylidene fluoride composite membranes. *Journal of Membrane Sciences*, 541, 198–204.

- Foo, K. Y., & Hameed B. H. (2012). Porous structure and adsorptive properties of pineapple peel based activated carbons prepared via microwave assisted KOH and K_2CO_3 activation. *Microporous Mesoporous Materials*, 148, 191–195.
- Foo, K.Y., & Hameed, B (2010). Insights into the modeling of adsorption isotherm systems. *Chemical. Engineering Journal*, 156, 2–10.
- Fosmire, G. J (2006). Zinc toxicity. *American Journal of Clinical Nutrition*. 51(2), 3.
- Franko, A., Budihna, M. V., Dodic-Fikfak, M. (2015). Long-term effects of elemental mercury on renal function in miners of the Idrija Mercury mine. *Annals of Occupational Hygiene*, 49, 521–527.
- Freundlich, H.M.F. (1906). Over the adsorption in solution, *Zeitschrift Physikalische Chemie* 57, 385-470.
- Fu, F., & Wang, Q. (2011) Removal of heavy metal ions from wastewaters: a review. *Journal of Environmental Management*, 92, 407–418.
- Fu, J., Xin, Q., Wu, X., Chen, Z., Yan, Y., Liu, S., Wang, M., & Xu, Q. (2016). Selective adsorption and separation of organic dyes from aqueous solution on polydopamine microspheres. *Journal of Colloids Interface Sciences*, 461, 292-304.
- Ganesh, E. N. (2013). Single walled and multi walled carbon nanotube structure. *Synthesis and Applications*, 2(4), 311–318.
- Gao, Z., Bandosz, T. J. Zhao, Z. Han, M. Qiu, J. (2009). Investigation of factors affecting adsorption of transition metals on oxidized carbon nanotubes, *Journal of Hazardous Materials*, 167, 357–365.
- Gómez, S., Rendtorff, N. M., Aglietti, E. F., Sakka, Y., & Suárez, G. J. A. S. S. (2016). Surface Modification of Multiwall Carbon Nanotubes by Sulfonitric Treatment. *Applied Surface Science*, 379, 264-269.
- Grobert, N. (2007). Carbon nanotubes-becoming clean. *Mater Today*, 10(1), 28–35.
- Grosso, V., Vuono, D., Bahattab, M. A., Di Profio, G., Curcio, E., Al-Jilil, S.A., Alsubaie, F., Alfife, M., Nagy, J. B., Drioli, E. (2014). Polymeric and mixed matrix polyimide membranes. *Separation and Purification Technology*, 132, 684–696.
- Gunay, A., Arslankaya, E., & Tosun, I. (2017). Lead removal from aqueous solution by natural and pretreated clinoptilolite: Adsorption equilibrium and kinetics. *Journal of Hazardous Materials*, 146 (2), 362 – 371.
- Gupta, S., & Babu, B. V. (2009). Utilization of waste product (tamarind seeds) for the removal of Cr (VI) from aqueous solutions: Equilibrium, kinetics, and regeneration studies. *Journal of Environmental Management*, 90 (10), 3013–3022.
- Gupta, V. K. Ali, T., Saleh, A., Nayak, A., & Agarwal, S. (2012). Chemical treatment technologies for waste-water recycling—an overview, *Royal Society of Chemistry Advances*, 2 (16), 6380–6388.
- Gupta, V. K., Pathania, D., & Sharma, S. (2017). Adsorptive remediation of Cu(II) and Ni(II) by microwave assisted H_3PO_4 activated carbon. *Arabian Journal of Chemistry*, 10, S2836–S2844.

- Gusain, R., Kumar, N., Fosso-kankeu, E., & Ray, S. S. (2019). Efficient removal of Pb (II) and Cd (II) from industrial mine water by a hierarchical MoS₂/SH-MWCNT nanocomposite. *ACS Omega* 2019, 4, 13922–13935.
- Gzara, L., Rehan, Z. A., Khan, S. B., Alamry, K. A., Albeirutty, M. H., El-Shahawi, M. S., Rashid, M. I., Figoli, A., Drioli, E., & Asiri, A. M. (2016). Preparation and characterization of PES-cobalt nanocomposite membranes with enhanced anti-fouling properties and performances. *Journal of Taiwan Institute of Chemical Engineering*, 65, 405–419.
- Hameed, B. H. (2007). Evaluation of papaya seeds as a novel non-conventional low-cost adsorbent for removal of methylene blue. *Journal of Hazardous Materials*, 162, 939–944.
- Hamid, A.A., Al-Ghobashy, M.A., Fawzy, M., Mohamed, M.B., Mohamed, M.S.A., Abdel-Mottaleb. (2013). Phytosynthesis of Au, Ag, and Au–Ag bimetallic nanoparticles using aqueous extract of sago pondweed (*Potamogeton pectinatus* L.) *American Chemical Society Sustainable Chemistry and Engineering*, 1,1520–1529.
- Happi E.T., Robert, C., Ronkart, S. N., Wathélet, B., & Paquot, M. (2008). Dietary fibre components and pectin chemical features of peels during ripening in banana and plantain varieties. *Bioresource Technology*, 99, 4346–4354.
- He, Z. B., Maurice, J. L., Lee, C. S., Cojocar, C. S., & Pribat, D. (2010). Nickel catalyst faceting in plasma-enhanced direct current chemical vapor deposition of carbon nanofibers. *The Arabian Journal for Science and Engineering*, 35(1C), 1–19.
- Hintsho, N., Ahmed, S., Pranav, K., Tripathi, B. P., & Shane, D. (2015). The effect of CO₂ on the CVD synthesis of carbon nanomaterials using fly ash as a catalyst, *Royal Society of Chemistry*, 5, 53776–53781.
- Hirlekar, R., Yamagar, M., Garse, H., Vij, M., & Kadam, V. (2009). Carbon nanotubes and its applications: a review. *Asian Journal of Pharmaceutical Clinical Resources*, 2(4), 17–27.
- Ho, Y. S., & McKay, G. (1999). The sorption of lead (II) ions on peat. *Water Resources*, 33, 578–584.
- Ho, Y. S., & McKay, G. (2000). The kinetic of sorption of divalent metal ions into sphagnum moss peat. *Water Research*, 34, 735–742.
- Hu, K., Hu, X., Zeng, L., Zhao, M., & Huang, H. (2010). Hydrogels prepared from pineapple peel cellulose using ionic liquid and their characterization and primary sodium salicylate release study. *Carbohydrate Polymer*, 82, 62–68.
- Hu, L., Zheng, G., Yao, J., Liu, N., Weil, B., Eskilsson, M., Karabulut, E., Ruan, Z., Fan, S., Bloking, J. T., & McGehee, M. D. (2013a). Transparent and conductive paper from nanocellulose fibers. *Energy and Environmental Science*, 6, 513–518. <https://doi.org/10.1039/C2EE23635D>.
- Hu, X., Wang, J., & Huang, H. (2013b). Impacts of some macromolecules on the characteristics of hydrogels prepared from pineapple peel cellulose using ionic liquid. *Cellulose*, 20, 2923–2933. <https://doi.org/10.1007/s10570-013-0075-4>.

- Huang, J., Liu, Y., Sun, B., & Shang, Z. (2017). Microwave-assisted alkali extraction of bagasse hemicellulose enhanced by an enzymatic pretreatment process. *Journal of Bioresources and Bioproducts*, 2(3), 105–109.
- Hurst, S. J., Lytton-Jean, A. K. R., & Mirkin, C. A. (2006). Maximizing DNA loading on a range of gold nanoparticle sizes. *Analytical Chemistry*, 78(24), 8313–8.
- Ibigbami, T.B., Dawodu, F.A., Akinyeye, O.J. (2016). Removal of heavy metals from pharmaceutical industrial wastewater effluent by combination of adsorption and chemical precipitation methods. *American Journal of Applied Chemistry*. 1, 24-32.
- Ibrahim, S., Fatimah, I., Ang, H. M. & Wang, S. (2010). Adsorption of anionic dyes in aqueous solution using chemically modified barley straw. *Water Science Technology*, 62, 1177–1182.
- Iijima, S. (1991). Helical microtubules of graphitic carbon. *Nature*, 354(6348), 56–58.
- Iloms, E., Ololade, O. O., Ogola, H. J. O., & Selvarajan, R. (2020). Investigating Industrial Effluent Impact on Municipal Wastewater Treatment Plant in Vaal, South Africa. *International Journal of Environmental Research and Public Health*, 17(3), 1096.
- Inbaraj, B. S. Wang, J. S. Lu, J. F., Siao, F.Y., & Chen, B. H. (2009). Adsorption of toxic mercury (II) by an extracellular biopolymer poly(c-glutamic acid). *Bioresource Technology*, 100, 200–207.
- Inyinbor, A. A., Adekola, F. A., & Olatunji, G. A. (2016). Kinetics, isotherms and thermodynamic modeling of liquid phase adsorption of Rhodamine B dye onto *Raphia hookerie* fruit epicarp. *Water Resources and Industry*, 15, 14–27.
- Iravani, S., Korbekandi, H., Mirmohammadi, S. V., & Zolfaghari, B. (2014). Synthesis of silver nanoparticles: chemical, physical and biological methods. *Research in Pharmaceutical Sciences*, 9(6), 385–406.
- Islam, R., Foisal, J. Al, Rahman, M., Lisa, L. A., & Paul, D. K. (2016). Pollution assessment and heavy metal determination by AAS in waste water collected from Kushtia industrial zone in Bangladesh. *African Journal of Environmental Science and Technology*, 10(1), 9–17. <https://doi.org/10.5897/AJEST2014.1994>.
- Isogai, A., Saito, T., & Fukuzumi, H. (2011). TEMPO-oxidized Cellulose Nanofibers, *Nanosciences*, 3 (1) 71-85.
- Jacobs, J. T., Testa, S, M (2005). *Overview of chromium (VI) in the environment: background and history*. Chromium (VI) handbook. Boca Raton: CRC Press 22.
- Jain, K., Patel, A. S., Pardhi, V. P., & Flora, S. J. S. (2021). Nanotechnology in wastewater management: A new paradigm towards wastewater treatment. *Molecules*, 26(6), 1-26.
- Jaishankar, M., Tseten, T., Anbalagan, N., Mathew, B. B., Beeregowda, K. N (2014). Toxicity, mechanism and health effects of some heavy metals. *Interdisciplinary Toxicology*, 7(2), 12.

- Jeong, H., Park, J., & Kim, H. (2013). Determination of NH_4^+ in Environmental Water with Interfering Substances Using the Modified Nessler Method. *Journal of Applied Chemistry*, 6(3), 1-9.
- Journet, C., Maser, W. K., Bernier, P., Loiseau, A., De La Chapelle, M. L., Lefrant, D., Deniard, P., Lee, R., & Fischer, J. E. (1997). Large-scale production of single-walled carbon nanotubes by the electric-arc technique. *Nature*, 388(6644), 756–758.
- Kalishwaralal, K., Deepak, V., Pandian, R. K., Kottaisamy, B. S. M., Kartikeyan, K. S., & Gurunathan, B. S. (2010). Biosynthesis of silver and gold nanoparticles using *Brevibacterium casei*. *Colloids Surface B: Biointerfaces*, 77, 257–62.
- Kanthapazham, R., Ayyavu, C., & Mahendiradas, D (2016). Removal of Pb^{2+} , Ni^{2+} and Cd^{2+} ions in aqueous media using functionalized MWCNT wrapped polypyrrole nanocomposite. *Desalination and Water Treatment*, 57(36), 16871–16885.
- Kanu, I. & Achi, O. K. (2011). Industrial Effluents and their Impact on Water Quality of Receiving Rivers in Nigeria. *Journal of Applied Technology in Environmental Sanitation*, 1(1), 75-86
- Kariim, I., Abdulkareem, A. S., Abubakre, O. K., Bankole, M. T., Tijani, J. O., & Mohammed, I. A. (2016). Studies on the suitability of alumina as metallic catalyst support for MWCNTs in a CVD Reactor. 60(2), 296-305.
- Karkeh-abadi, F., Saber-Samandari, S. (2016). The impact of functionalized CNT in the network of sodium alginate-based nanocomposite beads on the removal of Co (II) ions from aqueous solutions. *Journal of Hazardous Materials*, 312, 224–233.
- Katarzyna, P., Mariusz, T., Jolanta, G. (2006). Relationship between organic carbon and other measures of organic matter in the waters of lake Isag. *Limnological Review*, 6, 233-238.
- Kaur, N., Sharma, S, Kaur, S., & Khosla, E. (2016) Reverse micellar extraction of acid dyes from simulated textile effluent. *Journal of Chemical, Biological and Physical Sciences (JCPBS)*, 6,180–197.
- Kean, T., & Thanou, M. (2010). Biodegradation, bio-distribution and toxicity of chitosan. *Advanced Drug Delivery Reviews*, 62, 3–11.
- Kedzior, S. A., Dubé, M. A., & Cranston, E. D. (2017). Cellulose nanocrystals and methyl cellulose as costabilizers for nanocomposite latexes with double morphology. *ACS Sustainable Chemistry and Engineering*, 5, 10509–10517.
- Khaled, Z. A., & Ginam, H. (2014). Correlation between biochemical oxygen demand and chemical oxygen demand for various wastewater treatment plants in Egypt to obtain the biodegradability indices. *International Journal of Sciences: Basic and Applied Research*, 13(1), 42-48.
- Khalid, A., Abdel-Karim, A., Atieh, M. A., Javed, S., & McKay, G. (2018). PEG-CNTs nanocomposite PSU membranes for wastewater treatment by membrane bioreactor. *Separation and Purification Technology*, 190, 165–176.
- Khalil, H. S. A., Alwani, M. S., & Omar, A. K. M. (2007). Chemical composition, anatomy, lignin distribution, and cell wall structure of Malaysian plant waste fibers. *Bioresources*, 1(2), 220-232.
- Khan, I., Saeed, K., & Khan, I. (2019). Nanoparticles: Properties, applications and toxicities. *Arabian Journal of Chemistry*, 12, 908-931.

- Khan, M. J., Shameli, K., Sazili, A. Q., & Selamat, J. (2019). Rapid green synthesis and characterization of silver nanoparticles arbitrated by curcumin in an alkaline medium. *Molecules*, 24, 719, <https://doi.org/10.3390/molecules24040719>.
- Khawas, P., & Deka, S. C. (2016). Isolation and characterization of cellulose nanofibers from culinary banana peel using high intensity ultrasonication combined with chemical treatment. *Carbohydrate Polymer*, 137:608–616. <https://doi.org/10.1016/j.carbpol.2015.11.020>.
- Khorrami, S. A. & Lofti, R. (2013). Influence of carrier gas flow rate on carbon nanotubes growth by TCVD with Cu catalyst. *Journal of Saudi Chemical Society*, 20, 432–436.
- Kim, E. S., Liu, Y., & Gamal El-Din, M. (2013). An in-situ integrated system of carbon nanotubes nanocomposite membrane for oil sands process-affected water treatment. *Journal of Membrane Science*, 429, 418–427.
- Kim, J., & van der Bruggen, B. (2010). The use of nanoparticles in polymeric and ceramic membrane structures: Review of manufacturing procedures and performance improvement for water treatment. *Environmental Pollution*, 158, 2335–2349.
- Kim, S., Park, S., Kim, D., & Jin, C. (2020). Thermal Diffusivity of Ag/CNT - Added Ag Nanocomposites Prepared by Spark Plasma Sintering. *International Journal of Precision Engineering and Manufacturing*. <https://doi.org/10.1007/s12541-020-00334-8>.
- Kocaoba, S., Orham, Y., & Akyuz, T. (2014). Kinetics and equilibrium studies of heavy metal ions removal by use of natural zeolites. *Desalination*, 214(3), 1 – 10.
- Koseoglu-Imer, D., & Koyuncu, I. (2017). Fabrication and application areas of mixed matrix flat-sheet membranes. In *Application of Nanotechnology in Membranes for Water Treatment*, Figoli, A., Hoinkis, J., Altinkaya, S.A., Bundschuh, J. (Eds.), CRC Press Taylor & Francis Group: London, UK, 20(4), 87-90.
- Kulkarni, N. & Muddapur U. (2014). Biosynthesis of metal nanoparticles: a review. *Journal of Nanotechnology*, 7(1), 1–8.
- Kumar, N., Fosso-Kankeu, E., Ray, S.S. (2019). Achieving controllable MoS₂ nanostructures with increased interlayer spacing for efficient removal of Pb (II) from aquatic systems. *American Chemical Society Applied Material and Interfaces*, 11, 19141–19155.
- Kumar, S., Ahlawat, W., Bhanjana, G., Heydarifard, S. & Dilbaghi, N. (2014) Nanotechnology-based water treatment strategies. *Journal Nanoscience Nanotechnology*, 14, 1838–1858.
- Kumar, M., and Ando, Y. (2010). Chemical vapor deposition of carbon nanotubes: A review on the growth mechanism and mass production. *Journal of Nanoscience and Nanotechnology*, 10 (6), 3739-3758.
- Lagergren, S. (1898). Zurtheorie der sogenannten adsorption gelösterstoffe, *Kungliga Svenska Vetenskaps akademien. Handlingar*, 24, 1-39.
- Lagerwall, J. P. F., Schutz, C., Salajkova, M., Noh, J., Hyun, P. J., Scalia, G., & Bergstr, M. L. (2014). Cellulose nanocrystal-based materials: from liquid crystal self-assembly and glass formation to multifunctional thin films. *NPG Asia Materials*, 6, 80-4

- Lalia, B. S., Kochkodan, V., Hashaikh, R., & Hilal, N. (2013). A review on membrane fabrication: Structure, properties and performance relationship. *Desalination*, 326, 77–95.
- Landi, B. J., Raffaele, R. P., Castro, S. L., & Bailey, S. G. (2005). Single-wall carbon nanotube-polymer solar cells. *Progress in Photovoltaics: Research and Application*, 13(2), 165–172.
- Langmuir, I. (1916). The constitutional and fundamental properties of solids and liquids. *Journal of American Chemical Society*, 38(4), 2221–2295.
- Larrude, D. G., Maia, M. E. H., & Freire Jr, L. F. (2014). Synthesis and Characterization of Silver Nanoparticle-Multiwalled Carbon Nanotube Composites. *Journal of Nanomaterials*, 6(12), 1-7.
- Lasheen, M. R., El-Sherif, I. Y., Sabry, D. Y., El-Wakeel, S. T., & El-Shahat, M. F. (2015). Removal of heavy metals from aqueous solution by multiwalled carbon nanotubes: equilibrium, isotherms, and kinetics. *Desalination and Water Treatment*, 53(13), 3521–3530. <https://doi.org/10.1080/19443994.2013.873880>.
- Le, N. L. & Nunes, S. P. (2016). Materials and membrane technologies for water and energy sustainability. *Sustainable Materials and Technologies*, 7, 1–28.
- Lenntech Filter Cartridges, (2018). Available online: <https://www.lenntech.com/Data-sheets/Atlas-16-WATERTREATMENT-L.pdf> (accessed on 15 March 2018).
- Li, W., Zhang Y., Li, J., Zhou, Y., Li, R., Zhou, W (2015). Characterization of cellulose from banana pseudo-stem by heterogeneous liquefaction. *Carbohydrate Polymers*, 132, 513-519.
- Lieu, P. T., Heiskala, M., Peterson, P. A. & Yang, Y. (2001). The roles of Iron in health and disease. *Molecular Aspect of Medicine*. 22, 1-87.
- Lijima, S., (1991). Helical microtubules of graphitic carbon. *Nature* 56, 354-359.
- Lin, K., Pan, J., Chen, Y., Cheng, R., Xu, X. (2009) Study the adsorption of phenol from aqueous solution on hydroxyapatite nanopowders. *Journal of Hazardous Materials*, 161, 231-240.
- Lin, N., & Dufresne, A. (2014). Surface chemistry, morphological analysis and properties of cellulose nanocrystals with gradiented sulfation degrees. *Nanoscale*, 6, 5384–5393.
- Lin, W., Hu, X., You, X., Sun, Y., Wen, Y., Yang, W., Zhang, X., Li, Y., & Chen, H. (2018). Hydrophobic Modification of Nanocellulose via a Two-Step Silanation Method. *Polymers*, <https://doi.org/10.3390/polym10091035>.
- Liu, Z., Li, X., Xie, W., & Deng, H. (2017). Extraction, isolation and characterization of nanocrystalline cellulose from industrial kelp (*Laminaria japonica*) waste. *Carbohydrate Polymers*, 173, 353-359.
- López-Heras, M., Theodorou, I. G., Leo, B. F., Ryan, M. P., & Porter, A. E. (2015). Towards understanding the antibacterial activity of Ag nanoparticles: Electron microscopy in the analysis of the materials-biology interface in the lung. *Environmental Science Nanotechnology*, 2, 312–326.

- Lucaci, A. R., Bulgariu, D., Ahmad, I., Lis, G., Mocanu, A. M., & Bulgariu, L. (2019). Potential Use of Biochar from Various Waste Biomass as Biosorbent in Co (II) Removal Processes. *Water*, 11(4), 1565-11569
- Luo, X., Zeng, J., Liu, S., & Zhang, L. (2015). An effective and recyclable adsorbent for the removal of heavy metal ions from aqueous system: magnetic chitosan/cellulose microspheres. *Bioresource Technology*, headfoot, 8(22), 1-16.
- Ma, X., Yang, S.T, Tang, H., Liu, Y., & Wang, H. (2015). Competitive adsorption of heavy metal ions on carbon nanotubes and the desorption in simulated biofluids. *Journal of Colloid and Interface Science*, 448, 347–355.
- Madaeni, S. S., Ghaemi, N. (2007). Characterization of self-cleaning RO membranes coated with TiO₂ particles under UV irradiation. *Journal of Membrane Science*, 303, 221–233.
- Madaeni, S. S., Ghaemi, N., & Rajabi, H. (2015). *Advances in Polymeric Membranes for Water Treatment*. Elsevier Ltd.: Amsterdam, The Netherlands, 215-233.
- Manjuladevi, M., & Sri, O. M. (2017). Heavy metals removal from industrial wastewater by nano adsorbent prepared from *Cucumis melopeel* activated carbon. *Journal of Nanomedicine Research*, 5(1), 00102.
- Martin, S., & Griswold, W. (2009). Human health effects of heavy metals. *Environmental Science Technology Briefs from Citizens*, 15(1), 6-13
- Maximous, N., Nakhla, G., Wan, W., & Wong, K. (2010). Performance of a novel ZrO₂/PES membrane for wastewater filtration. *Journal of Membrane Sciences*, 352, 222–230.
- Mehmet, E. A., Sukru, D., Celalettin O, & Mustafa, K. (2006). Heavy metal adsorption by modified oak sawdust: thermodynamics and kinetics. *Journal of Hazardous Material*, 141(1), 77-85.
- Mezenner, N.Y., Bensmaili, A. (2009). Kinetics and thermodynamic study of phosphate adsorption on iron hydroxide-eggshell waste. *Chemical Engineering Journal*, 147, 87–96.
- Mierzwa, C., Arieta, V., Verlage, M., Carvalho, J., & Vecitis, C. D. (2013). Effect of clay nanoparticles on the structure and performance of polyethersulfone ultra filtration membranes. *Desalination*, 314, 147–158.
- Mohamed, A., & Robert, B. (2012). Synthesis and characterization of multi-walled carbon nanotube modified with octadecylamine and polyethylene glycol. *Arabian Journal of Chemistry Department Faculty of Science King Abdul Azeez University*, 4,7-34.
- Mohanta, D. & Nath, A. (2019). Environmentally benign fabrication of SnO₂-CNT nanohybrids and their multifunctional efficiency as an adsorbent, catalyst and antimicrobial agent for water decontamination. *Scientific Report*, 9, 12935. <https://doi.org/10.1038/s41598-019-49181-2>.
- Mohanta, D., & Nath, A. (2019). Environmentally benign fabrication of SnO₂-CNT nanohybrids and their multifunctional efficiency as an adsorbent, catalyst and antimicrobial agent for water decontamination. *Scientific Reports*, 11, 1–19.
- Mohapatra, D., Mishra, S., & Sutar, N. (2010). Banana and its by-product utilisation: an overview. *Journal of Scientific and Industrial Research*, 69, 323-329.

- Morais, S. C. F., & Pereira, M. L (2012). Heavy metals and human health, in Environmental health emerging issues and practice ed. A. Jacques Oosthuizen Edith Cowan University, Australia. 4(2), 42-49
- Mougel, J.-B., Adda, C., Bertoncini, P., Capron, I., Cathala, B., & Chauvet, O. (2016). Highly Efficient and Predictable Noncovalent Dispersion of Single-Walled and Multi-Walled Carbon Nanotubes by Cellulose Nanocrystals. *Journal of Physical Chemistry C*, 120 (39), 22694-22701.
- Muhammad, H., Al-Malack, L., & Abdullahi, A. B. (2016). Adsorption of heavy metals using activated carbon produced from municipal organic solid waste. *Desalination and Water treatment*.1-14.
- Mukhopadhyay, S., Fanguero, R., Arpac, Y., Entürk, Ü. (2008). Banana fibers: Variability and fracture behaviour. *Journal of Engineered Fabrics & Fibers*, 3(2) 2-11.
- Muthukumar, V.P., & Karuppan. M. (2016). Ultrasound assisted green synthesis of silver nanoparticles using weed plant. *Bioprocess and Biosystems Engineering*, 39, 401-441.
- Nasir, S., Hussein, M.Z., Zainal, Z., Yusof, N.A. (2018). Carbon-Based Nanomaterials/Allotropes: A Glimpse of Their Synthesis, Properties and Some Applications. *Materials*, 11, 295.
- National Environmental Standards Regulatory and Enforcement Agency (NESREA). (2011) Guideline for drinking water quality. Federal Ministry of Environment, Nigeria.
- Nepomuceno, N. C., Santos, A. S. F., Oliveira J. E., Glenn, G. M., & Medeiros, E. S. (2017). Extraction and characterization of cellulose nanowhiskers from Mandacaru (*Cereus jamacaru* DC.) spines. *Cellulose*, 24, 119–129. <https://doi.org/10.1007/s10570-016-1109-5>.
- Nuhoglu, Y., & Malkoc, E. (2005). Investigations of Nickel (II) removal from aqueous solutions using tea factory waste. *Journal of Hazardous Materials*, 127, 120-125.
- Nwabanne, J. T. & Okoye, A. C. (2013). Treatment of synthetic and battery industry wastewater by electrocoagulation. *Der Chemica Sinica*, 4(6), 32–39.
- Nwagwu, S. N., Kuyoro, E. O., Agboola, D. M., Salau, K. S., & Kuyoro, T. O. (2016). Pollution of Nigerian Aquatic Ecosystems by Industrial Effluents: Effects on Fish Productivity. *American Geophysical Union*, 2016, CT44B-0238.
- Ofomaja, A. E., & Ho, Y. S. (2007). Equilibrium sorption of anionic dye from aqueous solution by palm kernel fibre as sorbent. *Dyes Pigments*, 74, 60-66.
- Okoye, A. I., Ejikeme, P. M., & Onukwuli, O. D. (2010). Lead removal from wastewater using fluted pumpkin seed shell activated carbon: Adsorption modeling and kinetics. *International Journal of Environmental Science and Technology*, 7, 793-800. <http://dx.doi.org/10.1007/BF03326188>.
- Oren, A. H., & Kaya, A. (2016). Factors affecting adsorption characteristics on Zn²⁺ on two natural zeolites, *Journal of Hazardous Materials*, 131,1 - 3.
- Osibanjo, O., Daso, A. P., & Gbadebo, A. M. (2011). The impact of industries on surface water quality of River Ona and River Alaro in Oluyole Industrial Estate, Ibadan, Nigeria. *African Journal of Biotechnology*, 10 (4), 696-702.

- Otokunefor, T. V. & Obiukwu, C. (2005). Impact of refinery effluent on the physico-chemical properties of a water body in the Niger Delta. *Applied Ecology and Environmental Research*, 3, 61-72.
- Oyaro, N., Odendi, J., Murago, E. N. M., Gitonga, E. J. (2007). The contents of Pb, Cu, Zn and Cd in meat in Nairobi, Kenya. *Journal of Food, Agriculture and Environment*, 5 (3&4), 119-121.
- Pathak, P. D. & Mandavgane, S. A. (2015). Preparation, characterization of raw, and carbon from banana peel by microwave activation: application in citric acid adsorption. *Journal of Environmental Chemical Engineering*, 3, 2435-2447.
- Patil, V. V. V (2012). Banana fibre epoxy composites and its potential for engineering application [M.Tech thesis]. Vellore, India: VIT University.
- Peng, Y., & Chen, Q. (2012). Fabrication of one-dimensional Ag/multiwalled carbon nanotube nano-composite. *Nanoscale Research Letters*, 7(1), 195. <https://doi.org/10.1186/1556-276X-7-195>.
- Power, G. E. (2016). Correlating Total Organic Carbon (TOC) To Biochemical (BOD₅) and Chemical Oxygen Demand (COD). Water and Process Technology. Application Note. (<https://www.researchgate.net/file/postfileloader.html>. (05 April 2020).
- Prathna, T. C, Chandrasekaran, N., Raichur, A. M., & Mukherje A. (2011). Kinetic evolution studies of silver nanoparticles in a bio-based green synthesis process. *Colloids Surface A: Physicochemical Engineering Aspects*, 37, 212–6.
- Qalyoubi, L., Al-Othman, A., & Al-Asheh, S. (2021). Recent progress and challenges of adsorptive membranes for the removal of pollutants from wastewater. Part II: Environmental applications. *Case Studies in Chemical and Environmental Engineering*, 3, 100102.
- Qu, J., Tian, X., Jiang, Z., Cao, B., Akindolie, M.S., Hu, Q., Feng, C., Feng, Y., Meng, X., Zhang, Y. (2020). Multi-component adsorption of Pb(II), Cd(II) and Ni(II) onto microwave-functionalized cellulose: Kinetics, isotherms, thermodynamics, mechanisms and application for electroplating wastewater purification. *Journal of Hazardous Materials*, 5(387)121718. doi: 10.1016/j.jhazmat.2019.121718.
- Radhakrishnan, A., Nahi, J., & Beena, B. (2020). Synthesis and characterization of multi-carboxyl functionalized nanocellulose graphene oxide-zinc oxide composite for the adsorption of uranium (VI) from aqueous solutions: kinetic and equilibrium profiles. *Materials Today: Proceedings* 1-7.
- Ramana, D. K. V., Yu, J. S., & Sessaiah, K. (2013). Silver nanoparticles deposited multiwalled carbon nanotubes for removal of Cu (II) and Cd(II) from water: Surface, kinetic, equilibrium, and thermal adsorption properties. *Chemical Engineering Journal*, 6, 3-12
- Rasheed, I. A., Rehan, Z. A., Khalid, T., Zahid, M., & Ahmad, H. (2020). Chapter 18 - Prospects of nanocomposite membranes in commercial scale. In M. Sadrzadeh & T. Mohammadi (Eds.), *Nanocomposite Membranes for Water and Gas Separation*, 457–473.
- Ray, S. S., Okamoto, K., & Okamoto, M. (2003). Structure-property relationship in biodegradable poly(butylenes succinate)/layered silicate nanocomposites. *Macromolecules*, 36(7), 2355–67.
- Ray, S.S., Gusain, R., & Kumar, N. (2020.) Carbon nanomaterial-based adsorbents for water purification: Fundamentals and applications, *Elsevier: Amsterdam, The Netherlands*, 1-23.

- Reddy, G. A. K., Joy, J. M., Mitra, T., Shabnam, S., & Shilpa, T. (2012). Nano silver – a review. *International Journal in Advanced Pharmacy*, 2(1), 09–15.
- Renge V. C., Khedkar S. V., & Shraddha V. P. (2012). Removal of heavy metals from wastewater using low cost adsorbents: A Review. *Scientific Reviews & Chemical Communications*, 2 (4), 580-584.
- Rodríguez, C., & Leiva, Eduardo. (2020). Enhanced heavy metal removal from acid mine drainage wastewater using double-oxidized multi-walled carbon nanotubes. *Molecules*, 25, 10-11.
- Saelo, S., Assatarakul, K., Sane, A., & Suppakul, P. (2016). Fabrication of novel bioactive cellulose-based films derived from caffeic acid phenethyl ester-loaded nanoparticles via a rapid expansion process: RESOLV. *Journal of Agriculture and Food Chemistry*, 64, 6694–6707.
- Sahayaraj, K., Rajesh, S. (2011). Bionanoparticles: synthesis and antimicrobial applications, science against microbial pathogens: communicating current research and technological advances. In: Méndez-Vilas A, editor, FORMATEX, 8, 228–44.
- Salleh, M. A. M., Mahmoud, D. K., Karim, W. A.W., & Idris, A. (2011). Cationic and anionic dye adsorption by agricultural solid wastes: A comprehensive review. *Desalination*, 280, 1-13.
- Samberg, M. E., Oldenburg, S. J., & Monteiro-Riviere, N. A. (2010). Evaluation of silver nanoparticle toxicity in vivo skin and in vitro keratinocytes. *Environ Health Perspectives*, 118(3), 407–13.
- Samudro, G., & Mangkoedihardjo, S. (2010). Review on BOD, COD and BOD/COD ratio: a triangle zone for toxic, biodegradable and stable levels. *International Journal of Academic Research*, 2 (4), 235-239.
- Sawyer, C. N., McCarty, P. L., & Parkin, G. F. (2000). Chemistry for Environmental Engineering Fourth Edition. McGraw-Hill, Inc., New York.
- Sayed, E.T., Alawadhi, H., Elsaid, K., Olabi, A.G., Almakrani, M.A., Bin Tamim, S.T., Alafraji, G.H.M., & Abdelkareem, M.A. A (2020). Carbon-Cloth anode electroplated with iron nanostructure for microbial fuel cell operated with real wastewater. *Sustainability*, 12, 6538.
- Schadler, L. S. (2003). Polymer-based and polymer-filled nanocomposites. In: Ajayan PM, Schadler LS, Braun PV, editors. Nanocomposite science and technology. Weinheim: WILEY-VCH Verlag GmbH & Co KGaA, 2003.
- Segal, L., Creely, J. J., Martin, A. E., & Conrad, C. M. (1959). An Empirical Method for Estimating the Degree of Crystallinity of Native Cellulose Using the X-Ray Diffractometer. *Textile Research Journal*, 43, 432.
- Seiyaboh, E I. & Izah, S.C. (2017). Review of Impact of Anthropogenic Activities in Surface Water Resources in the Niger Delta Region of Nigeria: A Case of Bayelsa State. *International Journal of Ecotoxicology and Ecobiology*. 2, (2) 61-73.
- Senthilkumaar, S., Kalaamani, P., & Subburaam, C. V. (2006). Liquid phase adsorption of crystal violet onto activated carbons derived from male flowers of coconut tree. *Journal of Hazardous Materials*, 136, 800-808.
- Shah, M.P., Reddyb, P., Banerjee, G.V., Babu, P.R., & Kothari, I.L. (2005). Microbial degradation of banana waste under solid state bioprocessing using two ligno-

- cellulolytic fungi (*Phylosticta* spp. MPS-001 and *Aspergillus* spp. MPS-002). *Process Biochemistry*, 40 (1), 445–451.
- Shah, P., & Murthy, C. N. (2013). Studies on the porosity control of MWCNT/polysulfone composite membrane and its effect on metal removal. *Journal of Membrane Science*, 437, 90–98.
- Shaikh, H. M., Pandare, K. V., Nair, G., & Varma, A. J. (2009). Utilization of sugarcane bagasse cellulose for producing cellulose acetates: Novel use of residual hemicellulose as plasticizer. *Carbohydrate Polymers*, 76, 23–29.
- Shariatnia, S., Kumar, A. V., Kaynan, O., Asadi, A., & Hall, T. (2020). Hybrid Cellulose Nanocrystals-Bonded Carbon Nanotubes/Carbon Fiber Polymer Composites for Structural Applications Manufacturing and Mechanical Engineering Technology. *ACS Paragon Plus*, <https://doi.org/10.1021/acsanm.0c00785>.
- Sharma, P., & Dubey, R. S. (2005). Lead Toxicity in Plants. *Brazilian Journal of Plants Physiology* 17, 18.-24
- Sharmila, G., Muthukumaran, C., Saraswathi, H., Sangeetha, E., Soundarya, S., & Kumar, N. M. (2019). Green synthesis, characterization and biological activities of nanoceria. *Ceramic International*, 45, 12382–12386.
- Sharmin, N., Khan, R. A., Salmieri, S., Dussault, D., Bouchard, J., & Lacroix, M. (2012). Modification and characterization of biodegradable methylcellulose films with trimethylolpropane trimethacrylate (TMPTMA) by γ radiation: effect of nanocrystalline cellulose. *Journal of Agriculture and Food Chemistry*, 60, 623–629.
- Shen, J. N., Yu, C. C., Ruan, H. M., Gao, C. J., & van der Bruggen, B. (2013). Preparation and characterization of thin-film nanocomposite membranes embedded with poly(methyl methacrylate) hydrophobic modified multiwalled carbon nanotubes by interfacial polymerization. *Journal of Membrane Science*, 442, 18–26.
- Shi, F., Ma, Y., Ma, J., Wang, P., & Sun, W. (2012). Preparation and characterization of PVDF/TiO₂ hybrid membranes with different dosage of nano-TiO₂. *Journal of Membrane Science*, 389, 522–531.
- Sile-Yuksel, M., Tas, B., Koseoglu-Imer, D. Y., & Koyuncu, I. (2014). Effect of silver nanoparticle (AgNP) location in nanocomposite membrane matrix fabricated with different polymer type on antibacterial mechanism. *Desalination*, 347, 120–130.
- Singh N. B., & Agarwal, S. (2016). Nanocomposites—an overview. *Emerging Materials Research*, 5(1), 5–43.
- Singh, A., Goswami, A., & Nain, S. (2020). Enhanced antibacterial activity and photo - remediation of toxic dyes using Ag /SWCNT/PPy based nanocomposite with core – shell structure. *Applied Nanoscience*, 0123456789.
- Singh, G., Prince, J. A., Bhuvana, S., Boodhoo, K. V. K. & Anbharasi, V. (2014). Synthesis and characterization of PEG-Ag immobilized PES hollow fiber ultrafiltration membranes with long lasting antifouling properties. *Journal of Membrane Science*, 454, 538–548.

- Singh, J., Ali, A., & Prakash, V. (2014). Removal of lead (II) from synthetic and batteries wastewater using agricultural residues in batch/column mode. *International Journal of Environmental Science and Technology*, 11, 1759-1770.
- Singh, N. B., & Susan, A. B. H. (2018). Polymer nanocomposites for water treatments. In *Polymer-based Nanocomposites for Energy and Environmental Applications*. Elsevier Ltd, 345-349. <https://doi.org/10.1016/B978-0-08-102262-7.00021-0>
- Somorjai, G. A. (2014). Introduction to Surface chemistry and catalysis, *World Academy of Science, Engineering and Technology*, 56.
- Spinella, S., Maiorana, A., Qian, Q., Dawson, N. J., Hepworth, V., McCallum, S. A., & Gross, R. A. (2016). Concurrent cellulose hydrolysis and esterification to prepare a surface modified cellulose nanocrystal decorated with carboxylic acid moieties. *ACS Sustainable Chemistry and Engineering*, 4, 1538-1550.
- Srivastava, P., Singh, B., & Angove, M. (2005). Competitive adsorption behavior of heavy metals on kaolinite, *Journal of Colloidal Interface Science*. 290, 28–38.
- Suman, A., Kardam, M., Gera, V.K., Jain, A. (2015). Novel reusable nanocomposite for complete removal of dyes, heavy metals and microbial load from water based on nanocellulose and silver nano-embedded pebbles. *Environmental Technology*, 36, 706–714.
- Sumesh, E., Bootharaju, M. S., & Pradeep, T. (2011). A practical silver nanoparticle-based adsorbent for the removal of Hg^{2+} from water. *Journal of Hazardous Materials*, 189 (1–2), 450–457. <https://doi.org/10.1016/j.jhazmat.2011.02.061>.
- Sun, X., Yang, L., Li, Q., Zhao, J., Li, X., Wang, X., & Liu, H. (2014). Amino-functionalized magnetic cellulose nanocomposite as adsorbent for removal of Cr (VI): Synthesis and adsorption studies. *Chemical Engineering Journal*, 241, 175–183. <https://doi.org/10.1016/j.cej.2013.12.051>.
- Suteu, D., Zaharia, C., Bilba, D., Surpateanu, M. (2007). Conventional and unconventional materials for wastewater treatment. *Bulletin of the Transilvania University of Brasov (Romania)*, 4, 692 –696.
- Sweetly, D. J., Sangeetha. K., & Suganthi, B. (2015). The effect of battery recycling industry solid waste leachate on antioxidant status of *Trigonella foenum-graecum*. *Kongunadu. Research Journal*, 2(1), 133-137.
- Tao, J., Yang, J., Ma, C., Li, J., Du, K., Wei, Z., & Deng, X. (2020). Cellulose nanocrystals / graphene oxide composite for the adsorption and removal of levofloxacin hydrochloride antibiotic from aqueous solution. *Royal Society Open Science*, 7, 200857. <http://dx.doi.org/10.1098/rsos.200857>.
- Telisman, S., Colak, B., Pizent, A., Jurasovic, J., & Cvitkovic, P. (2007). Reproductive toxicity of low level lead exposure in men. *Environmental Research*, 105(2), 256-266.
- Temkin, M., & Pyzhev, V. (1940). Heavy Metals Removal and Isotherms Study. *Acta Physiochimica URSS*, 12, 217–222.

- Thess, A., Lee, R., Nikolaev, P., Dai, H., Petit, P., Robert, J., Xu, C., Lee, Y. H., Kim, S. G., & Rinzler, A. (1996). Crystalline ropes of metallic carbon nanotubes. *Science-AAAS-Weekly Paper Edition* 1996, 273(5274), 483–487.
- Tibolla, H., Pelissari, F. M., & Menegalli, F. C. (2014). Cellulose nanofibers produced from banana peel by chemical and enzymatic treatment. *LWT - Food Science and Technology*, 59, 1311–1318.
- Tibolla, H., Pelissari, F. M., Martins, J. T., Vicente, A. A., & Menegalli, F. C. (2018). Cellulose nanofibers produced from banana peel by chemical and mechanical treatments: Characterization and cytotoxicity assessment. *Food Hydrocolloids*, 75, 192–201.
- Tofighy, M. A., & Mohammadi, T. (2011). Adsorption of divalent heavy metal ions from water using carbon nanotube sheets, *Journal of Hazardous Materials*, 185, 140–147.
- Tofighy, M. A., & Mohammadi, T. (2015): Copper ions removal from aqueous solutions using acid-chitosan functionalized carbon nanotubes sheets, *Desalination and Water Treatment*, DOI: 10.1080/19443994.2015.1072738.
- Trache, D., Hussin, M. H., Haafiz, M. K. M., & Thakur, V. K. (2017). Recent progress in cellulose nanocrystals: sources and production. *Nanoscale*, 9, 1763–1786. <https://doi.org/10.1039/C6NR 09494E>.
- Tran, Q. H., Van Quy Nguyen, V. Q., & Le, A. T. (2013). Silver nanoparticles: synthesis, properties, toxicology, applications and perspectives. *Advances in Natural Sciences: Nanosciences and Nanotechnology*, 4(6), 1–21.
- Udo, E. J., & Ogunwale, A. (1986). *Laboratory manual for the analysis of soil, plant and water samples*, 2nd ed: Ibadan, Nigeria: *University Press Limited*. 132-133.
- United State Environmental Protection Agency (USEPA). Water monitoring and Assessment. Available online: <https://archive.epa.gov/water/archive/web/html/vms52.html> (accessed on 2nd February 2021).
- Ursino, C., Castro-Muñoz, R., Drioli, E., Gzara, L., Albeirutty, M., & Figoli, A. (2018). Progress of Nanocomposite Membranes for Water Treatment. *Membranes*, 8(2), 18. MDPI AG. Retrieved from <http://dx.doi.org/10.3390/membranes8020018>.
- Van der Bruggen, B., Curcio, E., & Drioli, E. (2004). Process intensification in the textile industry: The role of membrane technology. *Journal of Environmental Management*, 73, 267–274.
- Vander Wal, R. L., Berger, G. M., & Ticich, T. M. (2003). Carbon nanotube synthesis in a flame using laser ablation for in situ catalyst generation. *Applied Physics A*, 77(7), 885–889.
- Velma, V., Vutukuru, S. S., Tchounwou, P. B. (2009). Ecotoxicology of hexavalent chromium in freshwater fish: a critical review. *Reviews on Environmental Health*, 2009. 4(2), 16.
- Vijay, K. P. P. N., Pammi, S. V. N., Kollu, P., Satyanarayana. K. V. V., & Shameem, U. (2014). Green synthesis and characterization of silver nanoparticles using *Boerhaavia diffusa* plant extract and their anti-bacterial activity. *Industrial Crops and Products*, 52, 562–6.

- Vu, H. H. T., Gu, S., Thriveni, T., Khan, M. D., Tuan, L. Q., & Ahn, J. W. (2019). Sustainable Treatment for Sulfate and Lead Removal from Battery Wastewater. *Sustainability*, 11(13), 3497-3499.
- Waalkes, M. W. Z., Rodriguez, E. (2001). *Cadmium*. In: Sullivan J.B Jr. Krieger G.R., Clinical environmental health and toxic exposures. Vol. 2nd Edition. 2001: Lippincott Williams & Wilkins.
- Wang, L., Hu, D., Kong, X., Liu, J., Li, X., Zhou, K., & Zhou, C. (2018). Anionic polypeptide poly (Γ -glutamic acid)-functionalized magnetic Fe_3O_4 -GO-(o-MWCNTs) hybrid nanocomposite for high-efficiency removal of Cd(II), Cu(II) and Ni(II) heavy metal ions. *Chemical Engineering Journal*, 346(Ii), 38-49. <https://doi.org/10.1016/j.cej.2018.03.084>.
- Waziri, M., & Ogugbuaja, V. (2010). Interrelationships between physicochemical water pollution indicators: a case study of river Yobe Nigeria. *American Journal of Scientific and Industrial Research*, 1(1), 76-80.
- Wei, L., Lu, J., Xu, H., Patel, A., Chen, Z. S., & Chen, G. (2015). Silver nanoparticles: Synthesis, properties, and therapeutic applications. *Drug Discovery*, 20, 595-601.
- Werner. (2018). "BOD, COD, TOC and TOD - Sum Parameters in Environmental Analysis. "Arts, Lar Process Analysers Ag (Www.Chemeurope. Com).
- Wilbur, S., Henry, M.A., Abadin, M.H., Fay, M., Yu, D., Tencza, B., Ingerman L., Klotzbach, J., & James, S. (2012). Toxicological profile for chromium. Atlanta (GA): Agency for Toxic Substances and Disease Registry (US).
- Worch, E. (2021). *Adsorption Technology in Water Treatment*. Berlin, Boston: De Gruyter. <https://doi.org/10.1515/9783110715507>.
- World Health Organization. (WHO). (2004). Guidelines for drinking-water quality. Joint FAO/WHO Expert Committee on Food Additives: Sixty-first meeting, Rome, 5, 10-19.
- World Health Organization. (WHO). (2017). Guidelines for Drinking-water Quality. 4th Edn. 631, [https://doi.org/10.1016/S1462-0758\(00\)00006-6](https://doi.org/10.1016/S1462-0758(00)00006-6).
- Xia, S., & Ni, M. (2015). Preparation of poly (vinylidene fluoride) membranes with graphene oxide addition for natural organic matter removal. *Journal of Membrane Science*, 473, 54-62.
- Xu, D., Hou, B., Qian, L., Zhang, X., & Liu, G. (2019). Non-enzymatic electrochemical sensor based on silver nanoparticle-decorated carbon nanotubes. *Molecules*, 24, 3411.
- Yadav, C., Saini, A., & Maji, P. K. (2017). Energy efficient facile extraction process of cellulose nanofibres and their dimensional characterization using light scattering techniques. *Carbohydrate Polymers*, 165, 276-284.
- Yin, J., & Deng, B. (2015). Polymer-matrix nanocomposite membranes for water treatment. *Journal of Membrane Science*, 479, 256-75.
- Yu, F., Yanqing, W., Jie, M., & Chi, Z. (2013). Adsorption of lead on multi-walled carbon nanotubes with different outerdiameters and oxygen contents: Kinetics, isotherms and thermodynamics. *Journal of Environmental Sciences*. 25, 193 - 205.

- Yu, J. H., Du, Y. M., & Zheng, H. (1999). Blend films of chitosan-gelatin. *Journal of Wuhan University of Natural Sciences in Education*, 45, 440–444.
- Yu, S., Zuo, X., Bao, R., Xu, X., Wang, J., & Xu, J. (2009). Effect of SiO₂ nanoparticle addition on the characteristics of a new organic-inorganic hybrid membrane. *Polymer*, 50, 553–559.
- Yuan, X., Xia, W., An, J., Yin, J., Zhou, X., & Yang, W (2015). Kinetic and Thermodynamic Studies on the Phosphate Adsorption Removal by Dolomite Mineral. *Journal of Chemistry*, 2015, 1–8.
- Zahid, M., Rashid, A., Akram, S., Rehan, Z. A., & Razzaq, W. (2018). *A Comprehensive Review on Polymeric Nano-Composite Membranes for Water Treatment*. 8(1), 1–20.
- Zamudio, A., Elias, A.L., Rodriguez-Manzo, J.A., Lopez-Urias, F., Rodriguez-Gattorno, G., Lupo, F. (2006). Efficient anchoring of silver nanoparticles on N-doped carbon nanotubes. *Small*, 2 (3), 346–350.
- Zapata, P. A., Larrea, M., Tamayo, L., Rabagliati, F. M., Azócar, M. I., & Páez, M. (2016). Polyethylene/silver-nanofiber composites: A material for antibacterial films. *Material Science and Engineering C*, 69, 1282–1289.
- Zhan, Y., Hu, H., He, Y., Long, Z., & Wan, X. (2016). Novel Amino-functionalized Fe₃O₄/ carboxylic multi-walled carbon nanotubes: One-pot synthesis, characterization and removal for Cu (II). *Russian Journal of Applied Chemistry*, 89(11), 1894–1902.
- Zhang, Y., Karimkhani, V., Makowski, B. T., Samaranayake, G., & Rowan, S. J. (2017). Nanoemulsions and Nanolatexes Stabilized by Hydrophobically Functionalized Cellulose Nanocrystals. *Macromolecules*, 50, 6032–6042.
- Zhang, Y., Wang, Y., Zhang, H., Li, Y., Zhang, Z., & Zhang, W. (2020). Recycling spent lithium-ion battery as adsorbents to remove aqueous heavy metals: Adsorption kinetics, isotherms, and regeneration assessment. *Resources, Conservation and Recycling*, 156, [104688]. <https://doi.org/10.1016/j.resconrec.2020.104688>.
- Zhitkovich, A. (2005). Importance of chromium-DNA adducts in mutagenicity and toxicity of chromium (VI). *Chemical Research in Toxicology*. 18(1), 8.
- Zhou, J., Yang, S., Yu, J., & Shu, Z (2011). Novel hollow microspheres of hierarchical zinc–aluminum layered double hydroxides and their enhanced adsorption capacity for phosphate in water. *Journal of Hazardous Materials*, 192, 1114–1121.

APPENDICES

APPENDIX A: Preparation of Reagents

Preparation of 30% HNO_3 in 500 cm^3

Approximately 213.37 cm^3 of conc. HNO_3 was diluted with distilled water in a 500 cm^3 volumetric flask and later made up to the 500 cm^3 mark.

Preparation of 30% H_2SO_4 in 100 cm^3

Around 30.61 cm^3 of conc. H_2SO_4 was diluted with distilled water in a 100 cm^3 volumetric flask and later made up to the 100 cm^3 mark.

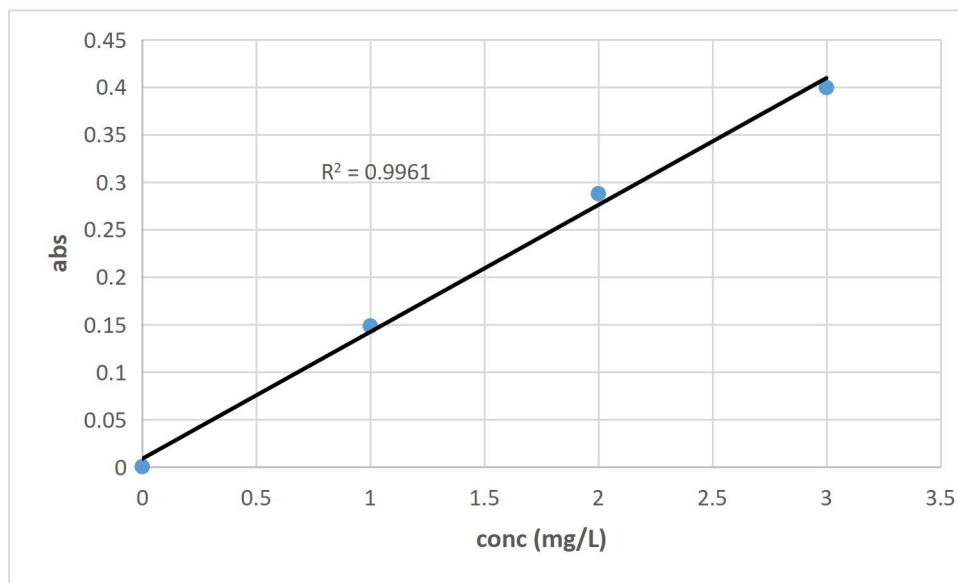
Preparation of 1 mM AgNO_3

About 0.17 g of silver (v) nitrate AgNO_3 was dissolved in 50 cm^3 of distilled water in a 100 cm^3 beaker, and later transferred to a 1000 cm^3 volumetric flask and made up to the mark with distilled water in a dark room.

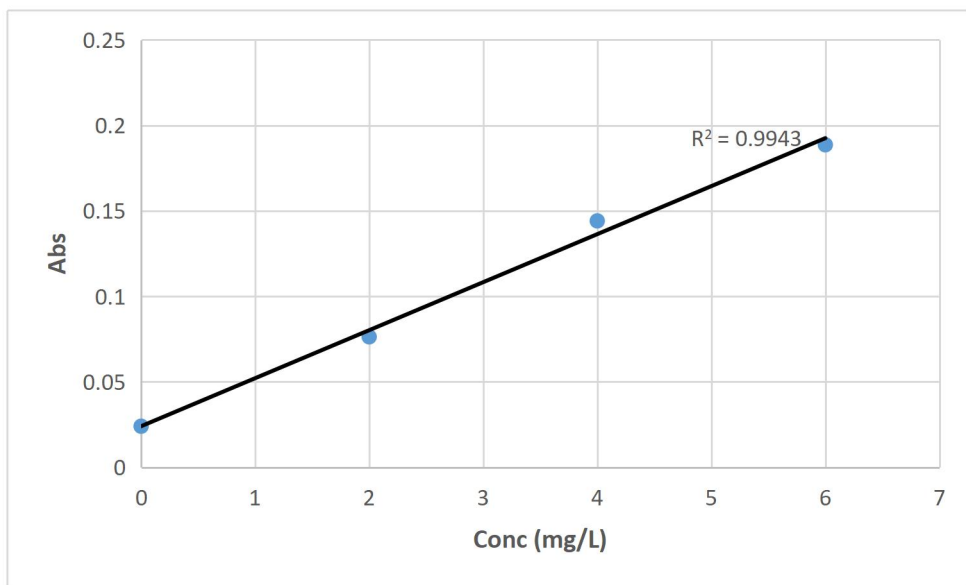
Preparation of 0.5 M NaOH in 100 cm^3

Approximately, 20 g of sodium hydroxide NaOH pellets was dissolved in distilled water in a 1000 cm^3 volumetric flask and subsequently made up to the 1000 cm^3 .

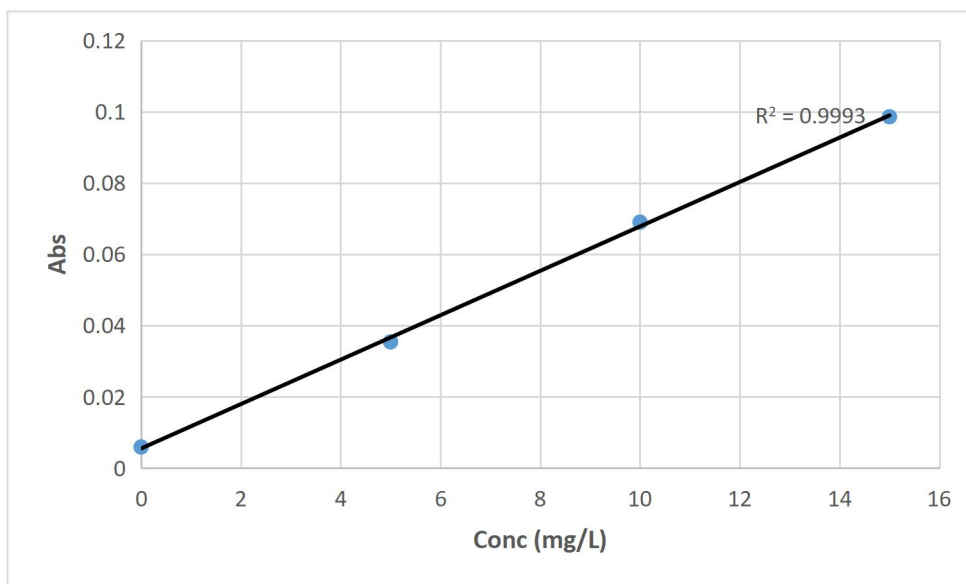
APPENDIX B: Calibration Curves



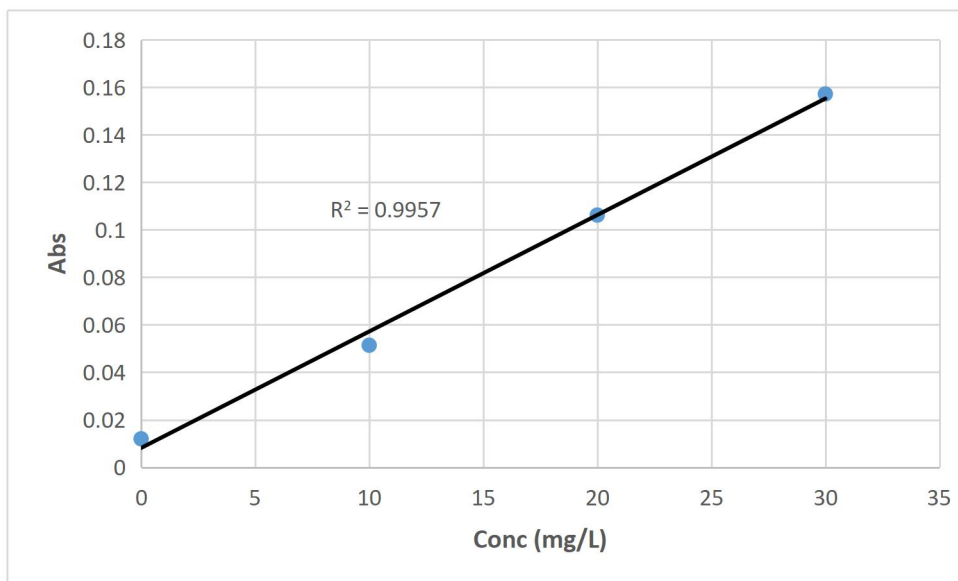
Zn Calibration Curve from AAS Analysis



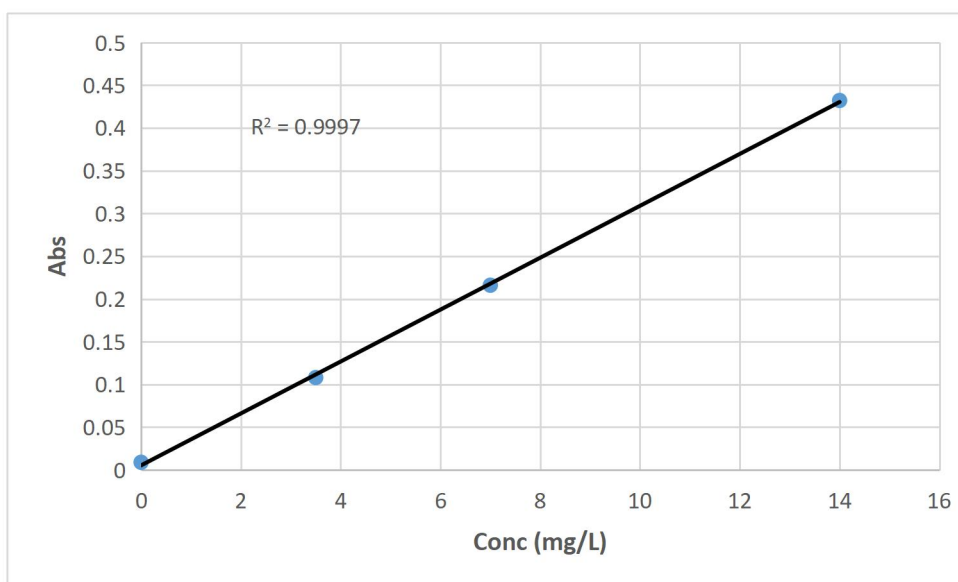
Cu Calibration Curve from AAS Analysis



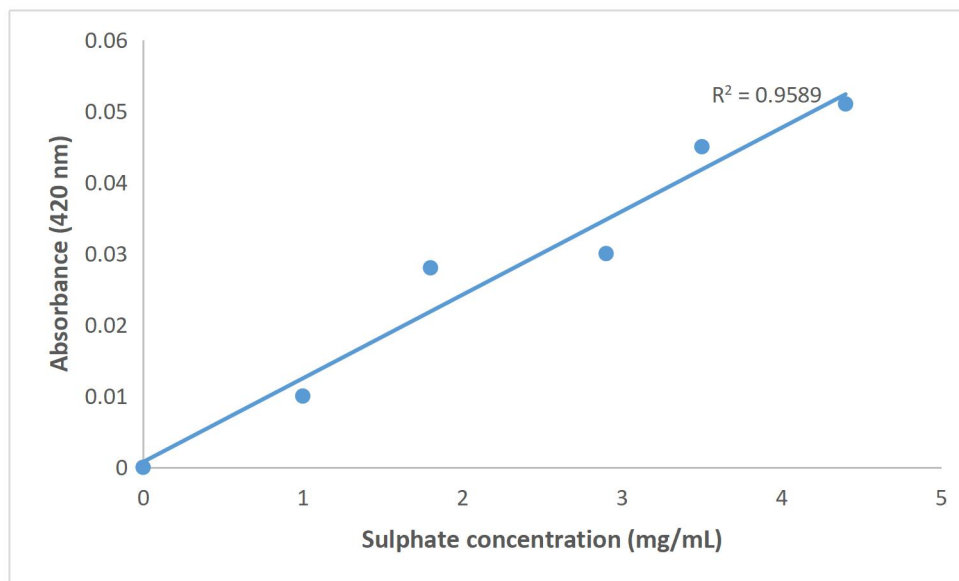
Fe Calibration Curve from AAS Analysis



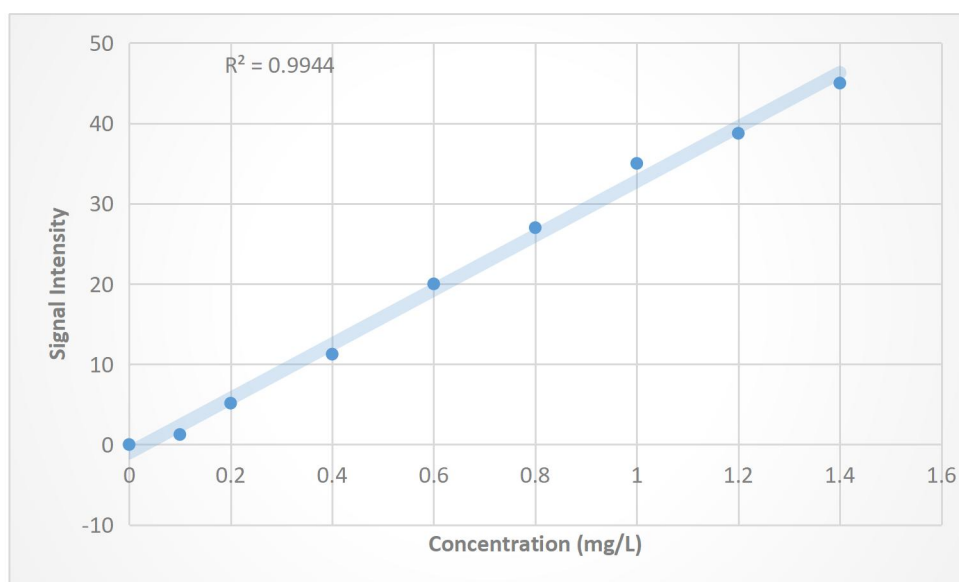
Pb Calibration Curve from AAS Analysis



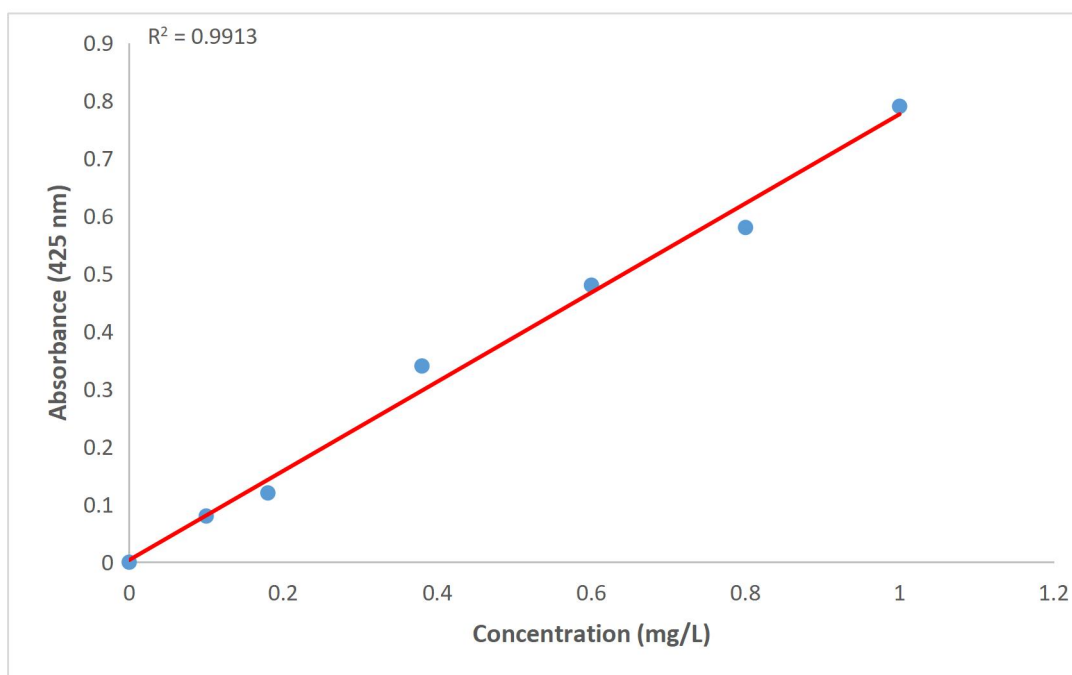
Ni calibration curve from AAS Analysis



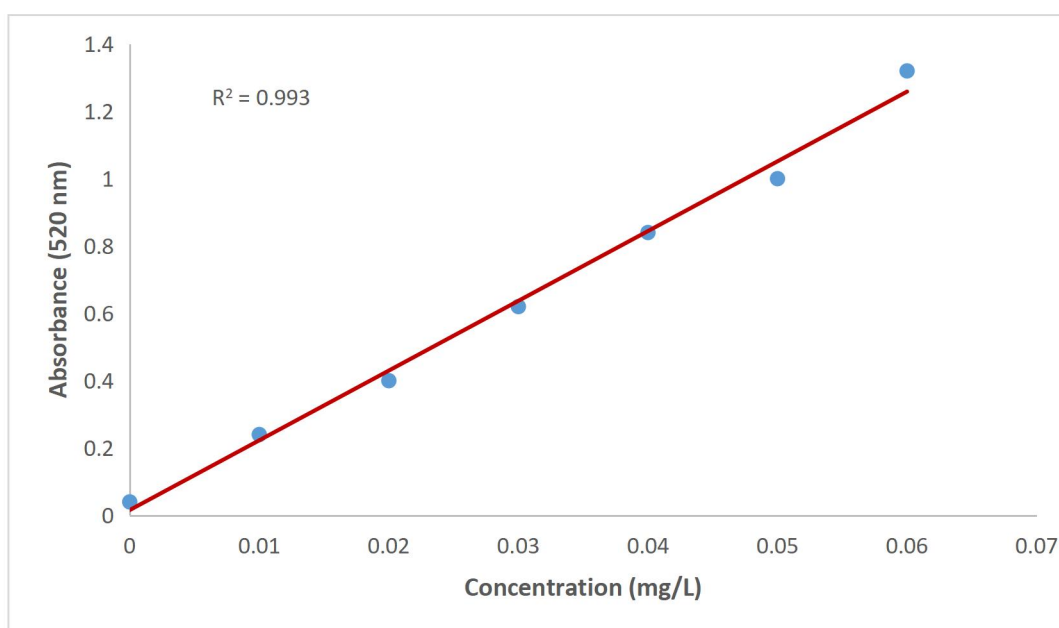
Standard Calibration Curve for the Determination of Sulphate Concentration



Standard Calibration Curve for the Determination of Fluoride Concentration

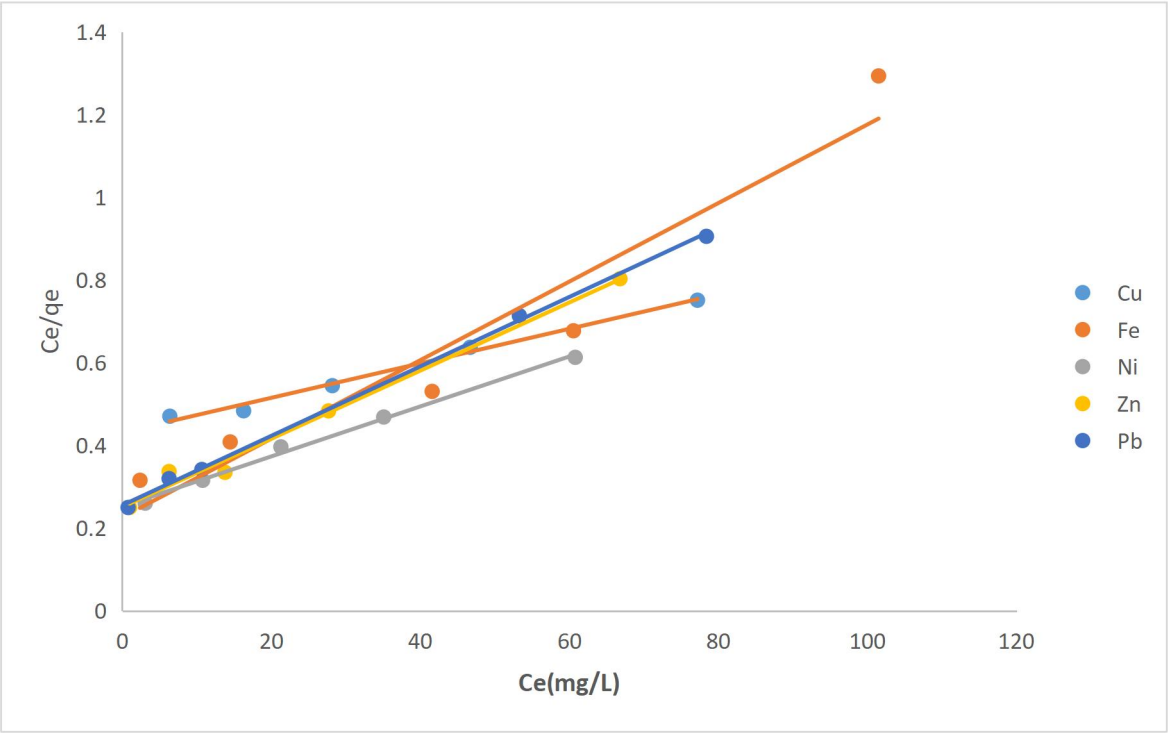


Standard Calibration Curve for the Determination of Ammonium Concentration

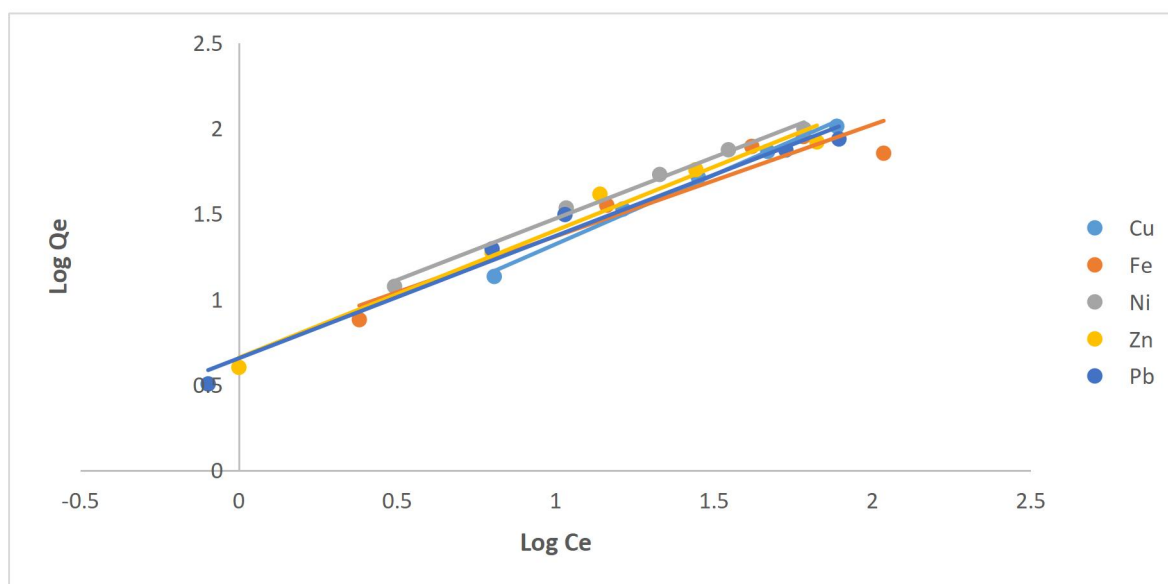


Standard Calibration Curve for the Determination of Cyanide Concentration

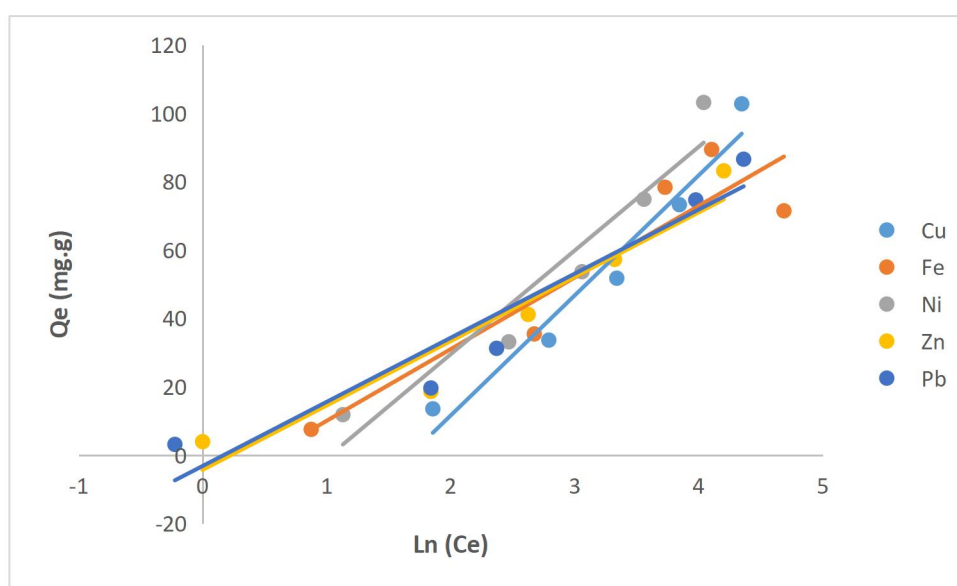
APPENDIX C: Adsorption Isotherm Plots for Heavy Metal Removal by Adsorbents



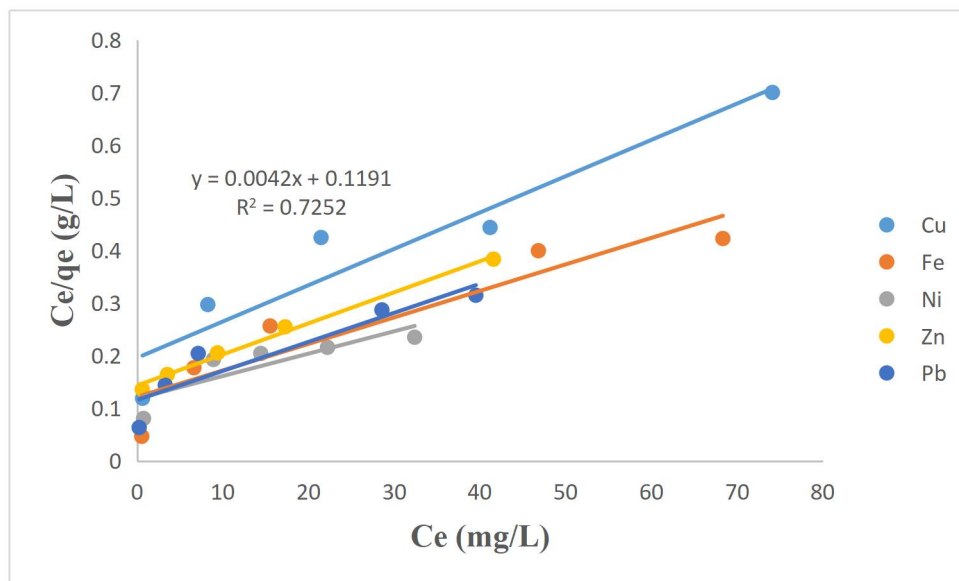
Langmuir Isotherms for Ag-CNTs Adsorbent



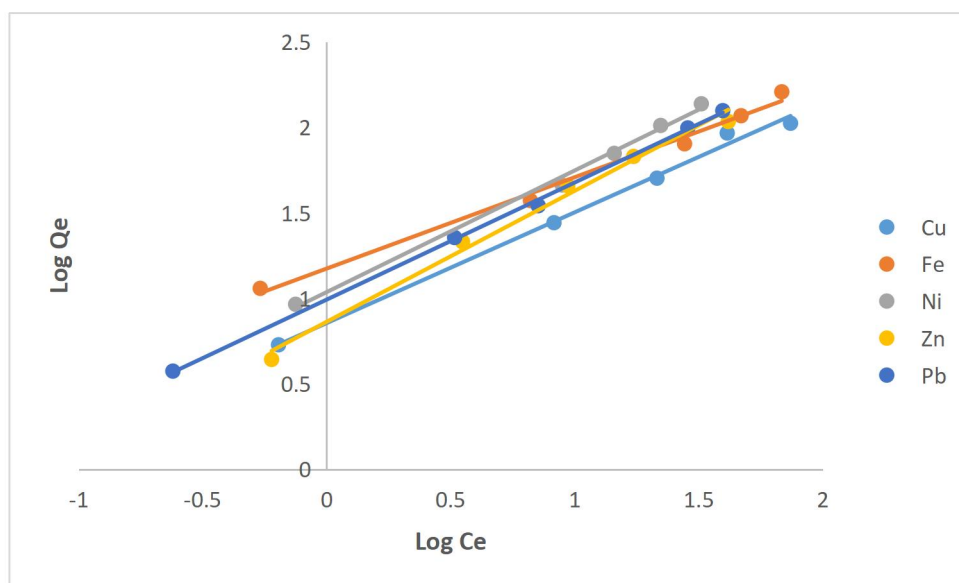
Freundlich Isotherms for Ag-CNTs Adsorbent



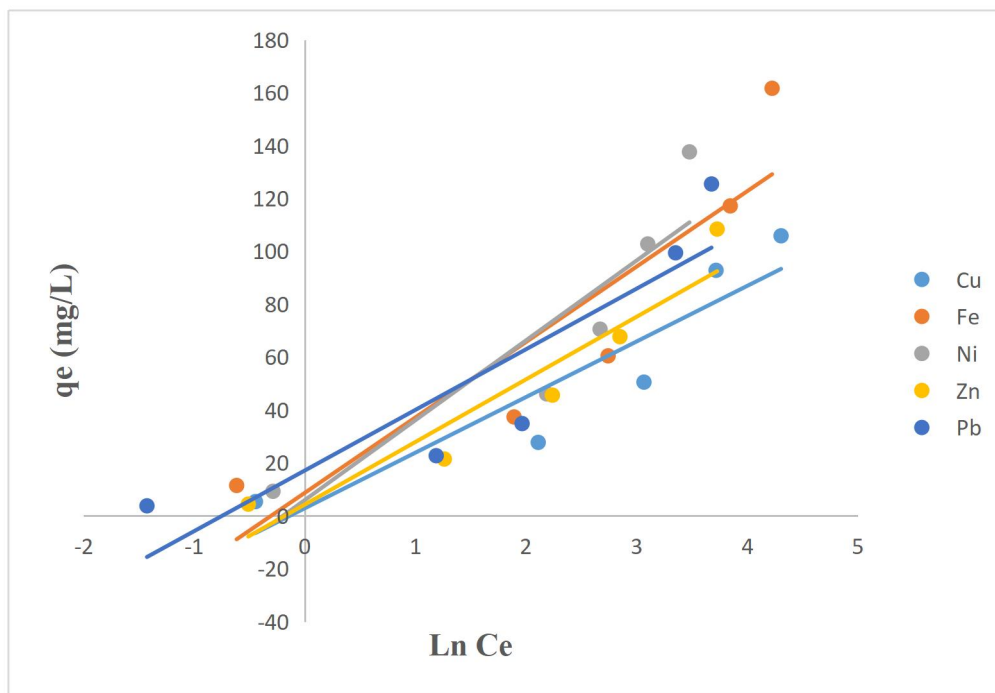
Temkin Isotherms for Ag-CNTs Adsorbent



Langmiur Isotherms for Ag-CNTs-CNCs Adsorbent

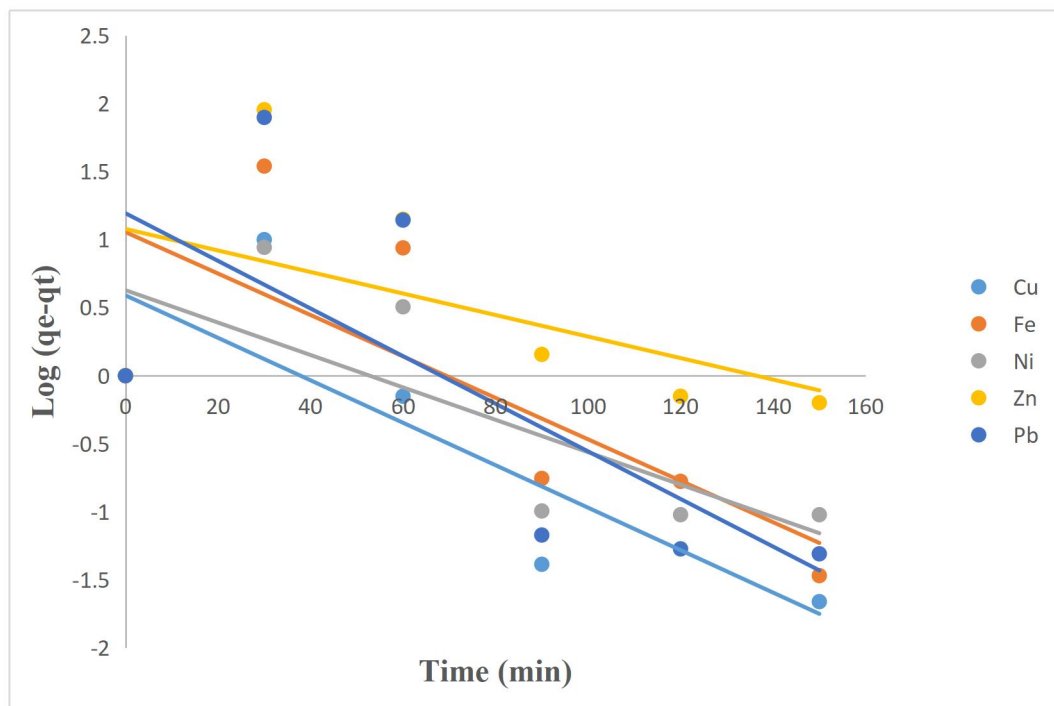


Freundlich Isotherms for Ag-CNTs-CNCs adsorbent

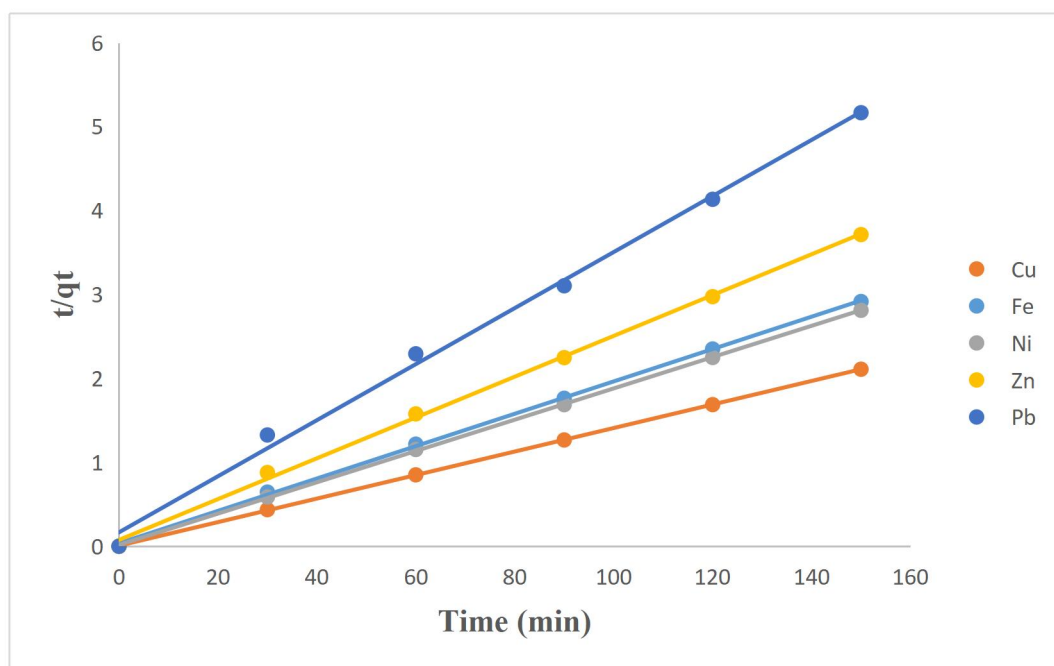


Temkin Isotherms for Ag-CNTs-CNCs adsorbent

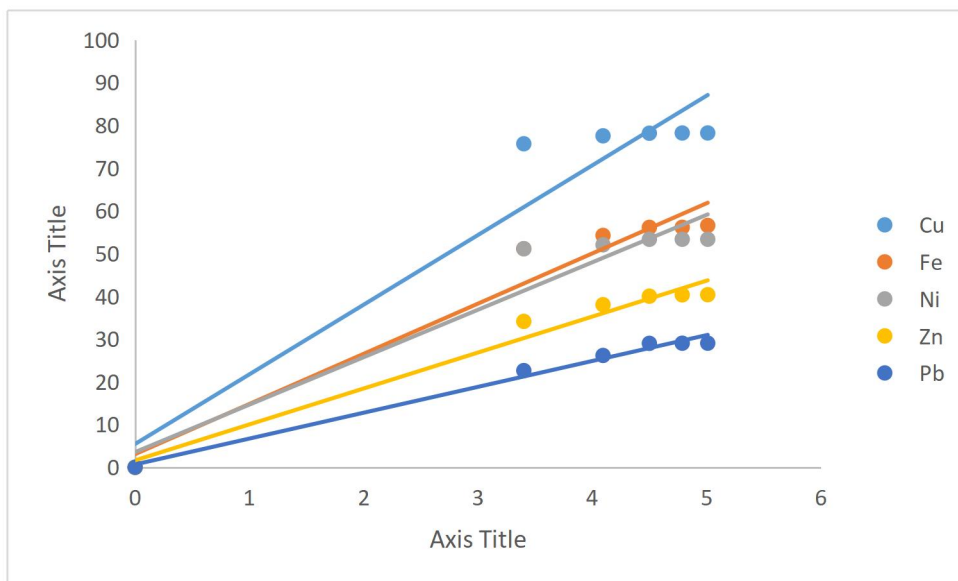
APPENDIX D: Kinetics Plots for Heavy Metal Adsorption by Prepared Adsorbents



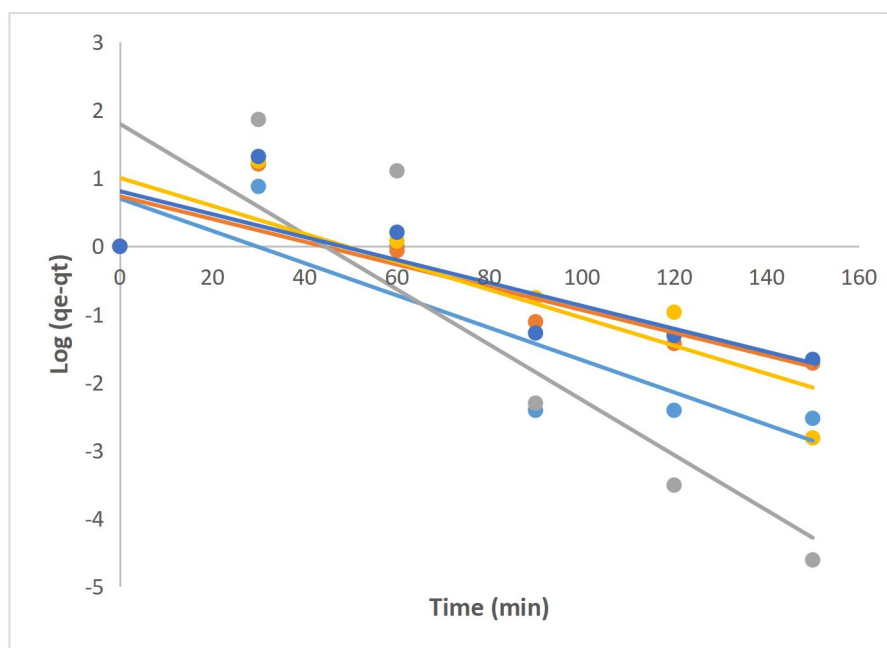
Pseudo First Order Kinetics for Ag-CNTs Adsorbent



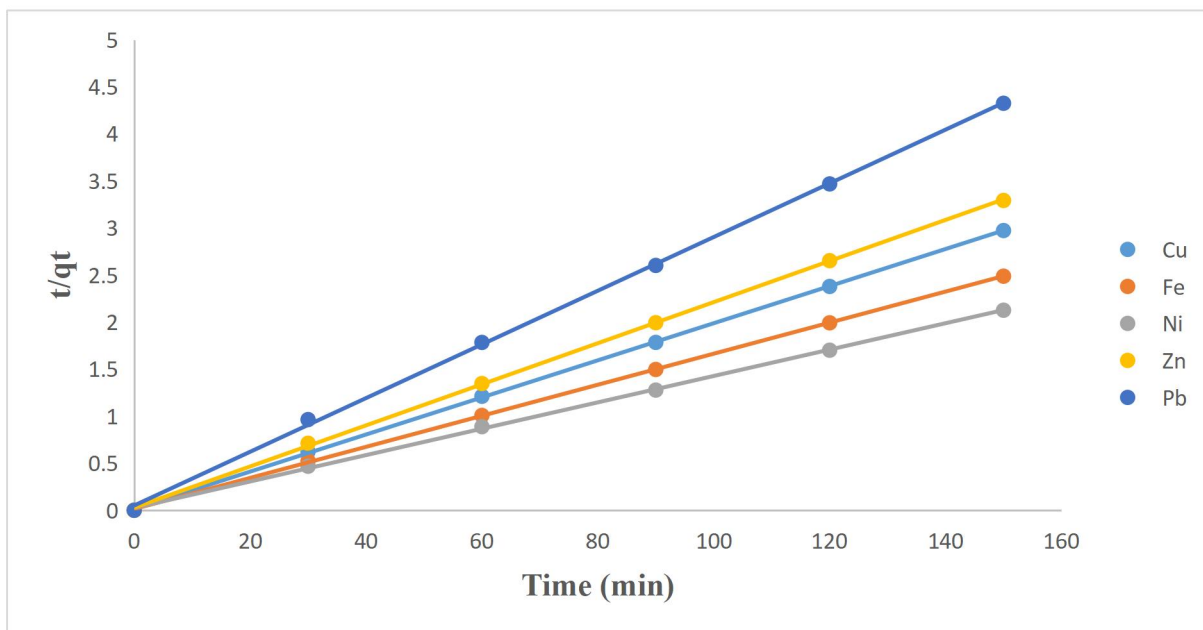
Pseudo Second Order Kinetics for Ag-CN Adsorbent



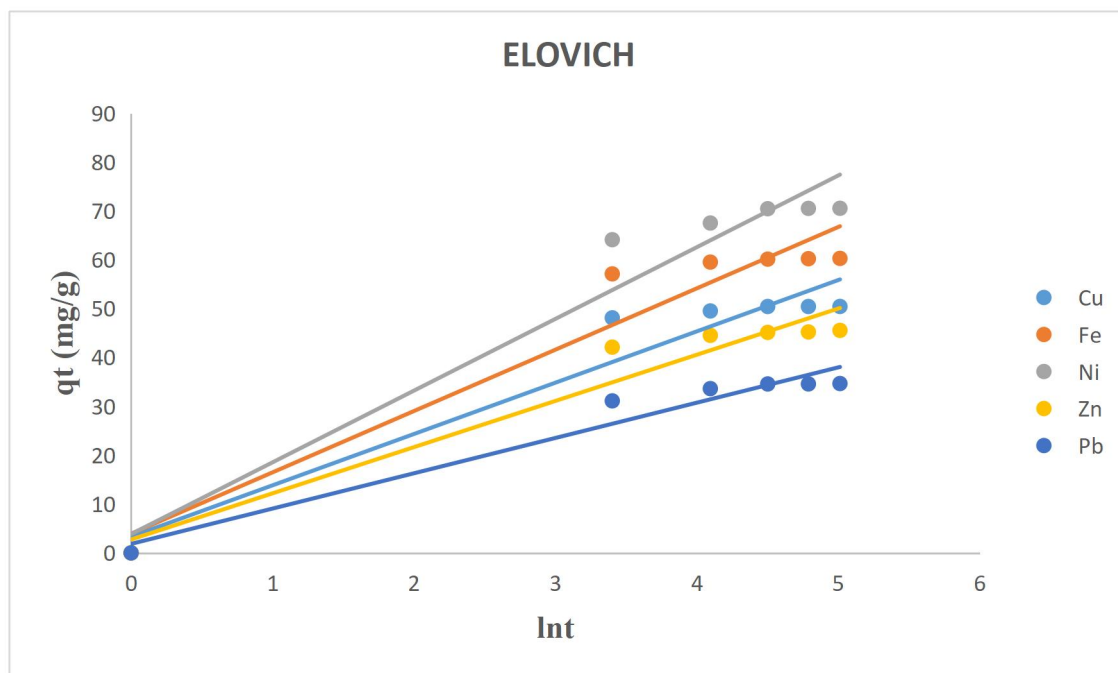
Elovich Kinetics Model for Ag-CNTs Adsorbent



Pseudo First Order Kinetics for Ag-CNTs-CNCs Adsorbent



Pseudo Second Order Kinetics for Ag-CNTs-CNCs Adsorbent



Elovich Kinetics Model for Ag-CNTs-CNCs Adsorbent